

(Dissertation for Doctoral Degree at Chiba University)

Delineation of debris-covered glaciers based on a  
combination of geomorphometric parameters and  
Landsat [TIR/(NIR/SWIR)] band ratio

February 2017

Chiba University  
Graduate School of Science  
Division of Geosystem and Biological Science  
Department of Earth Sciences  
Haireti Alifu

Delineation of debris-covered glaciers based on  
a combination of geomorphometric parameters  
and Landsat [TIR/(NIR/SWIR)] band ratio

January 2017

Chiba University

Graduate School of Science

Division of Geosystem and Biological Science

Department of Earth Sciences

Haireti Alifu

---

**Delineation of debris-covered glaciers based on a  
combination of geomorphometric parameters and  
Landsat [TIR/(NIR/SWIR)] band ratio**

---

Thesis

submitted in fulfilment of the requirements for the degree of Doctor  
of Sciences at Chiba University, 2017

By

Haireti Alifu

Committee approval:

Professor Akihiko Kondoh

Professor Nozomu Takeuchi

Associate professor Atsushi Higuchi

Professor Hiroaki Kuze

Professor Ryutaro Tateishi

## Acknowledgments

First and foremost, I would like to acknowledge and express my heartfelt gratitude to my advisors, Professor Akihiko Kondoh and Professor Ryutaro Tateishi, for their support, guidance, and assistance. For that, I will be forever grateful.

Also, I am indebted to my committee members, Professor Nozomu Takeuchi, Associate Professor Atsushi Higuchi, and Professor Hiroaki Kuze for their valuable comments, which significantly helped me to improve on this thesis. It is my great fortune to have had them on my committee.

Spatial thanks to Dr. Brian Johnson (The Institute for Global Environmental Strategies), who through the innumerable back and forth emails, patiently explained to me the how to write the academic papers and how to logically describe the idea and discussion of the matter. Without Brian's generous assistance, assuredly this thesis would have been impossible.

I also, wish to thank my laboratory members, colleagues and friends for their kind of help, assistance and concern. Aikebaier Maitiniyazia, Baixiulian, Dr. Bayan Alsaideh, Eunice Nduati, Hama Tadashi, Kayser Keram, Muzapper Omar, Mamtily, Richa Bahtarai, Dr. Saeid Gharechelou, Takuma Wakaizumi, Dr. Xiaokaiti Haji and Assistant Professor Yang Wei.

I also wish to express my appreciation for the fiscal support from the Japanese foundations (Watanuki International Scholarship Foundation and Japan and China Chinese Overseas by Japan-China Science and Technology Exchange Association) and the Chinese foundations (Chinese government award for outstanding self-finance students abroad, Outstanding International Students Scholarship for whose come from Xinjiang region). Their generosity and kind support played a vital role in supporting my life and studies in Japan.

Furthermore, I would like to thank the Cold and Arid Regions Environmental and Engineering Research Institute (CAREERI), Chinese Academy of Sciences team, and M. Rankl (Institute of Geography, University of Erlangen-Nuremberg, Germany) for providing the SCGI results and glacier velocity maps for this study.

Finally, I express deep gratitude to my parents, wife (thanks for hard days spent together with me) and sons for their love, supports, affection and *dua* during life and studies in the Japan. The success would not have been realized without their advice, encouragement and support.

Thank you very much to all.

---

## Abstract

Glaciers are considered to be key indicators of climate change. Glaciers are important freshwater resources as well as contributors to rising sea level, which threaten coastal settlements. However, supraglacial debris (debris cover on the glacier surface) alters the terminus dynamics of glaciers and thereby modifies the response of glaciers to climate change. Experimental and short-period (ablation season) studies indicate that a thick debris cover reduces ablation, whereas a thin debris layer increases ice melt underneath. Therefore, mapping and monitoring of debris-covered glaciers are essential for assessment of the impacts of climate change and management of water resources. For this reason, various methods for mapping of debris-covered glaciers have been developed and tested. However, most of these methods are highly region-specific, not universally established, and optimized for a small area. Furthermore, existing methods have difficulties when applied to (a) mapping of debris-covered glaciers covered by thick debris layers; and/or (b) mapping of debris-covered glaciers when the glacier terminus region has a gentle slope. Therefore, as an attempt to solve these problems, in this study, a new approach was developed using optical and thermal remote sensing data in combination with additional geomorphometric parameters. The proposed solution to the problems described above was based on the fact that supraglacial debris has different characteristics in the visible, near-infrared (NIR) to the shortwave-infrared (SWIR) region, in the thermal infrared region (TIR), and different landscape properties. The novelty of the present study lies in developing

---

a new approach that is a combination of the new band ratio technique [TIR/(NIR/SWIR)] with geomorphometric parameters (slope, plan, and profile curvature) using Landsat data and digital elevation model (DEM) to delineate the debris-covered glaciers. The theory behind [TIR/(NIR/SWIR)] band ratio images is that these images can utilize the benefits of both optical and thermal data sets. The (NIR/SWIR) band ratio (part of the equation) helps to identify clean glacier-ice, whereas the TIR band contributes to distinguishing supraglacial debris from the surrounding periglacial debris region. The [TIR/(NIR/SWIR)] band ratio image could detect the actual glacier terminus, whereas the geomorphometric analysis allowed the glacier margin to be detected more accurately. The method was tested by mapping glaciers in the Karakoram/Tianshan (China), and Glacier Bay, Alaska regions because these glaciers were considered to be challenging using previous methods. The final results of the glacier outlines showed relatively higher accuracy compared to the reference data sets from the Randolph Glacier Inventory, Second Chinese Glacier Inventory, glacier velocity maps, and manual delineation of the high-resolution images. However, the proposed method has limitations, such as cases in which the glacial moraine is too small or not represented in the DEM, the glacier is in a shaded area, and a river channel is connected with the glacier tongue. Thus, manual editing is required as a final step. Nonetheless, for mapping debris-covered glaciers, the proposed method was similar to manual delineation in terms of accuracy and faster than manual delineation.

---

---

**[This thesis interpolates material from four papers based on the Ach1-Ach4. Chapter 2 uses material from References (Ach3), Chapter 3 is based on Reference (Ach1). Finally, Chapter 4 builds on References of Ach2 and Ach4. Some material from each of these papers has also been incorporated into introductory Chapter.]**

Ach.1. Haireti Alifu, Ryutaro Tateishi and Brian Johnson (2015), A new band ratio technique for mapping debris-covered glaciers using Landsat imagery and a digital elevation model, **International Journal of Remote Sensing**, Volume:36, Issue:8, pp.2063-2075, DOI: 10.1080/2150704X.2015.1034886. Copyright © 2016 Taylor & Francis

Ach.2. Haireti Alifu, Brian Johnson and Ryutaro Tateishi, (2016), Delineation of Debris-Covered Glaciers Based On a Combination of Geomorphometric Parameters and A TIR/NIR/SWIR Band Ratio, **IEEE Journal of Selected Topics in Applied Earth Observations and Remote Sensing**, Volume: 8, Issue:2, pp.781 – 792, DOI: 10.1109/JSTARS.2015.2500906. © [2016] IEEE. (In reference to IEEE copyrighted material which is used with permission in this thesis, the IEEE does not endorse any of [Chiba University]'s products or services. Internal or personal use of this material is permitted.)

Ach.3. Haireti Alifu, Ryutaro Tateishi, Bayan Alsaadiehb and Saeid Gharecheloub, (2016), Multi-criteria technique for mapping of debris-covered and clean glacier ice in the Shaksgam Valley using Landsat TM and ASTER GDEM, **Journal of Mountain Science**, Volume: 13, Issue: 4, pp. 703-714, April 2016, DOI: 10.1007/s11629-015-3649-9.

Ach.4. Haireti Alifu, Ryutaro Tateishi, Eunice Nduati and Aikebaier Maitiniyazi, (2016), Glacier changes in Glacier Bay, Alaska, during 2000–2012, **International Journal of Remote Sensing**, Volume: 37, Issue: 17, pp. 4132-4147, July 2016. DOI: 10.1080/01431161.2016.1207267. Copyright © 2016 Taylor & Francis

---

# Contents

Abstract.....	i
Contents.....	iv
List of Figures .....	- 1 -
List of Tables .....	- 4 -
Chapter 1    Introduction.....	- 6 -
1.1    Importance of glacier studies .....	- 6 -
1.2    Mountain glaciers.....	- 12 -
1.3    Clean glacier-ice and debris-covered glaciers.....	- 14 -
1.3.1    Role of debris cover on glacier surfaces.....	- 16 -
1.4    Thesis structure .....	- 18 -
1.5    Literature review — mapping of glaciers .....	- 19 -
1.5.1    Definition of glacier.....	- 19 -
1.5.2    Advantages and limitations of remote sensing technology in glaciology.....	- 24 -
1.5.3    Methods for mapping clean glacier-ice.....	- 25 -
1.5.4    Methods for mapping debris-covered glaciers.....	- 31 -
1.6    Objectives.....	- 44 -
Chapter 2    An evaluation of existing method.....	- 45 -
2.1    Introduction .....	- 45 -
2.2    Study area – Shaksgam Valley.....	- 46 -
2.3    Data sources .....	- 48 -
2.4    Method .....	- 52 -
2.5    Results and discussions .....	- 63 -
2.6    Limitation of method.....	- 70 -
2.7    Conclusions .....	- 72 -
Chapter 3    Early stage of the new method for mapping of debris-covered glaciers — Based on the combination of [TIR/(NIR/SWIR)] band ratio image and slope.....	- 73 -
3.1    Introduction .....	- 73 -
3.2    Study area – Yengisogat glacier and Koxkar glacier .....	- 74 -
3.3    Data sources .....	- 76 -
3.4    Method .....	- 80 -
3.4.1    Introducing of the [TIR/(NIR/SWIR)] band ratio image.....	- 80 -
3.4.2    Delineating the final debris-covered glacier boundary by combining classified map with slope information .....	- 88 -

---

3.5	Accuracy assessment.....	- 91 -
3.6	Results and discussions .....	- 93 -
3.7	Limitation of method.....	- 100 -
3.8	Conclusions .....	- 101 -
Chapter 4	Final stage of the new method for mapping of debris-covered glaciers — Based on the combination of [TIR/(NIR/SWIR)] band ratio and geomorphometric parameters	- 102 -
4.1	Introduction .....	- 102 -
4.2	Study area – Shaksgam Valley and Glacier Bay .....	- 103 -
4.3	Data sources .....	- 105 -
4.4	Method .....	- 109 -
4.4.1	Thresholding of [TIR/(NIR/SWIR)] band ratio imagery .....	- 109 -
4.4.2	Geomorphometric Analysis .....	- 113 -
4.4.3	Overlay operation.....	- 122 -
4.5	Accuracy assessment.....	- 125 -
4.6	Results and discussions .....	- 141 -
	Glacier outlines derived from presented method — Shaksgam Valley .....	- 141 -
	Glacier outlines derived from presented method — Glacier Bay .....	- 143 -
4.7	Limitation of method.....	- 153 -
4.8	Conclusions .....	- 155 -
Chapter 5	General conclusions .....	- 156 -
References	.....	- 159 -

---

# List of Figures

Figure 1.1– Percentage of water contain on the Earth.....	- 8 -
Figure 1.2– Components of mountain glaciers.....	- 13 -
Figure 1.3.1– Characteristics of supraglacial debris cover.....	- 16 -
Figure 1.5.1.1– Examples of glacier outlines mapping in this study.....	- 22 -
Figure 1.5.1.2– Example of stereo-viewing of Google Earth images of debris-covered glacier terminus.....	- 22 -
Figure 1.5.1.3– Examples of manual digitizing the debris-covered glacier in this study...-	23 -
Figure 1.5.3.1– Spectral response of Snow and Ice.....	- 28 -
Figure 1.5.3.2– Comparisons of band ratio methods derived from Landsat TM.....	- 30 -
Figure 1.5.4.1– The schematic cross-section of a typical valley glacier showing the boundary of supraglacial debris and periglacial debris.....	- 31 -
Figure 1.5.4.2– Example of the thermal image derived from Landsat data.....	- 36 -
Figure 2.2.1– Location of study area Shaksgam Valley and selected glaciers.....	- 47 -
Figure 2.4.1– Schematic workflow for mapping glaciers based on method developed by Bhambri et al. (2011).....	- 51 -
Figure 2.4.2– Examples of clustering analysis.....	- 55 -
Figure 2.4.3– Examples of converted part of bedrock outerside of lateral moraine.....	- 56 -
Figure 2.4.4– Examples of thermal thresholding.....	- 56 -
Figure 2.4.5– Generating of final supraglacial debris.....	- 58 -
Figure 2.4.6– Examples of clean glacier-ice mapping.....	- 59 -
Figure 2.4.7– Examples of overlay operation.....	- 61 -
Figure 2.4.8– Examples of manually corrected area such as turbid water near the glacier tongue.....	- 62 -
Figure 2.5.1– Examples of misclassification area derived from thermal mask.....	- 68 -
Figure 2.5.2– Comparisons of glacier outlines from different sources.....	- 69 -
Figure 3.2.1– The overall location of study areas in this chapter.....	- 75 -
Figure 3.4.1.1– [TIR/(NIR/SWIR)] band ratio images generated by multi-temporal Landsat images.....	- 82 -
Figure 3.4.1.2– Visual comparisons of Yengisogat glacier terminus region represented by thermal (TIR) band, NIR/SWIR band ratio and [TIR/(NIR/SWIR)] band ratio image.....	- 83 -
Figure 3.4.1.3– Visual comparisons of Koxkar glacier terminus region represented by thermal (TIR) band, NIR/SWIR band ratio and [TIR/(NIR/SWIR)] band ratio image.....	- 84 -
Figure 3.4.1.4– Example of classification map of Yengisogat glacier using [TIR/(NIR/SWIR)] band ratio.....	- 86 -

---

Figure 3.4.1.5– Example of classification map of Koxkar glacier using [TIR/(NIR/SWIR)] band ratio.....	- 87 -
Figure 3.4.2.1– Generation of final Yengisogat glacier outline.....	- 89 -
Figure 3.4.2.2– Generation of final Koxkar glacier outline.....	- 90 -
Figure 3.5.1– Comparisons of the results for the delineation of glaciers using the different methods.....	- 92 -
Figure 3.6.1– Comparison of the results derived from existing method (chapter 2) and method described in this section.....	- 95 -
Figure 3.6.2– Yengisogat glacier and five classes which described in Figure 3.6.3-6.....	- 97 -
Figure 3.6.3– Normalized histogram showing frequency of each class in the (NIR/SWIR) band ratio derived from Landsat TM data.....	- 98 -
Figure 3.6.4– Normalized histogram showing frequency of each class in the thermal band from Landsat TM data.....	- 98 -
Figure 3.6.5– Normalized histogram showing frequency of each class in the [TIR/(NIR/SWIR)] band ratio derived from Landsat TM data.....	- 99 -
Figure 4.2.1– Studied glaciers which are located in Glacier Bay National Park, Alaska..	- 103 -
Figure 4.4.1.1– Examples of thresholding of [TIR/(NIR/SWIR)] band ratio.....	- 111 -
Figure 4.4.1.2– Examples of thresholding of [TIR/(NIR/SWIR)] band ratio.....	- 112 -
Figure 4.4.2.1– Examples of Plan and profile curvature image computed from ASTER GDEM V2.....	- 114 -
Figure 4.4.2.2– Examples of Plan and profile curvature image calculated from IFSAR DEMs.....	- 115 -
Figure 4.4.2.3– Examples of clustering of plan curvature and profile curvature.....	- 116 -
Figure 4.4.2.4– Examples of clustering of plan curvature and profile curvature.....	- 117 -
Figure 4.4.2.5– Examples combining the mean of slope, plan curvature, and profile curvature.....	- 120 -
Figure 4.4.2.6– Examples combining the mean of slope, plan curvature, and profile curvature.....	- 121 -
Figure 4.4.3.1– Examples of generating of final glaciers outlines in Shaksgam Valley by combining the results from thresholding of [TIR/(NIR/SWIR)] band ratio and geomorphometric analysis.....	- 123 -
Figure 4.4.3.2– Examples of generating of final glaciers outlines in Glacier Bay by combining the results from thresholding of [TIR/(NIR/SWIR)] band ratio and geomorphometric analysis.....	- 124 -
Figure 4.5.1– Comparisons of the selected clean glacier-ice outlines derived from proposed method with reference datasets.....	- 126 -
Figure 4.5.2– Comparisons of the Yengisogat glacier outlines derived from proposed method with reference datasets.....	- 127 -
Figure 4.5.3– Comparisons of the selected debris-covered glaciers outline derived from proposed method with reference dataset.....	- 128 -

---

---

Figure 4.5.4– Comparison between glacier outlines derived from proposed method and SCGI in the case of region 1.....	132 -
Figure 4.5.5– Comparison between glacier outlines derived from proposed method and SCGI in the case of region 2.....	133 -
Figure 4.5.6– Comparison between glacier outlines derived from proposed method and SCGI in the case of region 3.....	134 -
Figure 4.5.7– Comparison between glacier outlines derived from proposed method and SCGI in the case of region 4.....	135 -
Figure 4.5.8– Comparison between glacier outlines derived from proposed method and SCGI in the case of region 5.....	136 -
Figure 4.5.9– Comparisons of the Fairweather, Desolation and Crillon glacier outlines (Glacier Bay, Alaska) derived from proposed method with reference datasets.....	138 -
Figure 4.5.10– Comparisons of the Lituya and Cascade glacier outlines (Glacier Bay, Alaska) derived from proposed method with reference datasets.....	139 -
Figure 4.6.1– Small debris-covered glaciers which are studied in this study.....	145 -
Figure 4.6.2– Examples of differences in Yengisogat glacier outlines .....	147 -
Figure 4.6.3– Examples of overestimated Yengisogat glacier outline reported in Chapter (3) comparing with results derived from presented method and references data sets.....	148 -

---

## List of Tables

Table 1.5.3 Examples of clean glacier-ice mapping studies.....	- 27 -
Table 1.5.4 Examples of debris-covered glacier mapping studies.....	- 42 -
Table 2.5.1 Percentage distribution of glaciers in the Shaksgam Valley derived from this study .....	- 63 -
Table 2.5.2 Comparison between glacier areas derived from proposed method and Second Chinese Glacier Inventory (SCGI).....	- 64 -
Table 2.5.3 Comparison of selected four different glacier areas from three different studies.....	- 66 -
Table 3.6.1 Comparisons of separated each part of Yengisogat glacier derived from this study and reference data sets.....	- 94 -
Table 3.6.2 Comparisons of separated each part of Koxkar glacier derived from this study and reference data sets.....	- 94 -
Table 4.3 Manual delineation of selected glaciers for validation purpose.....	- 107 -
Table 4.5.1 Comparisons of Yengisogat glacier area derived from this study, Second Chinese Glacier Inventory (SCGI) and manual delineation of Google Earth™ images.....	- 129 -
Table 4.5.2 Comparisons of Teram Kangri glacier area derived from this study, Second Chinese Glacier Inventory (SCGI) and manual delineation of ALOS PRISM images.....	- 129 -
Table 4.5.3 Comparisons of Kulqin glacier area derived from this study, Second Chinese Glacier Inventory (SCGI) and manual delineation of ALOS PRISM images.....	- 130 -
Table 4.5.4 Comparisons of Small debris-covered glacier area derived from this study, Second Chinese Glacier Inventory (SCGI) and manual delineation of Google Earth™ images...	- 130-
Table 4.5.5 Comparisons of clean glacier-ice area derived from this study, Second Chinese Glacier Inventory (SCGI) and manual delineation of Google Earth™ images .....	- 131 -
Table 4.5.6 Comparisons between glacier areas derived from proposed method and SCGI.....	- 131 -
Table 4.5.7 Comparisons of Fairweather glacier area derived from this study and Randolph Glacier Inventory .....	- 137 -
Table 4.5.8 Comparisons of Desolation glacier area derived from this study and Randolph Glacier Inventory (RGI) .....	- 137 -
Table 4.5.9 Comparisons of Crillon glacier area derived from this study and Randolph Glacier .....	- 140 -
Table 4.5.10 Comparisons of Lituya glacier area derived from this study, Randolph Glacier Inventory (RGI) and Google Earth images™ .....	- 140 -
Table 4.5.11 Comparisons of Cascade glacier area derived from this study and Randolph .....	- 140 -
Table 4.6.1 Comparisons of Yengisogat glacier area from four different studies.....	- 149 -

---

---

Table 4.6.2 Comparison of data used in the early and final stage of method.....- 150 -

---

## **Chapter 1 Introduction**

---

### **1.1 Importance of glacier studies**

In the Earth's recent history, glaciers once covered 30% of the land area of the planet (Hooke 2005). At present, glaciers cover about 10% of the land surface of the Earth (Petersen et al. 2016). Most glaciers are located in Antarctica, Greenland, and high-altitude mountainous regions (Petersen et al. 2016). Glaciers provide many benefits to humans, as well as to vegetation in ecosystems. To recognize why glaciers are important, we need to realize what benefits glaciers offer. Moreover, we may start to understand why observation of glaciers are important. Therefore, as a beginning this thesis will begin with a description of the benefits of glaciers.

**Glaciers are a key indicator of climate change** (IPCC 2013). Variations in glacier area, volume, surface characteristics, and physical properties (i.e., albedo, debris-cover, ice velocity) indicate changes in air temperature, precipitation, and geomorphology (Ranzi et al. 2004, Haeberli et al. 2007). Thus, glaciers provide valuable information about climate change, especially in very remote areas where climate stations are rare. In addition, glaciers are widespread globally; therefore,

## INTRODUCTION

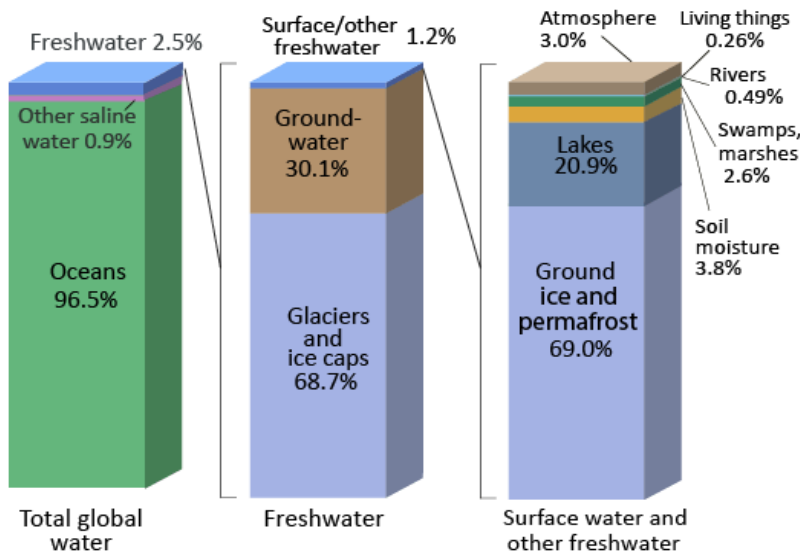
---

changes of glacier parameters provide proxy data for evaluating the nature of global climate fluctuations, and can also be useful for assessing the accuracy of climate models (Haeberli 1995, Oerlemans 2005, Nesje and Dahl 2016). Glaciers can provide information on short-term meteorological variations (Wirz et al. 2015) and reflect secular changes that occur over several decades or centuries (Zemp et al. 2015). For example, striking signal characteristics of changes in mountain glacier length are apparent by looking at cumulative values and different size categories (Haeberli 1995). Moreover, these changes give reliable, most efficiently smoothed signals of secular trends of climate variation with a delay of several years to several decades (Hoelzle et al. 2003, Zemp et al. 2015). Furthermore, large ice sheets such as those in Greenland and Antarctica have even greater response times, several thousands of years or more (Williams 1983). In contrast, small glaciers reflect yearly changes in climate almost without any delay by changes in ice velocity and mass balance (Haeberli 1995).

**Glaciers are an important freshwater resource.** Water covers about 71% of the Earth's surface (Gleick 1993). However, only 2.5% of Earth's water is freshwater, which is vital to life (Figure 1). Almost 70% of fresh-water is locked up in glaciers (Gleick 1993). Thus, glaciers are also known as “freshwater towers,” which make a significant contribution to water resources for supporting life, especially in arid and semi-arid regions (Thomas and Rai, 2005). Glaciers provide water to surrounding basin and rivers during hot, dry seasons and years.

---

## Where is Earth's Water?



Source: Igor Shiklomanov's chapter "World fresh water resources" in Peter H. Gleick (editor), 1993, *Water in Crisis: A Guide to the World's Fresh Water Resources*.  
NOTE: Numbers are rounded, so percent summations may not add to 100.

Figure 1.1– Percentage of water contain on the Earth (Source: Gleick, P. H. 1993)

**Continental glaciers such as Antarctica and Greenland can provide information about Earth's past climate.** Available meteorological observations for climate reconstruction are limited to a few decades. Fortunately, past climatic and environmental conditions can be inferred from ice cores drilled from ice sheets (Dansgaard et al. 1965, Petit et al. 1999). Measurement of the concentrations of carbon dioxide, methane, and other greenhouse gasses trapped in the ice cores provides the past air temperature at that time that the snow accumulated on the glacier's surface (Petit et al. 1999). In this way, the direction

and magnitude of future climate changes can be predicted from the information on Earth's past climate provided by glaciers (Lorius et al. 1990).

**The commercial value of glaciers.** Glacier ice itself used to be a profitable export commodity, part of the tourist industry, and was used for hydroelectric power generation (Gurnell 1983, Henrik 2008). Before refrigerators were invented, exported glacier ice was used for cooling and preserving food products (Blain 2006). Nowadays, glacier ice is used to make drinking products such as mineral water or alcohol with a high price (Henrik 2008). In contrast, meltwater from glaciers can be used to generate electric power (Kearsley 1993). Moreover, the tourism opportunities offered by glaciers, such as skiing, ice climbing, and trekking, constitute another important example of a use value of glaciers (Kearsley 1993).

**Glaciers have many benefits as mentioned above, but are also a source of hazards such as icebergs, surging, and ice avalanches as well as sea level rise (Kääb et al. 2005).** Tidewater glaciers can suddenly discharge a large amount of ice to the ocean, creating a potential hazard to transportation and shipping, as well as offshore oil installations (McNabb et al. 2015). Surging glaciers dramatically accelerate, advancing many times compared to their average speed, and block the river channel near the glacier tongue, thereby generating a glacier-dammed lake (Haemmig et al. 2014). Sudden outburst floods from glacier-dammed lakes have

---

## INTRODUCTION

---

threatened the safety of human beings and caused great economic damage (Haemmig et al. 2014). Similarly, there are glacier and permafrost hazards in high mountains, such as the Alps, as well as other regions (Kääb 2005). In history, ice avalanches have had volumes of millions of cubic meters and have covered whole villages (Margreth and Funk 1999). Moreover, melt water from glaciers is regarded as the main source of sea level rise (Pfeffer et al. 2008). Sea-level rise is a severe problem due to the global-scale rise in temperature, which has caused the rate of glacier melting to increase. Poore et al. (2000) reported that if all the current glacier ice on Antarctica and Greenland were to melt, the oceans would rise by approximately 80 m and inundate most of the coastal cities of the world.

The benefits and hazards of glaciers provide reasons for why monitoring of glaciers is necessary. The knowledge base obtained from observing glaciers is useful for understanding glacier “behavior” better and for becoming better placed to avoid future disasters. Moreover, information on glacier change can be used by policy-makers to make long-term plans to cope better with the economic impacts of climate change (Solomon et al. 2007). The benefits of glaciers are far greater than their disadvantages. In addition, natural hazards created by glaciers are another important reason for studying them.

Many different aspects might be involved with glacier monitoring. Observations of the areal extent of glaciers are often difficult to perform in the field, because

---

## INTRODUCTION

---

glaciers occur in extremely cold polar regions or high mountainous areas that are inaccessible or inhospitable to humans. Furthermore, most glaciers are big and change slowly, so repeat measurements are needed over large areas and long time periods. Fortunately, the remote sensing technique provides a unique tool for the scientific understanding of glaciers and allows extension of human observations in time and space. Satellite images provide a means of delineating the areal extent of glaciers for the entire globe (Pfeffer et al. 2014). The knowledge base of the worldwide extent, timing, and relative magnitude of glaciation is important for understanding the mechanism responsible for abrupt climate change (Clement and Peterson 2008). However, delineation of glaciers using satellite images is still challenging, because many glaciers in high mountain regions are partially or entirely covered by varying thicknesses of debris (Whalley et al. 1986). Mapping of debris-covered glaciers is a difficult task using remote sensing imagery, because the debris cover is similar to nearby valley rock. Therefore, in this research, the main focus is developing a new method for mapping of debris-covered glaciers. Therefore, the characteristics of debris-covered glaciers are described in the next section, followed by discussions of the current problems with existing methods.

### **1.2 Mountain glaciers**

There are two broad categories of glaciers: mountain or alpine glaciers (i.e.: glaciers in Himalaya, Alaska) and continental glaciers (i.e.: Greenland and Antarctica). Mountain or alpine glaciers can range from small masses of ice to a long and larger glacier system filling a mountain valley (Petersen et al. 2016). Mountain glaciers are made up of fallen snow that accumulates at high altitude, which is called the accumulation zone (Pidwirny 2006) (Figure 2). Over many years, accumulated snow builds up as snowflakes, which become packed into grains. The weight of the overlying snow causes the grains to become coarser and larger and change to firn (The equilibrium or firn line is the zone that separates bare ice from snow at the end of the ablation season, Figure 2) (Pidwirny 2006). Subsequently, snow starts to melt and quickly refreezes forming ice due to compaction and pressure (Petersen et al. 2016) (Figure 2). In this process, temperature is the main factor affecting how the snow changes and how long it takes to develop into glacier ice (Paterson 1994). When the weight of the ice and snow (thickening snowfield) becomes significant enough, the mass begins to move and flow into lower altitudes (Pidwirny 2006) (Figure 2). Glacier ice melts due to the higher temperature at lower altitudes: the zone of melting is named the

ablation zone (Figure 2). Glacier meltwater forms and contributes to rivers and is a resource for living beings.

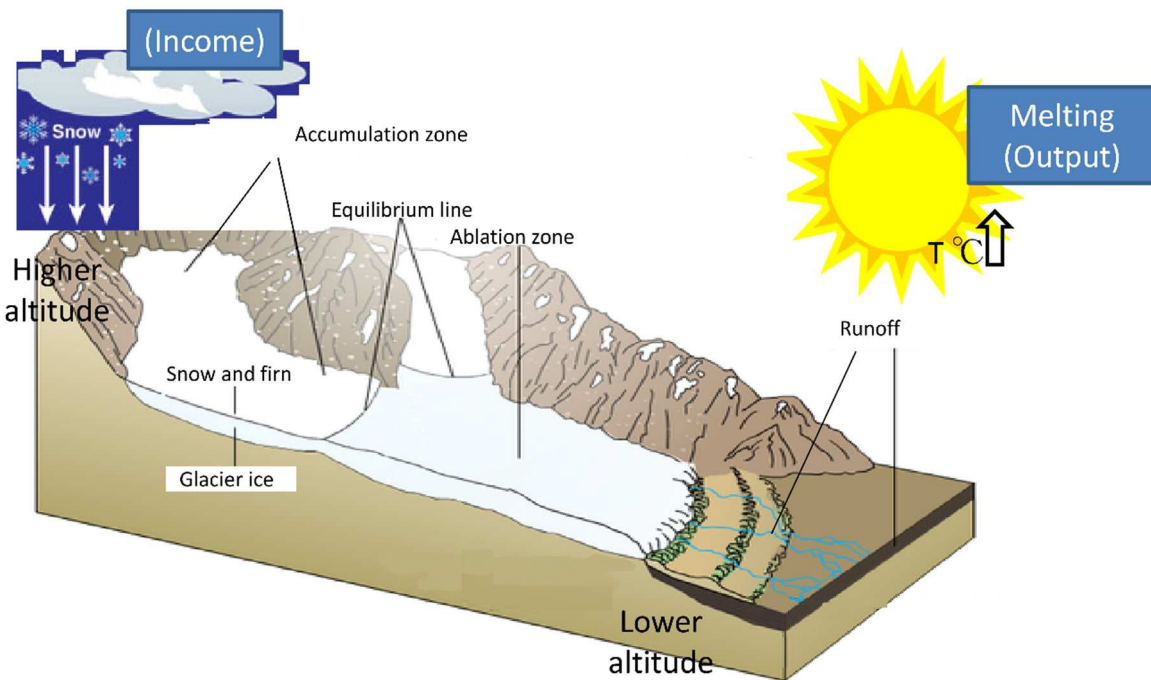


Figure 1.2– Components of mountain glaciers (Source: Glacial systems, The British Geographer, modified by Haireti).

Currently, mountain glaciers are distributed in the Rockies, the Cascades, Sierra Nevada, the Olympic Mountains, many Alaskan ranges of North America, the Coast Ranges, the Karakoram-Himalayas, the Pamirs, Kunlun mountain, the Tianshan, Ural to the Altay, and Kamchatka, Andes, the European Alps, the Pyrenees, and the Caucasus Mountains, Scandinavia, the Southern Alps of New Zealand (Petersen et al. 2016). They also exist in the East Africa on Mounts Kenya and Kilimanjaro at high elevations on tropical mountains (Petersen et al. 2016).

### **1.3 Clean glacier-ice and debris-covered glaciers**

On the basis of the glacier surface conditions, mountain glaciers can be split into two main categories: clean glacier-ice and debris-covered glaciers (Moribayashi and Higuchi, 1977).

Clean glacier-ice (Adhikary et al. 2000) occurs when a glacier has a clean or relatively clean ice (fine dust) surface (Kohshima et al. 1993). Clean glacier-ice has a high surface albedo that reflects back most of the solar radiation to space (Farmer 2015). Glacier melting and recession occurs during regional warming because the underlying land surface (rock or soil) absorbs more solar energy because its reflectivity is lower than that of glacier ice (Farmer 2015).

Mountain glaciers are often covered with varying amounts of debris (from fine to large particle size) consisting of dust, sand, silt, gravel, cobbles, and boulders (Bennett and Glasser, 2001). The debris cover on the glacier surface is derived from mass movement activities (Benn and Evans, 2014). Debris is often transferred from adjacent steep slopes to the glacier surface by rock falls, rock avalanches, debris flows, and snow/ice avalanches because of the instability of steep slopes in the high-mountain environment (debris also may become

## INTRODUCTION

---

entrained through englacial channels) (Hambrey et al. 1999, Shroder et al. 2000, Kääb et al. 2006, Hewitt 2009).

Debris-covered glaciers probably exist in all the major mountain regions of the world, and are especially well-developed in the Himalaya (Nakawo 1979, Racoviteanu et al., 2008), Karakoram (Owen and Derbyshire, 1993, Shroder et al., 2000), Caucasus (Stokes et al., 2007), Alaska (Berthier et al. 2010), New Zealand (Kirkbride 1993), and parts of the Andes (Racoviteanu et al., 2008b).

In particular, the nearly 800 million people living in the Himalaya and Karakoram regions mostly rely on water released from glaciers, especially during dry seasons (Bolch et al. 2012). A glacier mapping study based on recent satellite images estimated that the total glacier area of the Himalaya and Karakoram is ~40,800 km<sup>2</sup> (Himalaya, ~22,800 km<sup>2</sup>; the Karakoram, ~18,000 km<sup>2</sup>) (Bolch et al. 2012). In detail, ~10% of the total glacier area was debris-covered, and the debris-covered area has increased, especially in the Karakoram region (Bolch et al. 2012). Therefore, an understanding of the role of the debris cover is important for glacier dynamics, because debris thickness and distribution influence the ice melt rate (Östrem 1959).

### 1.3.1 Role of debris cover on glacier surfaces

The debris cover forms a secondary barrier between the glacier ice and the atmosphere. Solar energy must be transmitted to the underlying ice through the debris layer. Thus, the debris cover on the glacier surface (supraglacial debris) primarily affects surface ablation, altering the surface energy balance and surface boundary conditions compared to the clean glacier-ice (Scherler et al. 2011). In this way, a glacier's response to climate change can be modified (Scherler et al. 2011, Collier et al. 2015, Pratap et al. 2015).

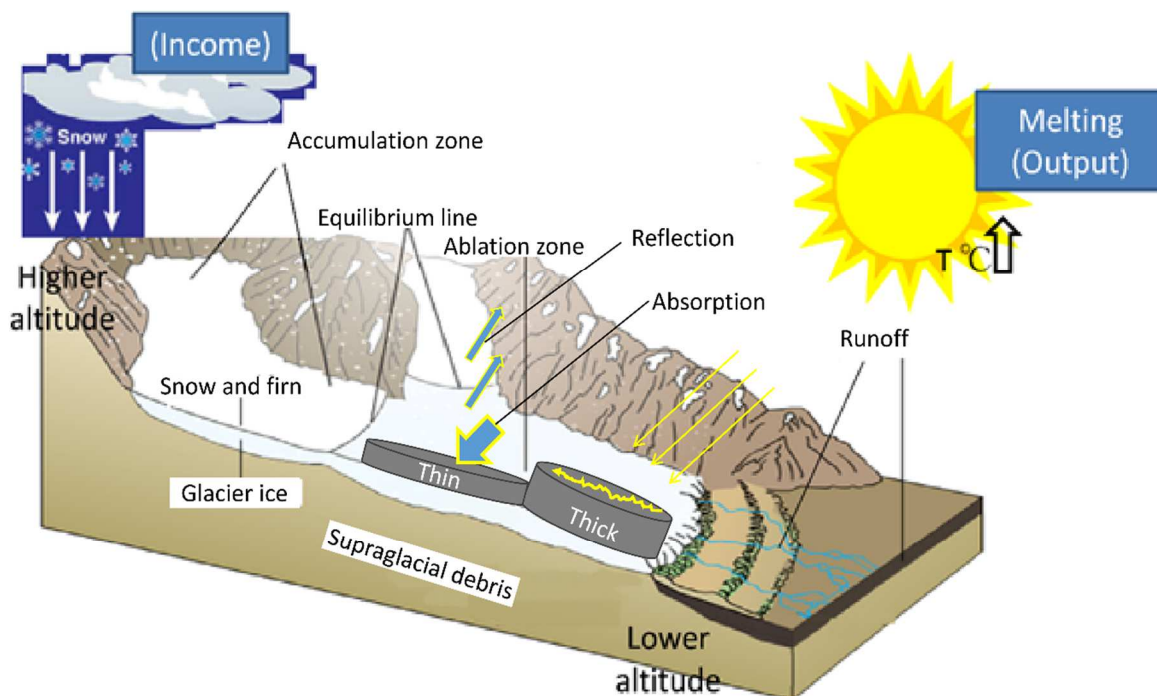


Figure 1.3.1– Characteristics of supraglacial debris cover (Source: Glacial systems, The British Geographer, modified by Haireti).

Several studies have been used field observations and simulation models to investigate glacier melting conditions in the central Himalayas and the

## INTRODUCTION

---

Karakoram regions (Collier et al. 2015, Minora et al. 2015, Pratap et al. 2015). Results from these studies suggest that debris cover enhances glacier ice melt when the debris cover is less than a few centimeters thick (Collier et al. 2015). This is due to lower surface albedo increases the absorption of solar heat (Figure 1.3.1). In contrast, a thick debris layer plays a role as an insulator: less heat energy can be transferred underneath to the glacier ice surface, which reduces glacier melting (Figure 1.3.1) (Östrem 1959, Nakawo and Young 1981, Nakawo and Young 1982, Nakawo and Rana 1999, Nicholson and Benn 2006, Juen et al. 2014, Collier et al. 2015, Minora et al. 2015, Pratap et al. 2015). Reduced ablation causes glacier tongues to be more stable and to react with greater delay to climate fluctuations than clean ice glaciers (Bolch 2011). This description highlights that understanding of debris-covered glaciers is important to produce accurate discharge models, predictions of fresh-water availability, and sea level rise. In addition, it is also important to realize that the retreat dynamics of debris-covered glaciers endanger downstream populations (Quincey et al. 2005, Juen et al. 2014). Therefore, mapping and monitoring of the extent of debris-covered glaciers can be used to assess the accuracy of climate change models, to estimate water availability in arid and semi-arid regions, and to obtain information on glacier health (Shukla et al. 2009, Bajracharya and Mool, 2010, Shukla et al. 2010, Racoviteanu and Williams, 2010, Bolch et al. 2012).

### **1.4 Thesis structure**

The structure of this thesis is:

- ◆ Chapter 1 provides background knowledge and a literature review that is relevant to this thesis. Topics such as the importance of the glacier studies, an introduction of glaciers and the role of the debris cover on the glacier, a review of existing methods for monitoring debris-covered glaciers and the current problems and objectives of this study are presented.
- ◆ Chapter 2 provides the results of experimental evaluation of an existing method developed by Bhambri et al. (2011).
- ◆ Chapter 3 delves into the early stage of the newly developed method, which is [TIR/NIR/SWIR] band ratio image integrated with the slope data.
- ◆ Chapter 4 introduces an improved method based on Chapter 3, which considers additional geomorphometric parameters such as plan curvature and profile curvature. The method is tested by applying it to a larger glacierized region.
- ◆ Chapter 5 reviews the findings and conclusions of thesis.

### **1.5 Literature review — mapping of glaciers**

#### **1.5.1 Definition of glacier**

Before reviewing the current methods used for glacier mapping, it is important to describe what area should be mapped as glacier area. The glaciers map in this study is following on definitions developed within the GLIMS (Global Land Ice Measurements from Space) project. And these definitions are adapted for the purpose of satellite-based glacier mapping based on official documents from the UNESCO (United Nations Educational, Scientific and Cultural Organization) guidelines for the compilation of the World Glacier Inventory (Müller et al. 1977).

Glacier inventory provides an indicator of climate variability and is a prerequisite to estimates of freshwater storage (Gao and Liu 2001). As the original inventory method was time-consuming and inapplicable for inaccessible areas, resulting detailed, repeated glacier inventory is still lacking (Ohmura 2009). Fortunately, to complete the glacier inventory, remote-sensing techniques, and automated computer processing were adopted in the 1980s, laying the foundation for the GLIMS project (Ohmura 2009). GLIMS is a project designed to monitor the world's glaciers primarily using data from optical satellite instruments (Raup et al. 2007; <http://www.glims.org/>).

---

## INTRODUCTION

---

The GLIMS definition of a ‘glacier’:

*A glacier or perennial snow mass consists of a body of ice and snow that is observed at the end of the melt season with minimal seasonal snow cover under cloud-free condition. In the case of tropical glaciers, after the transient snow melts. All tributaries and connected feeders that contribute ice to the main glacier, plus all debris-covered parts should include as the main glacier. Excluded is all exposed ground, including nunataks (Raup and Khalsa 2007). In the case of rock glaciers, GLIMS does not currently include it. Because of rock glaciers difficult to distinguish from in medium-resolution satellite images and most of the rock glaciers differ from debris-covered glaciers mainly by a much smaller size and a missing accumulation area (Racoviteanu et al. 2009) (thus, rock glacier isn’t included in this study) (Raup and Khalsa 2007, Rau et al. 2005).*

A definition of the glacier boundary under the debris might be deduced from the percentage ice content at depth and its characteristics (Kääb et al. 2014). Sub-surface ice content is not strictly seen at the surface, but might have an effect accessible at the surface such as a thermal signal, distinct topography, or be detectable in repeat images (Kääb et al. 2014). Thus, debris-covered glaciers boundary might be directly observed using satellite images through topography, debris lithology, or velocity as detected in repeat imagery (Kääb et al. 2014). A most used method such as manual delineation of panchromatic or multispectral

---

## INTRODUCTION

---

images might be useful for highly complex classifications for separating debris-covered ice from periglacial debris

(Some descriptions from the above are illustrated in Figure 1.5.1.1) (Kääb et al. 2014).

In generally, due to the lack of ground truth data, debris-covered glacier outlines derived from automatically methods based on medium-resolution satellite images (e.g. 30 m resolution of Landsat TM) often evaluated by comparing with manual delineation of the same set of glaciers by the same and different analysts based medium-resolution satellite or higher-resolution images (e.g. utilizing stereoviewing of higher resolution images in the Google Earth™, Figure 1.5.1.2) (Rastner et al. 2012, Paul et al., 2013). Especially, manual digitization of debris-covered glacier boundaries by an analyst experience of the region combines with clearly recognizable of geometric, topographic futures (ice crevasses, lateral and medial moraine\*) and spectral differences (supraglacial ponds, exposed ice, river channel connect to the glacier terminus) in higher resolution images can produce high quality and accuracy of glacier boundary outlines (Figure 1.5.1.3) (Rau et al. 2005, Raup et al. 2007, Paul et al. 2013, Nagai et al. 2013, Kääb et al. 2014, Fischer et al. 2014, Nuimura et al. 2014, Guo et al. 2015).

\***Lateral moraines** is angular and coarse-grained supraglacial debris, originating from valley sides (Benn and Ballantyne, 1994, Schomacker, 2011).

**Medial moraines** form when continuation of two merged lateral moraines from each flow unit (Schomacker, 2011).

## INTRODUCTION

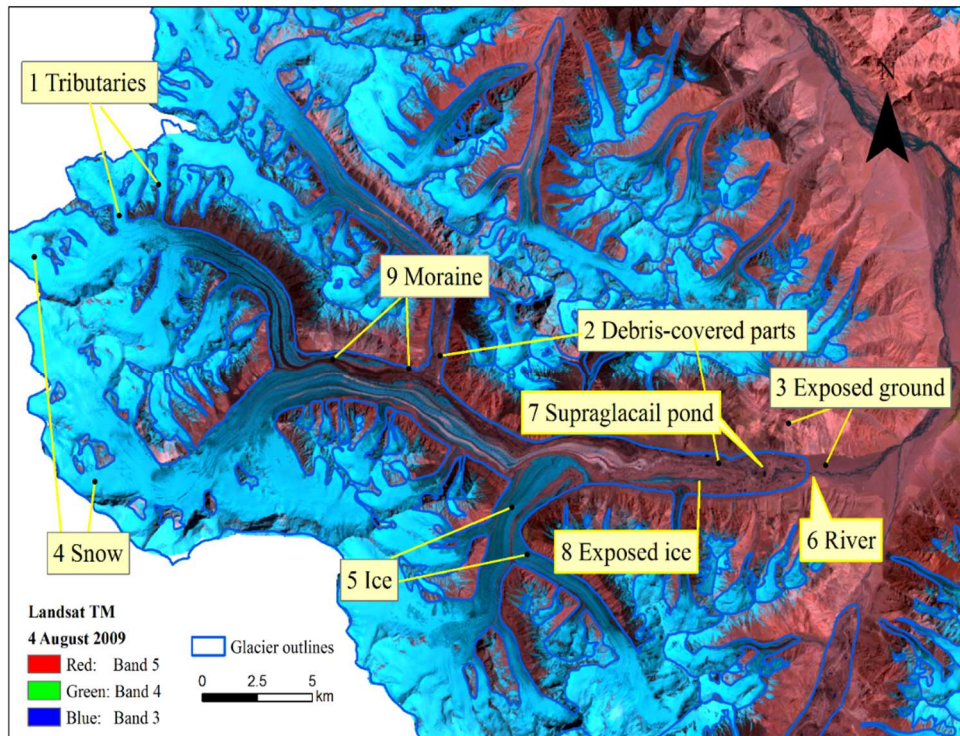


Figure 1.5.1.1- Examples of glacier outlines mapping in this study by following the GLIMS glacier definition and distinct futures (1~9) are help for identification glaciers boundary. Closer view of these distinct futures are available in Figure 1.5.1.3.

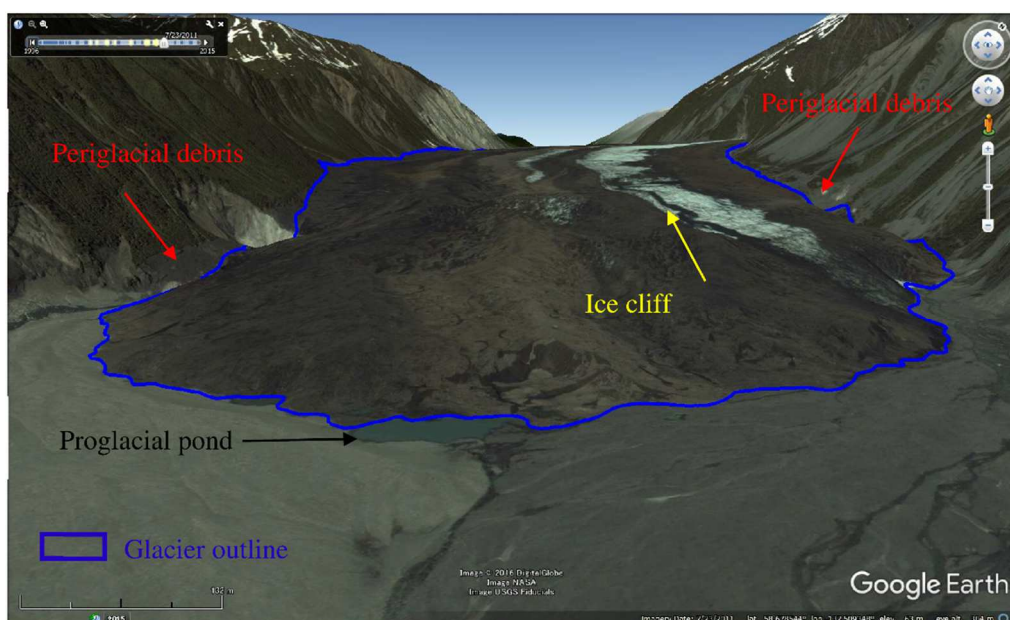


Figure 1.5.1.2- Example of stereo-viewing of Google Earth images of debris-covered glacier terminus. Small proglacial pond, ice cliff, and bumpy surface relief are identified.

## INTRODUCTION

---

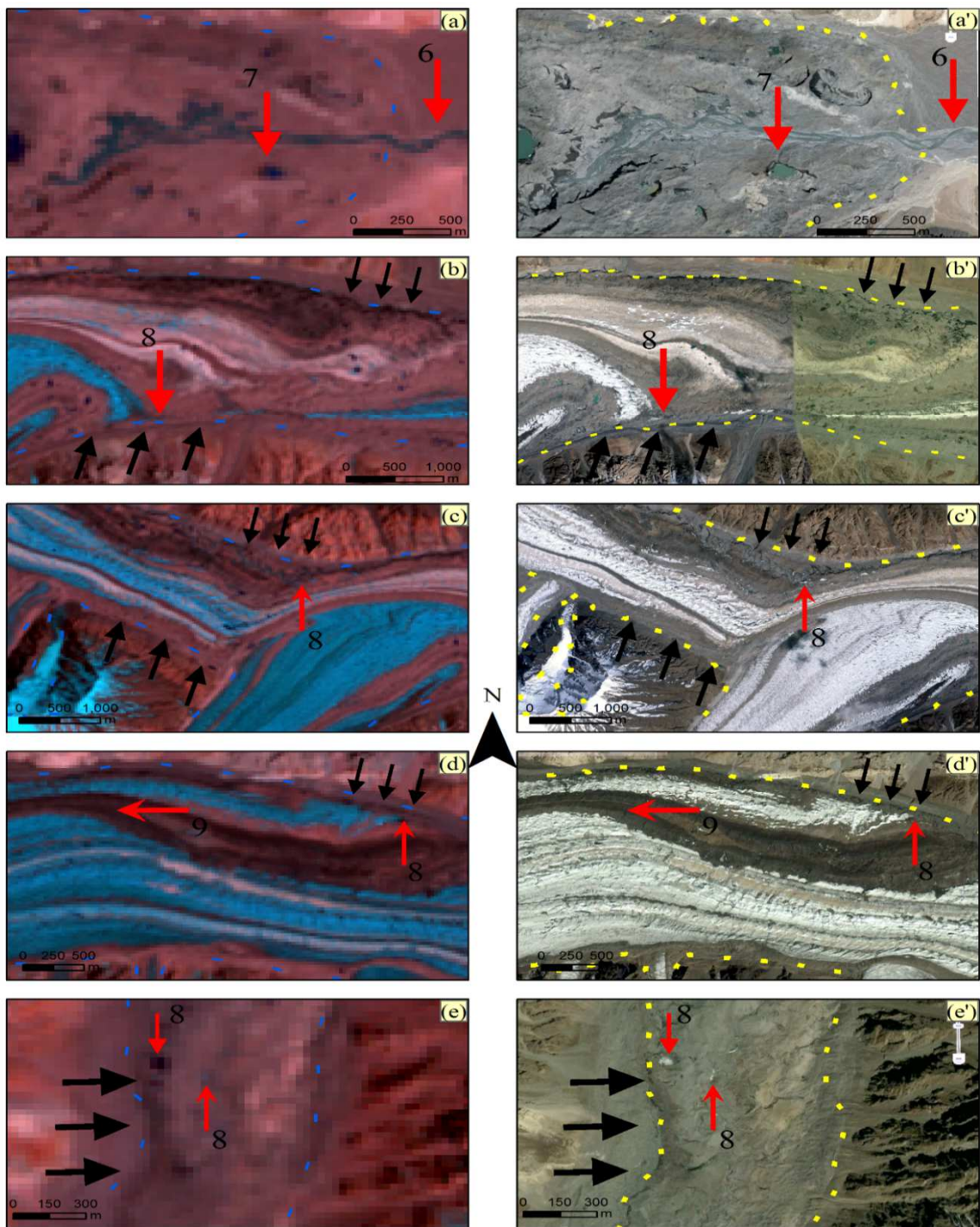


Figure 1.5.1.3- Examples of manual digitizing the debris-covered glacier in this study based on Google Earth images (a'-e') and glacier outline from SCGI (a-e). Figures show that distinct supraglacial debris futures [supraglacial ponds (7), river channel (6), exposed ice (8), medial moraine (9) and lateral moraine (black pointed)] are roughly identifiable by Landsat false colour composite images (a-e) whereas clearly visible in higher resolution google earth images (a'-e').

### **1.5.2 Advantages and limitations of remote sensing technology in glaciology**

Field-observation glacier studies provide the research results of the highest accuracy. There are several ways to monitor glaciers based on traditional field observations, such as detecting the changes in the glacier terminus by measurement at two fixed dates (end of the ablation and accumulation seasons) or measuring alterations in the glacier surface level (Østrem and Brugman 1991, Pelto and Hedlund 2001, Kaser et al. 2002.). However, field observation methods are hard to apply, due to the remoteness of glacier locations, harsh weather conditions, and presence of glaciers in politically sensitive regions, which hampers ground-based monitoring by limiting activity to small areas. Moreover, the expensiveness of field work has resulted in less repeativity and poor data coverage. For these reasons, repeated glacier inventory data are still lacking in many glacierized regions (Ohmura 2009). Hence, mapping and inventorying of glaciers using satellite or airborne imagery is the most cost-effective tool for repeated glacier monitoring in many regions (Kargel 2014). Fortunately, remote sensing images are improving and filling up the multi-temporal observation of large glacier areas within the satellite era; however, glacier mapping methods using remote sensing still require improvement of their accuracy.

### **1.5.3 Methods for mapping clean glacier-ice**

Through developing of the remote sensing technology, several methods such as manual delineation, automated and semi-automatic mapping techniques have been designed and tested for clean glacier-ice with good accuracy, as reported in previous studies (Bhambri and Bolch 2009, Racoviteanu et al. 2010, Paul et al. 2013).

Human interpretation remains the best tool for extracting glacier information from high-resolution satellite imagery (Raup et al. 2007, Paul et al. 2013, Fischer et al. 2014). Manual delineation of glacier boundaries based on the false color composites (FCC) images of Landsat Multispectral Scanner (MSS) and Thematic Mapper (TM) was started to using for the generation of glacier inventories in Iceland and Austria (Williams 1986, Hall et al. 1992). Continuously, manual digitizing of glaciers using coarse resolution to higher resolution (60 m to 25 cm) of remote sensing images [Landsat MSS/TM/Enhanced Thematic Mapper Plus (ETM+), ALOS PRISM (Advanced Land Observing Satellite data Panchromatic Remote-sensing Instrument for Stereo Mapping), aerial orthophotographs and topographic maps derived from aerial orthophotographs] are used for generation of the glacier inventories in many high mountain regions (Table 1.5.3) (Shi et al. 2008, Nagai et al. 2013, Nuimura et al. 2014, Fischer et al. 2014, Guo et al. 2015).

In general, manual digitization of glacier boundaries using remote sensing images by an operator who is knowledgeable of the region can produce high-quality and accurate glacier boundary outlines, especially when using high-resolution imagery (Raup et al. 2007, Paul et al. 2013, Fischer et al. 2014). Therefore, glacier outline derived from manual delineation approach is often used as reference data (due to ground truth data is very rare in high mountain region) to evaluated the glacier boundary derived from automated and semi-automatic glacier mapping methods (Racoviteanu et al. 2010, Paul et al. 2013).

However, manual delineation process is time-consuming when applied to large glaciers or large glacierized regions, and its accuracy depends on the image quality, interpreter's ability (Racoviteanu et al. 2010, Paul et al. 2013). For example, Bolch et al. (2010) reported some of the glacier outlines from First Chinese Glacier Inventory (FCGI) were overestimated. This might be due to some of the images used in the FCGI have fresh snow cover which hampers the detection of actual glacier boundary, resulted some of the glacier outlines were overestimated (Shi et al. 2008). Moreover, higher resolution images are very expensive, limited coverage and not often covered the glacier regions.

Therefore, automated mapping techniques of the clean glacier-ice were developed based on the fact that snow and ice has a high reflectivity in the visible to near-infrared wavelengths (VNIR) (0.4–1.2  $\mu\text{m}$ ). On the other hand, snow and

## INTRODUCTION

---

ice have a very low reflectivity in the short wave infrared (SWIR) wavelength region (1.4–2.5 µm) (Figure 1.5.3.1).

Table 1.5.3 Examples of clean glacier-ice mapping studies.

Method	Authors	Location	Remote sensing data
Manual delineation	Nuimura et al. 2014	Asia	Landsat TM and ETM+ (30 m)
Manual delineation	Fischer et al. 2014	Swiss Alps	Aerial Orth photographs (25 cm)
Manual delineation	Nagai et al. 2013	Bhutan Himalaya	ALOS PRISM (2.5 m)
Manual delineation	Shi et al. 2008 (FCGI)	China	Old aerial photographs and topo maps
NDSI	Silverio and Jaquet 2005	Cordillera Blanca	Landsat TM (30 m)
NIR/SWIR	Paul et al. 2002	Swiss	Landsat TM (30 m)
RED/SWIR	Bolch et al. 2010	Western Canada	Landsat TM (30 m)
NIR/SWIR, RED/SWIR	Falaschi et al. 2013	Southern Patagonian	Landsat TM/ETM+ and ASTER (30 m)
NIR/SWIR, RED/SWIR	Guo et al. 2015 (SCGI)	China	Landsat TM/ETM+ (30 m)

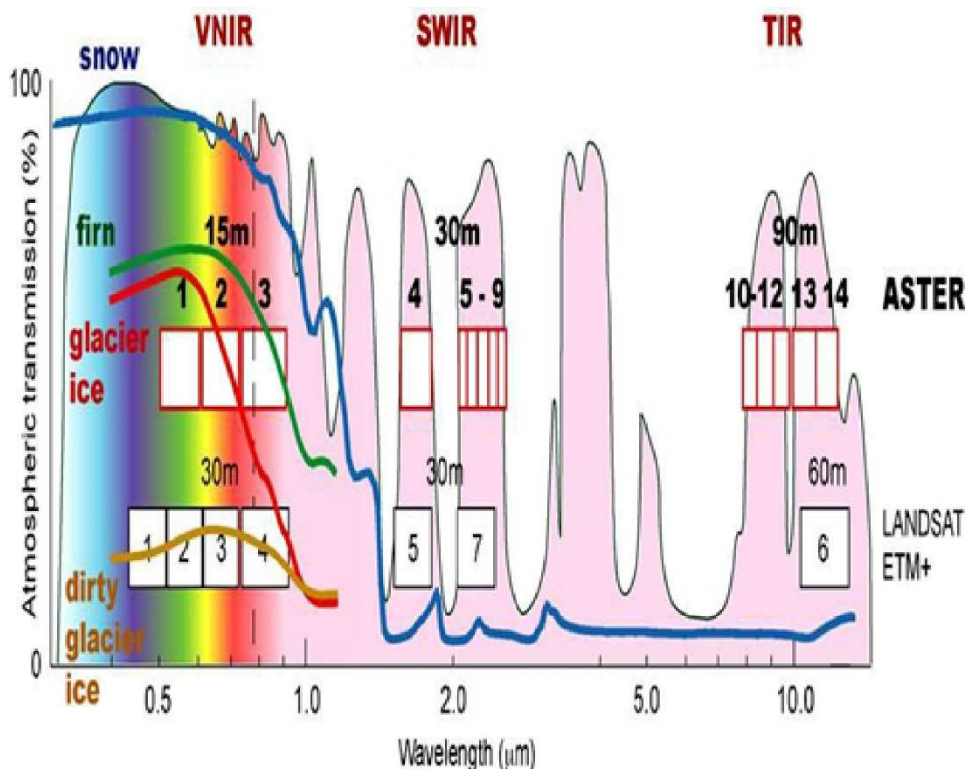


Figure 1.5.3.1– Spectral response of Snow and Ice (Source: Kääb, “Remote Sensing of Glaciers and Ice Caps”, Department of Geosciences, University of Oslo)

Rott (1994) and Bayr et al. (1994) proposed the method for clean glacier-ice mapping by thresholding of RED/SWIR and NIR/SWIR band ratio images. Similarly, Normalized Difference Snow Index (NDSI,  $[VIS - SWIR] / [VIS + SWIR]$ ) technique also used for glacier mapping in the past study (Silverio and Jaquet 2005). Moreover, a number of the glacier inventories such as: Swiss glacier inventory, inventory of glaciers in western Canada, Second Chinese glacier inventory (SCGI), first glacier inventory of the Monte San Lorenzo region

## INTRODUCTION

---

were generated by simple and robust ratio methods (RED/SWIR and NIR/SWIR) (Table 1.5.3) based on the satellite images.

The past studies concluded that mapping clean glacier-ice using band ratio technique is simple, fast and as accurate as manual delineation (Racoviteanu et al. 2010, Paul et al. 2013). However, results of the studies mentioned above indicate that band ratio methods are useful for clean glacier-ice detection, but the methods fail when they applied to debris-covered glaciers (Figure 1.5.3.2, pink mark) (Racoviteanu et al. 2010). Thus, manual digitization of debris-covered glaciers is necessary after application of such conventional band ratio techniques (Guo et al. 2015).

Comparison of ratio methods for clean glacier-ice mapping which summarized as follows:

- 1) NIR/SWIR band ratio is a more suitable method for clean glacier-ice than NDSI and RED/SWIR band ratio, due to NDSI and RED/SWIR band ratio misclassified proglacial lakes as clean glacier-ice (Figure 1.5.3.2, red mark) (Paul et al. 2002).
- 2) Beside, NIR/SWIR band ratio gives slightly better results than NDSI in the case of shadow and rocky areas in accumulation zone (Paul et al. 2002). (Figure 1.5.3.2, yellow mark).

## INTRODUCTION

---

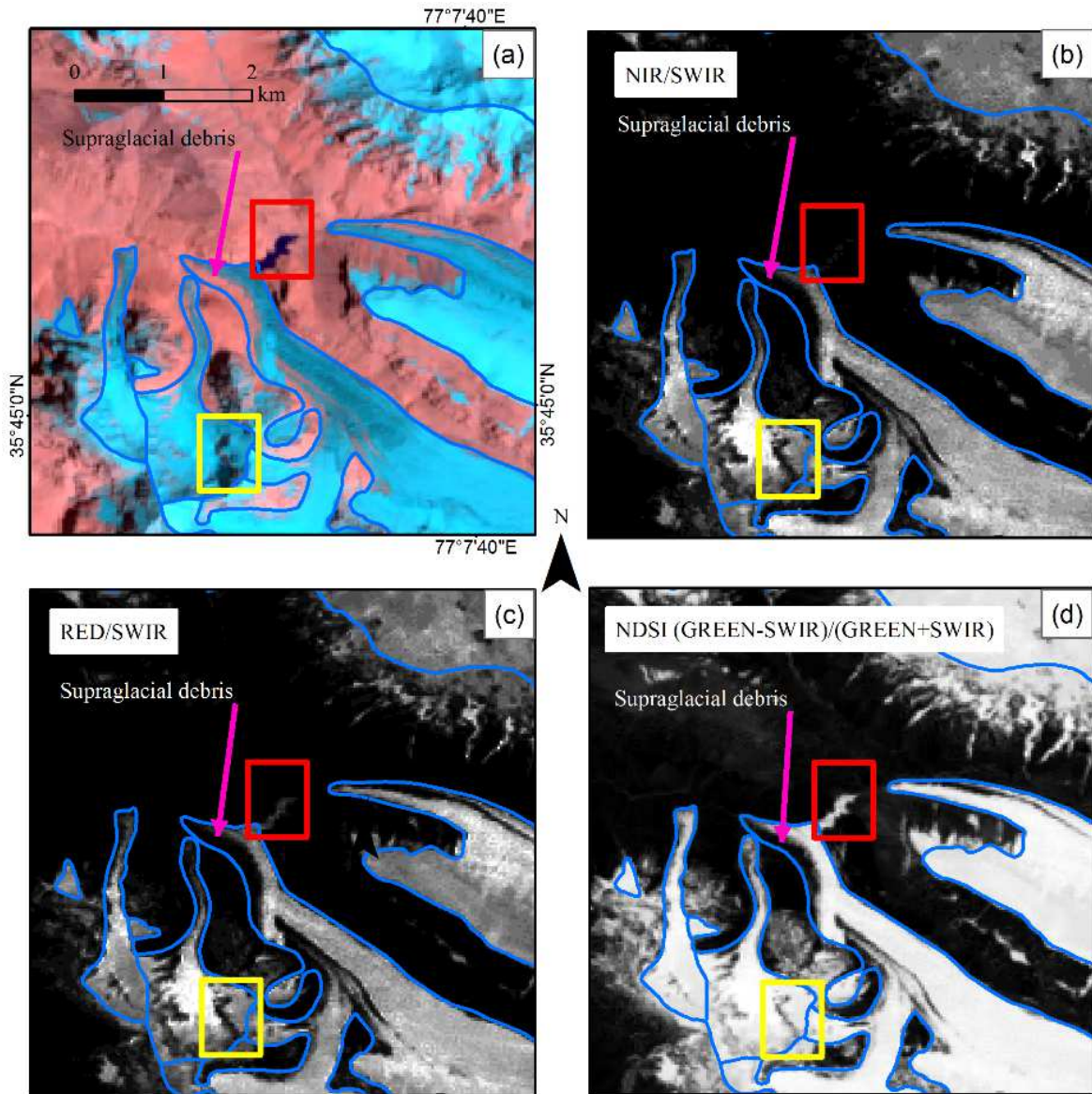


Figure 1.5.3.2– Comparisons of band ratio methods derived from Landsat TM. (a) Landsat TM image is false color composites with R = shortwave infrared band, G = red band, B = green band, same area with (b)-(d). Pink point mark shows the debris-covered glacier area. Red mark shows the proglacial lake. Yellow mark shows glacier ice under the shaded area. Glacier outline (blue) is from Second Chinese Glacier Inventory.

#### 1.5.4 Methods for mapping debris-covered glaciers

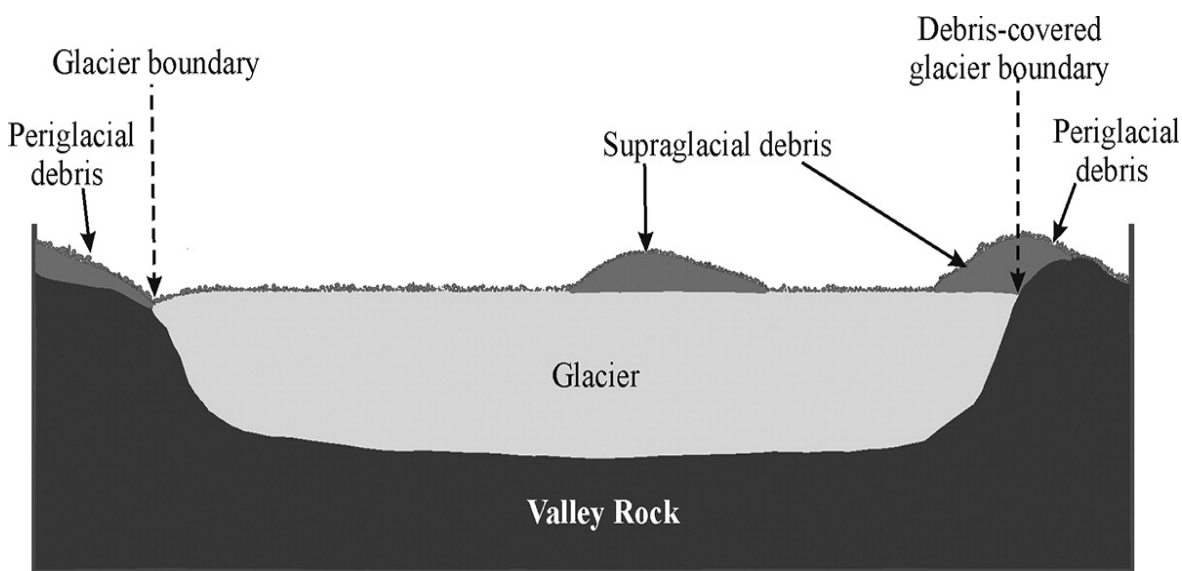


Figure 1.5.4.1- The schematic cross-section of a typical valley glacier showing the boundary of supraglacial debris and periglacial debris (Source: Shukla et al. 2010b).

Most of the glaciers in the Karakoram-Himalaya region are covered with varying thickness of debris cover (Nakawo 1979, Collier et al. 2015). Supraglacial debris (debris cover on the glacier surface, Figure 1.5.4.1) hinders glacier delineation using remote sensing data and has been recognized as a major challenge in glaciological studies (Whalley et al. 1986). Spectral response [or in the form of digital number values] of supraglacial debris involves a mixture of reflection from both debris/ice and ice that is completely covered by debris, which may not be spectrally distinguishable from adjacent periglacial debris (debris cover on the

outside of glacier margin, Figure 1.5.3.1). Moreover, the debris cover has a significant influence on glacier surface melting (section 1.3.1). Thus, the variation of the supraglacial area is considered to be essential for examining glacier runoff and measurement of water resources (Scherler et al. 2011). Also, dynamic changes of the debris cover over glaciers are correlated with local climatic variations and considered to be an important indicator of glacier health (Mihalcea et al. 2006, Stokes et al. 2007).

Therefore, in previous studies, several remote sensing techniques have been developed and applied to map debris-covered glaciers in various regions with varying degrees of success (Table 2.5.4). These techniques can be summarized into several categories, which are described below.

(i) Pixel-based image processing techniques

Artificial neural networks (ANNs) (Bishop et al. 1999, Shroder et al. 2000) and other supervised classification methods (Shukla et al. 2009), as well as band ratio approaches, [e.g., Normalized Difference Glacier Index (NDGI) and Normalized Difference Snow Ice Index (NDSII) (Keshri et al. 2009)] have been used to delineate debris-covered glaciers in the Himalay region based on spectral variations of the glacier surface.

Bishop et al. (1999) and Shroder et al. (2000) proposed ANN technology based on SPOT (Satellite Pour l'Observation de la Terre) Panchromatic data for

---

## INTRODUCTION

---

recognizing spatial reflectance variation to determine the extent of debris-covered glaciers (Raikot, Sachen, and Shaigiri glaciers) located in the Nanga Parbat massif of Pakistan. Similarly, Shukla et al. (2009) used multi-source satellite images such as IRS-P6 (Indian Remote-Sensing Satellite) Advanced Wide Field Sensor (AWiFS), IRS-1C LISS-III (Linear Imaging Self Scanning Sensor), and the Terra ASTER (Advanced Spaceborne Thermal Emission and Reflection Radiometer) to estimate the debris cover over the Samudra Tapu glacier, Chenab basin, Himalaya. In that study, supervised classification of topographically corrected reflectance images was used to map different land-cover classes on the glacier terrain such as snow, ice, mixed ice and debris, debris, valley rock, and water.

Keshri et al. (2009) developed new ratio indexes (NDGI and NDSII), which combine the Normalized Difference Snow Index (NDSI) to perform hierarchical classification of the snow, ice, and ice mixed debris classes within the single glacier in the Chenab basin, Himalaya region using ASTER images.

These studies indicated that exposed ice was misclassified as debris or thick debris cover (Bishop et al. 1999). Misclassification occurred due to ice crevasses having lower reflectance, similar to that of debris, which is caused by the complex topography of the supraglacial debris region that alters the magnitude of the reflectance (Bishop et al. 1999). Moreover, selection of appropriate threshold

values is difficult when using multi-ratio images and is challenging to apply to different sensors and dates. In addition, glacier outlines from topographic maps or existing outlines were used to create a mask corresponding to the debris-covered glacier area (which eliminates the periglacial area) before applying their methods to glacier terrain mapping (Keshri et al. 2009, Shukla et al. 2009). Therefore, these methods are unable to separate supraglacial debris from periglacial debris, when applied to a larger glacierized region. Therefore, spectral information, which has often been used for glacier mapping, does not always provide sufficient results (Kääb et al. 2014).

### (ii) Thermal-based methods

Satellite-based thermal infrared (TIR) measurements can capture land surface temperature data over large and inaccessible areas (Brenning et al. 2012). TIR is the optical region of the spectrum in the 3–5  $\mu\text{m}$  (i.e.: MODIS (Moderate Resolution Imaging Spectroradiometer)) and 8–14  $\mu\text{m}$  (i.e.: Landsat data) wavelength regions. This radiation is transferred well in these wavelength regions, due to emitted emission, and the signals are only slightly influenced by atmospheric absorption (Kerle et al. 2004). From the results of field work in the earliest study, Lougeay (1974) proposed that the thermal sensing technique has the potential to map debris-covered glaciers, because the various types of debris-covered ice show high thermal contrast in thermal infrared regions but similar

---

## INTRODUCTION

---

surface configuration and albedo values. Alternatively, Taschner and Ranzi (2002) detected the supraglacial debris margin of the Belvedere glacier in the Italian Alps based on radiometric temperature computed from the TIR bands of ASTER and Landsat TM. Furthermore, Ranzi et al. (2004) used ASTER thermal bands and conducted field observations and energy-balance modeling in test glaciers (Belvedere and Miage glaciers, Italian Alps), further proving that the supraglacial debris has a lower radiometric temperature than the surrounding periglacial debris. Thus, Ranzi et al. (2004) concluded that thermal-based methods are unable to detect debris-covered glaciers when the debris layer is thicker than 40–50 cm.

Thermal-based methods rely on measurement of emission radiance from objects: the emission radiance is dependent on the reflectivity of the object with respect to incoming solar heat and the thermal conductivity of target (Pellikka and Rees. 2009, Vihma 2011, Farmer 2015). Valley rock materials generally have higher thermal emissions than clean glacier ice, resulting in higher temperature values being captured in the TIR bands (Figure 1.5.4.2) (Warren and Bramdt, 2008). However, a thin debris layer on a glacier surface has a lower temperature than the surrounding valley rock due to the cooling effect of the underlying glacier ice (Figure 1.5.4.2) (Nakawo and Rana, 1999). In general, mapping debris-covered glaciers based on thermal data has the shortcoming that the recorded thermal emissions from such a surface are not strictly dependent on the ice underneath

---

but are also influenced by roughness, incoming shortwave radiation, thermal conductivity of the surface layer, meteorological conditions, and coarse spatial resolution (Suzuki 2011, Kääb et al. 2014). In addition, TIR imagery acquired from early morning daytime is recommended for use in glacier mapping, because these images potentially better indicate the thermal differences in the ground materials because of the effect of heating by daytime solar radiation (Kääb et al. 2014).

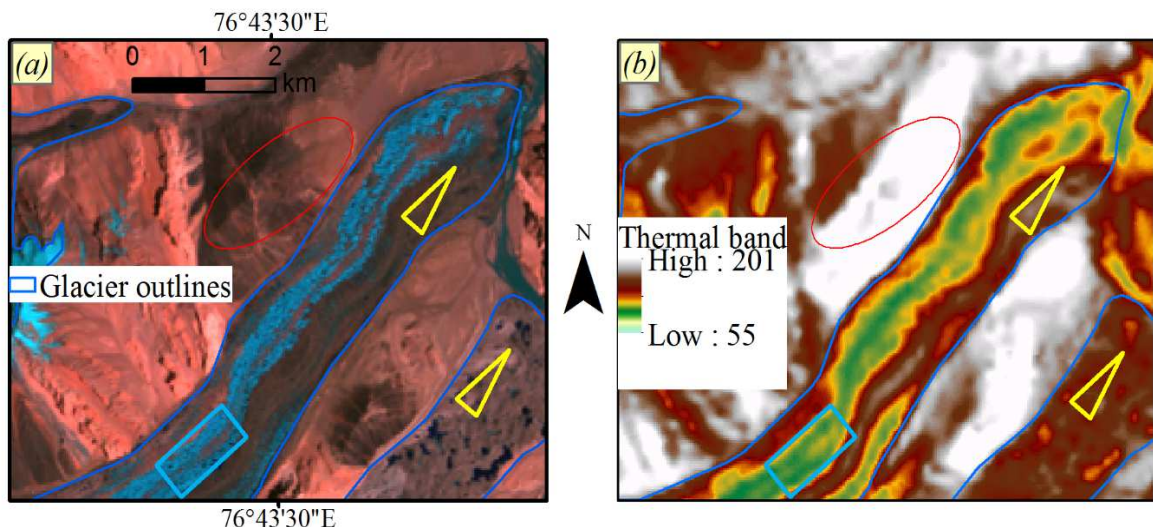


Figure 1.5.4.2- Example of the thermal image derived from Landsat data. (a) Glacier terminus region represented by Landsat images (acquisition time: 4 August 2009): R = shortwave infrared band, G = red band, B = green band. (b) Glacier terminus region represented by the thermal band of same Landsat data (a). Marked area are clean glacier-ice (blue), valley bed (red) and supraglacial debris (yellow).

### (iii) Geo-morphometric based methods

Bishop et al. (2001) investigated the utility of mapping the Raikot glacier (in Pakistan) based on the clustering of morphometric parameters derived from a digital elevation model (DEM) generated from SPOT Panchromatic stereo-pair

images. Bolch and Kamp (2006) proposed using cluster analysis to combine surfaces with similar characteristics based on morphometric parameters (plan curvature and profile curvature) to map the glaciers in the European Alps and northern Tien Shan of Kazakhstan and Kyrgyzstan. Morphometric parameters were derived from DHM25L2 DEM, the Shuttle Radar Topography Mission (SRTM), and DEM generated from ASTER images. However, determination of the boundary between glacier terminus and outwash plain was problematic where the transition between the glacier terminus region, and the un-glaciated terrain was gentle (Bolch and Kamp 2006). Furthermore, glaciers without any lateral moraines were difficult to delineate using geo-morphometric based methods (Bolch and Kamp 2006).

#### (iv) Multi-criteria techniques

Several methods have been developed that combine the different approaches mentioned above, after it was realized that mapping of debris-covered glaciers using spectral information, thermal information, or geomorphometric parameters alone did not provide satisfactory results. Paul et al. (2004) first proposed use of multispectral information [NIR/SWIR, Normalized Difference Vegetation Index (NDVI), and intensity–hue–saturation images using Landsat TM data] together with a slope data to delineate debris-covered glaciers in the Swiss Alps. However, this approach fails to map the debris-covered glaciers in the Himalaya region

---

when using its original form because of the requirement for the slope threshold to be shifted to suitable values for delineating the glacier termini (Bolch et al. 2007, Shukla et al. 2010a). Furthermore, thresholding of NDVI has to be used very carefully, because of the presence of vegetation cover on the surface of some debris-covered glaciers (Bolch et al. 2007).

Bolch et al. (2007) presented automated delineation of debris-covered glaciers in the Khumbu region of the Himalaya based on the ASTER's thermal bands with various geomorphometric parameters (slope, plan curvature, and profile curvature) derived by DEM generation from ASTER images. However, this method cannot detect the actual supraglacial area if the lateral parts of the debris-covered glaciers are missing, or are too small to be represented in the ASTER DEMs (Bolch et al. 2007). Also, this automated method is challenging when the glacier surface is covered by a thick debris layer (Bolch et al. 2007).

Another method, proposed by Khan et al. (2015), used supervised classification of different band combinations in the VNIR and SWIR wavelength regions together with a slope layer to map debris-covered glaciers in the upper Indus Basin of Pakistan using Landsat images and SRTM. However, misclassification occurred in transitional areas between the glacier and periglacial debris (Khan et al. 2015). Also, bare surfaces along rivers located on lower slopes were misclassified as debris cover (Khan et al. 2015). The approach proposed by

---

## INTRODUCTION

---

Bhardwaj et al. (2015) was used to incorporate multispectral (VNIR and SWIR) and TIR of Landsat 8 data to map selected debris-covered glacier faces in the Baspa river basin of the Indian Himalaya. This method involved manual delineation of the glacier boundary using pan-sharpened Landsat 8 bands. However, that study did not separate supraglacial debris from the periglacial debris region (i.e., the debris cover on the adjacent glacier margin). Racoviteanu and Williams (2012) proposed a decision tree algorithm based on multi-spectral (VNIR to SWIR), topographic variables (elevation and slope), and kinetic temperature computed from thermal bands using ASTER data to map the debris-covered glaciers in the Sikkim Himalaya. Some inaccuracies were reported, particularly in areas with deep shadow and thick debris cover (Racoviteanu and Williams 2012). Also, this method has a limitation (thresholds for multiple variables) that currently makes the method difficult to apply at large scales (Racoviteanu and Williams 2012).

Semi-automated methods have been developed based on cluster analysis of geomorphometric parameters (slope, plan, and profile curvature) derived from DEMs [DEMs generated from ASTER pair images and ASTER Global Digital Elevation Model Version two (GDEM V2) data], the (NIR/SWIR) band ratio technique, and thermal masks derived from thermal bands (ASTER, Landsat TM/ETM+) to delineate debris-covered glaciers in the Himalaya region (Bhambri et al. 2011, Bhardwaj et al. 2014). These methods have difficulty in detecting the

---

## INTRODUCTION

---

debris-covered glacier terminus region if covered by a thick debris layer and debris-covered ice under shadow (Bhambri et al. 2011, Bhardwaj et al. 2014). Thus, manual editing was necessary to improve the final glacier maps.

Shukla et al. (2010) and Karimi et al. (2012) used combinations of VNIR, SWIR, and/or TIR data (from different sensors, such as: IRS-P6 AWIFS, ASTER, Landsat TM, and Worldview-2) with geomorphometric parameters (e.g., slope, aspect, and elevation) derived from DEMs [digital topographic maps and airborne laser scanning data (LiDAR)] to delineate debris-covered glaciers (the Alamkouh galcier in the Alburz Mountains and Samudra Tapu glacier in and Himalaya region). In those studies, debris-covered glaciers surfaces and margins were adequately delineated based on the ANN and Maximum Likelihood Classifier methods. A similar study, that of Shukla et al. (2016), proposed the hierarchical knowledge-based classification method (HKBC) for the Kolahoi Glacier, in Kashmir Himalaya, to perform terrain mapping based on ASTER images and ASTER GDEM. The HKBC approach requires several input layers: the NIR/SWIR band ratio; spectral indices such as NDGI, the Normalized Difference Water Index, the Normalized Difference Debris Index (NDDI), image transformations (intensity hue saturation images); slope; and the thermal glacier mask. Therefore, HKBC involves the application of various thresholds; these may make it difficult to transfer the method to a large glacierized area. Moreover, cold rocky materials and the sandy area near the glacier snout have been misclassified

as debris-covered glacier during mapping using thermal data (Shukla et al. 2010). Nevertheless, approaches that combine optical and thermal data from multiple sensors require cloud-free images for both data sets, which may decrease the practical applicability of these methods to large regions. Additionally, the SWIR detectors of one of the commonly used data sources, ASTER data, failed in April 2008. In summary, all of these discussed previous approaches (including the combined methods) have the following characteristics.

- (a) Most of the methods have been applied to and tested on a single glacier or small region.
- (b) Some of the methods did not take account of supraglacial debris separated from periglacial debris (supraglacial debris area was extracted using glacier outlines from existing sources or manually delineated from satellite images, before mapping of the supraglacial terrain).
- (c) Some of the approaches that combine optical and thermal data from multiple sensors require cloud-free images for both data sets, which may decrease the practical applicability of these methods to wide regions.
- (d) Mapping of debris-covered glaciers covered with a thick debris layer is challenging.
- (e) It is difficult to map debris-covered glaciers when the transition from the debris-covered glacier terminus region to the unglaciated area is smooth.

## INTRODUCTION

---

Table 1.5.4 Examples of debris-covered glacier mapping studies.

Method	Authors	Location	Remote sensing data
Artificial neural networks	Bishop et al. 1999	Western Himalaya	SPOT (10 m)
	Shroder et al. 2000		
Supervised classification	Shukla et al. 2009	Himalaya	IRS-P6AWiFS (56 ~70 m) IRS-1C LISS-II (23.5 ~70 m) ASTER (15 ~ 90 m)
Ratio images: NDGI, NDSI, NDSII	Keshri et al. 2009	Himalaya	ASTER (VNIR to SWIR) (15~30 m)
Thermal-based	Taschner and Ranzi 2002	Italian Alps	Landsat TM (TIR: 120 m) ASTER (TIR: 90 m)
	Ranzi et al. 2004		ASTER (TIR: 90 m)
Geo-morphometric based	Bishop et al. 2001	Himalaya	SPOT (10 m)
	Bolch and Kamp 2006	Central Alps, Northern Tien Shan,	ASTER (15 m) SRTM (90 m) DHM25 (25 m)

## INTRODUCTION

---

Multi-criteria technique	Paul et al. 2004	Swiss	Landsat TM (30 ~ 120 m) DEM25 (20 m)
	Khan et al. 2015	Karakoram m	Landsat TM (30 ~ 120 m) ASTER (15~90 m)
	Bhardwaj et al. 2015	Himalaya	Landsat 8 (15 ~100 m) ASTER GDEM V2 (30 m)
	Racoviteanu and Williams 2012	Himalaya	ASTER (15~ 90 m) SRTM (90 m)
	Bolch et al. 2007	Himalaya	ASTER (15 ~ 90 m)
	Bhambri et al. 2011	Himalaya	ASTER (15 ~ 90 m)
	Bhardwaj et al. 2014	Himalaya	Landsat TM/ETM+ (15 ~120 m)
	Shukla et al. 2010	Himalaya	IRS-P6AWiFS (56 ~ 70 m) ASTER (15 ~ 90 m) DEM (1:50 000)
	Karimi et al. 2012	Iran	Worldview- 2 (48 cm ~ 2 m) Landsat TM (30 ~120 m)
	Shukla and Ali 2016	Himalaya	ASTER (15 ~ 90 m) ASTER GDEM V2 (30 m)

## **1.6      Objectives**

The literature review suggests that combining information from multi-spectral classification, geomorphometric analysis, and thermal characterization of the glacier is helpful to delineate debris-covered glaciers. Therefore, the principle objective of this study is to develop a new approach based on a combination of optical, thermal, and geomorphometric parameters to map glaciers that were considered to be challenging using previous methods. Therefore, there are several sub-objectives toward the final goal of this research: these sub-objectives are as following.

- 1) An existing method developed by Bhambri et al. (2011) was applied to map the glaciers in the Shaksgam Valley to determine the glaciers that are difficult to map using previous methods.
  
- 2) The early stage of the proposed method is assessed by mapping a single glacier selected from the literature review and experimental application of the first objective.
  
- 3) Make necessary modifications based on the early stage of the proposed method in order to apply the method to the large glacierized regions.

## **Chapter 2 An evaluation of existing method**

---

### **2.1 Introduction**

The method proposed by Bhambri et al. (2011) was used for the mapping of glaciers in the Shaksgam Valley. There were several reasons for conducting this work. First, this method was successfully used to map glaciers (debris-covered and clean glacier ice) in a larger area in the Himalaya region. A method that can delineate the glaciers in a large area is useful for rapid generation of a glacier inventory, and is thus, helpful for understanding the dynamic changes of glaciers and other related research (water management and climate change) (Haeberli 1995, Bajracharya and Mool, 2010, Bolch et al. 2012). However, it is uncertain whether this method can be applied to other regions.

The Shaksgam Valley was selected as a study area because this area is a large glacierized area with a heavy debris cover (Shi et al. 2008). Glaciers in this region have different landscape properties, which are suitable for examining the method developed by Bhambri et al. (2011). Furthermore, the Shaksgam Valley is a sensitive political area; therefore, use of remote sensing techniques to map the glaciers in this region is necessary.

## **2.2 Study area – Shaksgam Valley**

The Shaksgam Valley (Figure 2.2.1) is located on the north slope of Chinese Karakoram, in the southwest of the Xinjiang Uyghur Autonomous Region, China. Chinese Karakoram mountain occupies 5988.67 km<sup>2</sup>, in which the area covered by perennial snow (Liu et al. 2015). Glacier cover contains about 11.57% of total glacier area of China (Liu et al. 2015). Advection of the moist air masses from the India monsoon which causes the abundant precipitation at high altitudes resulting formation of large glaciers in this region and most of them are almost following the North direction.

The Shaksgam Valley has the largest concentration of glaciers in the mainland Asia (Shi et al. 2008). Eight glaciers over 50 km in length and more than 20 glaciers over 30 km long (Shi et al. 2008). The glacier meltwater contributes to the Indus and Yarkand rivers, and livelihood of around 130 million people (Sinha and Ravindra 2013). The equilibrium line altitude is around 5100-5400 m a.s.l. (Shi et al. 2008). Most of the glaciers terminus region terminate at elevations between 4200-4700 m a.s.l (Shi et al. 2008). The dynamics of Karakoram glaciers are known to show stable or advancing terminus positions and surging behavior compared to the worldwide retreat of many mountain glaciers (Copland et al. 2011, Bhambri et al. 2013, Rankl et al. 2014).

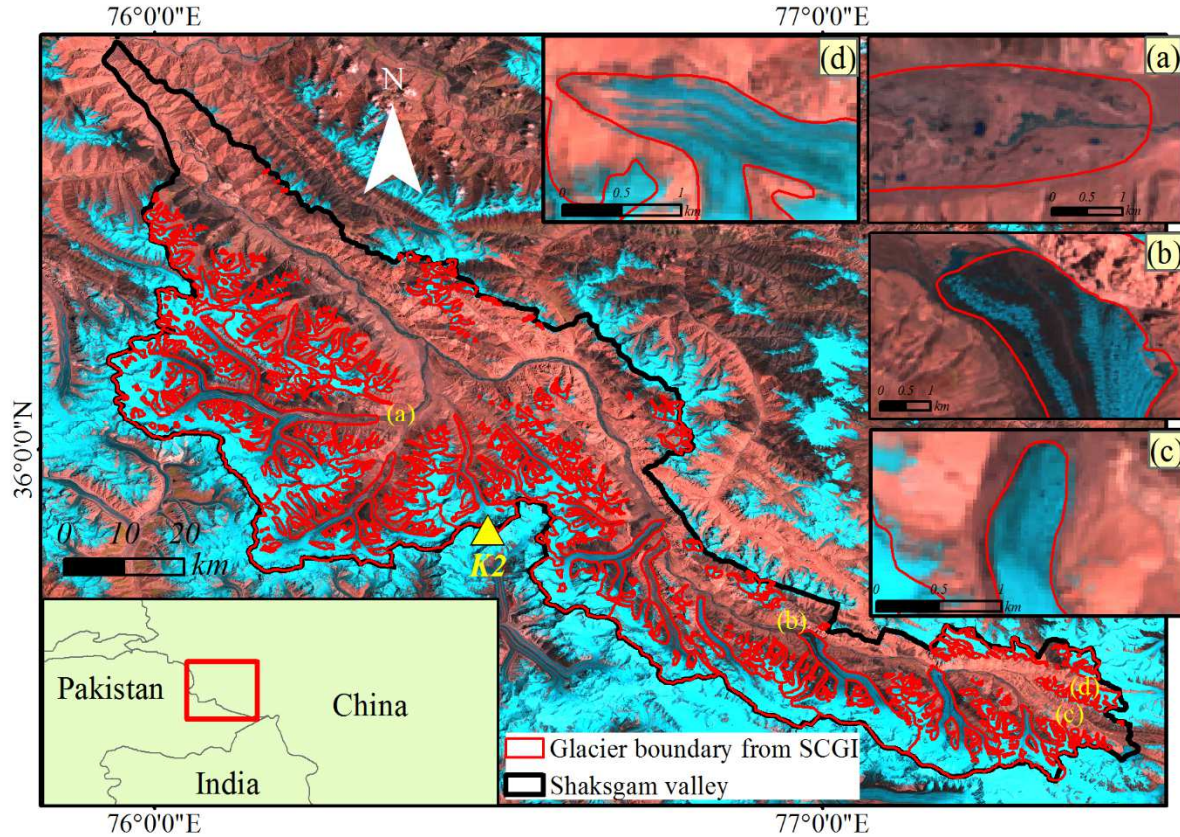


Figure 2.2.1- Location of study area of Shaksgam Valley and selected glaciers: (a) Yengisogat glacier terminus region, (b) Teram Kangri glacier terminus region, (c) Glacier B terminus region, (d) Glacier A terminus region, for manual delineation using Google Earth™ images. Landsat images: R = shortwave infrared band, G = red band, B = green band.

## **2.3 Data sources**

Landsat TM [acquisition time: 4 August 2009, Greenwich Mean Time (GMT): 05:18 (~11:18 am at local time)] and ASTER GDEM V2 data are used to map the glaciers in this chapter. The orthorectification of Landsat TM data with minimal seasonal snow and cloud cover is downloaded from (USGS) EarthExplorer (EE) (USGS EE; <http://earthexplorer.usgs.gov/>). Landsat TM provides seven spectral bands and a ground resolution of 30 m per pixel for the visible near infrared bands (VNIR) and shortwave infrared bands (SWIR) and 120 m per pixel for the thermal infrared band (TIR).

The improved ASTER GDEM V2 was released by the Ministry of Economy, Trade, and Industry (METI) of Japan and the United States National Aeronautics and Space Administration (NASA) in mid-October 2011. The second version of ASTER GDEM adds 260,000 additional stereo-pairs to improving coverage and reducing the occurrence of artifacts (Tachikawa et al. 2011). The refined production algorithm improved the spatial resolution, as well as increased horizontal (72 m) and vertical accuracy (17 m), also superior water body coverage and detection (Tachikawa et al. 2011). The ASTER GDEM V2 maintains the GeoTIFF format and the same gridding and tile structure as ASTER GDEM version one, with 30 m postings and 1 x 1 degree tiles.

---

The glacier extents from Second Chinese Glacier Inventory (SCGI) and manually delineation of selecting glaciers from high-resolution Google Earth™ images were used as reference data to compare and validate glacier outlines derived from this study.

SCGI dataset was provided by Cold and Arid Region Environment and Engineering Research Institute (CAREERI) at Lanzhou (<http://westdc.westgis.ac.cn/glacier>) (Guo et al. 2015). The glacier extent of SCGI was produced from Landsat scenes by following the GLIMS definition of the glacier (Guo et al. 2015, Liu et al. 2015). Conventional band ratio method was used as the first step in mapping the glaciers, and then intensive manual improvements were employed (Guo et al. 2015, Liu et al. 2015). In the case of debris-covered ice was delineating by manually (Guo et al. 2015, Liu et al. 2015). The primary result of SCGI was generated by 12 participants who's after in-depth training sessions on the pixel-mixing mechanisms and correct glacier discrimination from Landsat images (Guo et al. 2015). Identification of unique surface features such as supraglacial lakes, the outlets of subglacial streams near glacier termini, and the landforms and drainage systems of lateral moraine, relying on the difference of surface colours and textures in different band composites of Landsat images was an important theme during the training of all participants (Guo et al. 2015). The final check and improvements of SCGI were generated by five members who have rich experience (>3 years) for glacier

delineation (Guo et al. 2015). The overall accuracy of glacier outlines in SCGI was carried out by comparing the glacier outlines with the glacier marginal positions measured during field GPS investigation (maximum difference 1 year with Landsat data used for SCGI), and the glacier outlines delineated from high-resolution Google Maps™ images (Guo et al. 2015). Totally, 23 glaciers margin with >2320 measurements points were obtained by RTK-DGPS (real-time kinematic differential) (Guo et al. 2015). The randomly selected glaciers in different sub-regions were manually digitized by higher-resolution images in Google Maps™ with the nearest time with Landsat data used for SCGI (Guo et al. 2015). Finally, accuracy assessment showed that outlines of debris-covered ice is in the order of  $\pm 30$  m comparing to the glaciers margin detected by RTK-DGPS and 83% overall accuracy is obtained by comparing the glacier outlines based on manual delineation of high-resolution images from Google Maps™ (Guo et al. 2015).

Human interpretation remains the best tool for extracting glacier information from high-resolution satellite imagery (Raup et al. 2007, Paul et al. 2013, Fischer et al. 2014). Hence, we used freely available Google Earth™ software which is providing multi-temporal high-resolution images and corresponding DEM (see page 20-22 about the detailed explanation about identification of glacier area). Therefore, the former provide suitable source data for the creation of reference data by manual digitization of glacier outlines. In this study, four selected glaciers

---

(Figure 2.2.1) are manually delineated using Google Earth™ images. Acquisition date (16 July, 15 August, 22 August, 9 September, 30 September and 30 October of 2009) of chosen Google Earth™ images (which shown in the Figure 2.4.1) are similar with Landsat data used in this study.

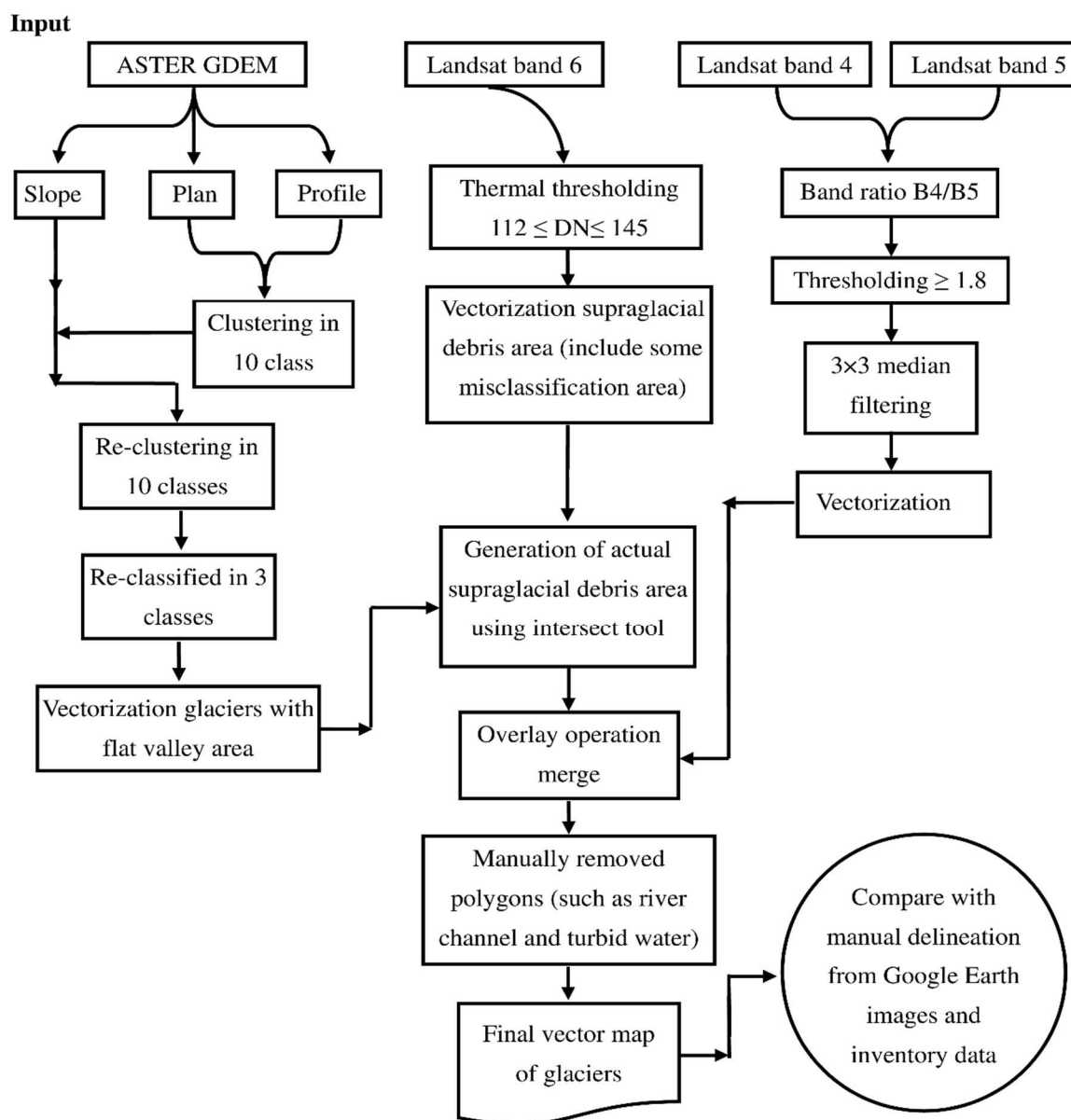


Figure 2.4.1- Schematic workflow for mapping glaciers based on method developed by Bhambri et al. (2011).

## **2.4      Method**

This section includes a description of detailed procedures of a multi-criteria technique developed by Bhambri et al. (2011) for mapping the glaciers in the Shaksgam Valley. The overall processing steps to generate the final glacier outlines are following as (Figure 2.4.1):

- 1) Supraglacial debris cover mapping
  - a) Extraction of morphometric parameters and cluster analysis
  - b) Selection of optimal threshold values from the thermal band to distinguish between supraglacial debris and periglacial debris
  - c) Generating final supraglacial debris
- 2) Clean glacier-ice mapping
- 3) Generation of final glacier outlines using overlay operation

1) Supraglacial debris cover mapping

*a) Extraction of morphometric parameters and cluster analysis*

Geomorphometric parameters such as the slope, plan, and profile curvature are used for delineation of the supraglacial debris cover. Mean slope was the best suited for delineation of the glacier terminus region (Bishop et al. 2001, Bolch and kamp 2006). However, it does not work well in the relevant gentle area (Bolch and kamp 2006). Plan curvature highlighted the crest of ridges and alpine-basin valley bottoms (Bolch and kamp 2006). Profile curvature enhanced the convexity associated with the lateral moraines and highlighted the concavity associated with glacier ablation valley boundary, where slopes are steep and concave (Bishop et al. 2001). Profile curvature enables the lateral moraines to be recognized, whereas plan curvature allows the differentiation of the glacier front to the valley floor of the direct glacier forefields (Bishop et al. 2001, Bolch and kamp 2006). Therefore, the combination of geomorphometric parameters derived from the DEM was helpful to represent glacier terrain characteristics thereby, to map debris-covered glaciers more accurately (Bishop et al. 2001).

The geomorphometric parameters (slope, plan, and profile curvature) were generated from ASTER GDEM (Figure 2.4.2.b) using Geographic Information System (GIS). In the beginning, the plan and profile curvature were integrating by ISODATA cluster algorithm and classified into ten classes with similar surface

---

properties (Figure 2.4.2.c). An unsupervised classification approach (ISODATA clustering algorithm) was used to ensure the concept of ``homogeneous morphology''. This algorithm is based on the global variance structure of morphometric parameters, and it iteratively adapts to the variance structure by statistical separability (Bishop et al. 2001). This type of clustering uses a process in which, during each iteration, all samples are specified to consisting cluster centers and new means are recomputed for every class (Ball and Hall 1965). The optimal number of specified classes are usually unknown (Richards and Jia 1999). Therefore, it is recommended to input a conservatively high number, analyze the resulting clusters, then, reclassify again with a reduced number of classes (Richards and Jia 1999). Subsequently, for delineating supraglacial debris region more accurately, the cluster analysis result of the plan and profile curvature was combined with the slope parameter, clustered again into new ten classes (Figure 2.4.2.d).

This new ten classes reclassified into the three categories (Figure 2.4.2.e, glaciers with flat valley area, concave terrain futures and convex terrains futures) by manually based on visually comparison of Landsat colour composite images (i.e. a false colour composites with Red = shortwave infrared, Green = red band, Blue = green band). The glaciers with the flat valley class's were converted into the vector map (Figure 2.4.2.f). However, the clustering of morphometric parameters could not accurately delineate the glacier boundaries where the transition from

---

the glacier terminus to unglaciated terrain was gentle (Figure 2.4.2.f). Also, converted part of bedrock outerside of lateral moraine (which belongs to periglacial debris class) near the accumulation zone of the debris-covered glacier (Figure 2.4.3) (Bolch and kamp 2006, Bhambri et al. 2011). Fortunately, these inaccuracies can be removed using additional information derived from thresholding of the Landsat thermal band.

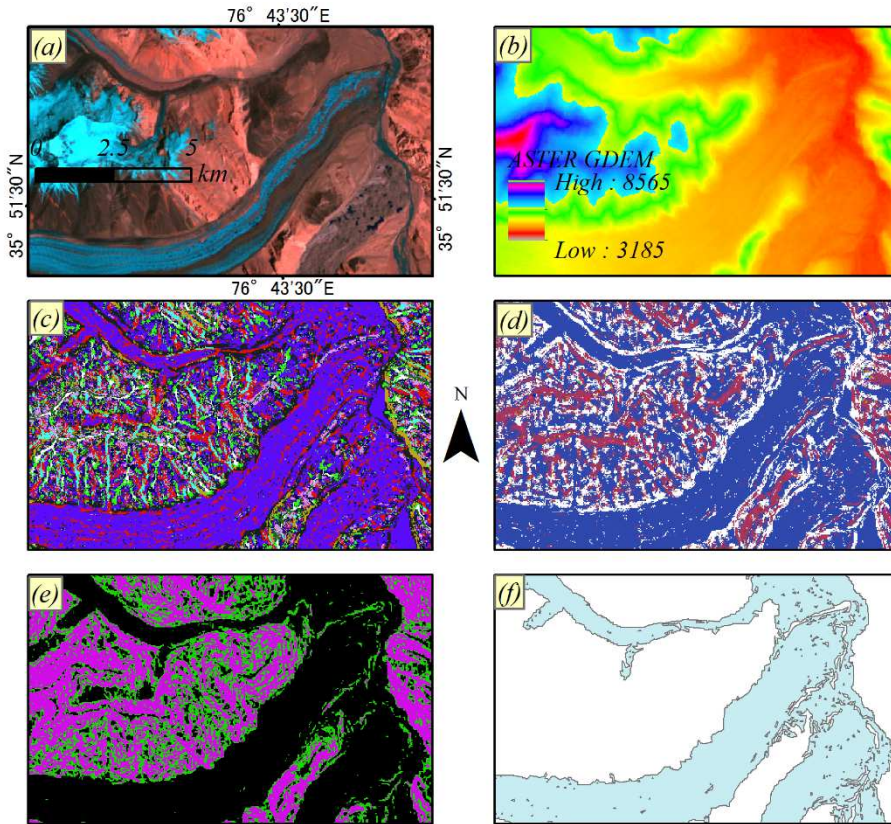


Figure 2.4.2- Examples of clustering analysis. (a) Glacier terminus region. (b) Glacier terminus region presents by ASTER GDEM. (c) Cluster analysis of plan and profile curvature into 10 classes. (d) Re-clustering of plan curvature, profile curvature and slope into 10 classes. (e) Re-classification result derived from clustering of plan curvature, profile curvature, and slope into three classes. (f) Vectorization of glaciers with flat valley area.

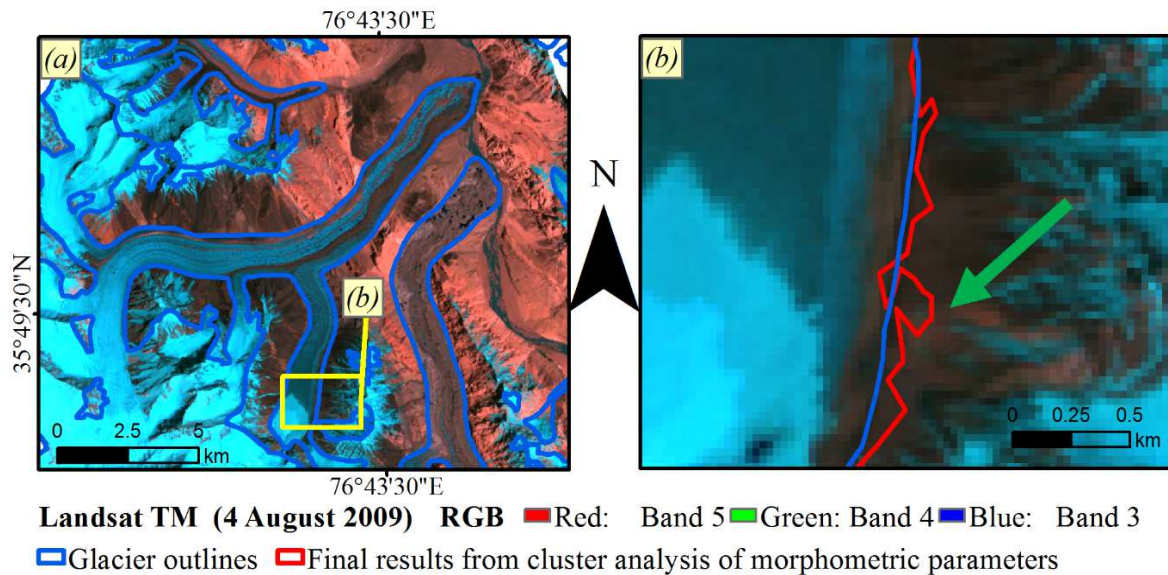


Figure 2.4.3- Examples of converted part of bedrock outerside of lateral moraine (green pointed). (a) Overall glaciers area. (b) Closer view of image (a).

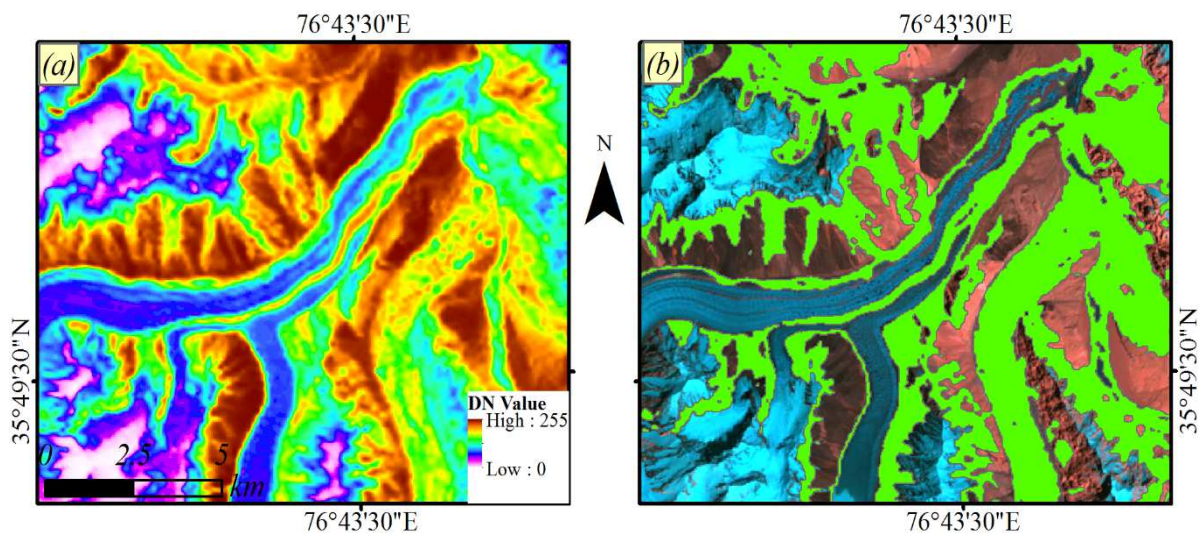


Figure 2.4.4- Examples of thermal thresholding. (a) Landsat TM thermal band. (b) Thermal mask vector layer (in green) for the supraglacial debris region overlaid onto Landsat TM false color composites image.

*b) Selection of optimal threshold values from the thermal band to distinguish between supraglacial debris and periglacial debris*

Ground truth estimation, as well as the measurement based on remote sensing studies, indicate that temperature difference exists between supraglacial debris, and adjacent periglacial debris (Ranzi et al. 2004, Shukla et al. 2010, Bhambri et al. 2011, Karimi et al. 2012). On the other hand, the permafrost possibility exists around the glaciers, but because of mountain permafrost under the layer of soil, rock or sediment, and this layer mostly thicker (0.5-8 m) than supraglacial debris (Gruver and Haeberli 2009, Gruber et al. 2016). Furthermore, its reliable detection requires temperature estimates spanning at least 2 years to understand the seasonal temperature evolution (Gruver and Haeberli 2009). Thus a purely thermal phenomenon of mountain permafrost can hardly be detected direct way by a TIR band (Owen and England 1998, Kääb 2005, Westermann et al. 2015, Gruber et al. 2016).

Consequently, a thermal band of Landsat TM was used to separate supraglacial debris from periglacial debris. The digital number (DN) values of supraglacial debris in the thermal band (Figure 2.4.4.a) were carefully checked by manually and where DN values are 112 and 145 were used to generate the thermal mask due to they can separate supraglacial debris with the unglaciated region. Then, thermal mask binary image was converted into a vector polygon map (Figure

---

2.4.4.b). Due to the shadowing effect and low spatial resolution of the Landsat TM TIR band, the interpretation of the final results of the thermal mask was not always straightforward.

*c) Generating final supraglacial debris*

Next, for generating outlines of the supraglacial debris (Figure 2.4.5.d), the intersect tool was applied to the vector layers derived from cluster analysis and containing the thermal mask.

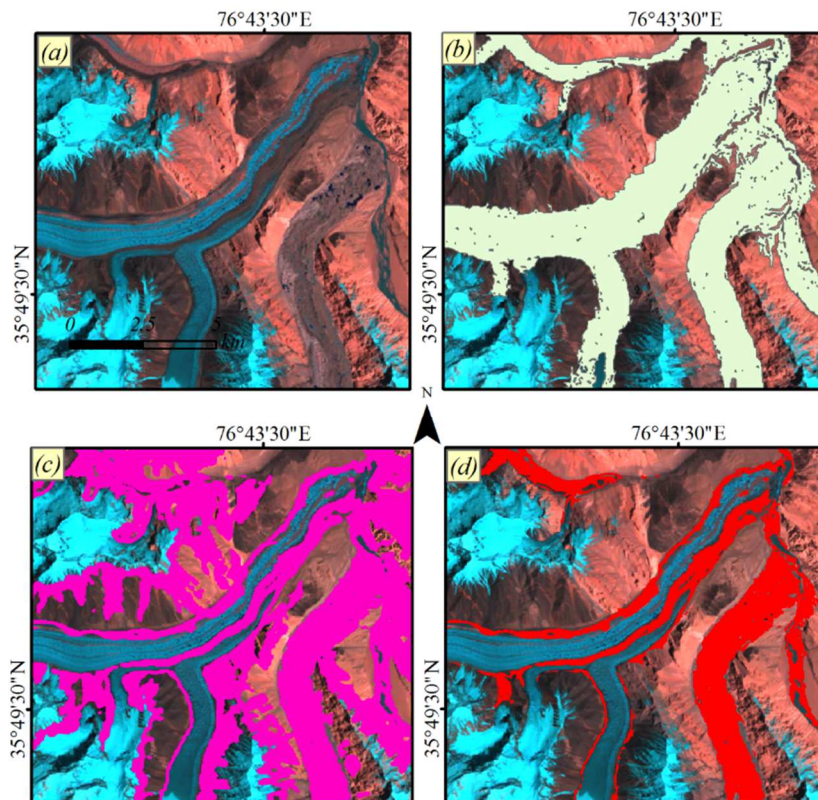


Figure 2.4.5- Generating of final supraglacial debris. (a) Gasherbrum and Urdok glacier terminus region. (b) Result derived from the geomorphometric analysis. (c) Thermal mask vector layer (in pink) for the supraglacial debris. (d) Final supraglacial debris outlines generated from the combination of vector layers derived from cluster analysis and containing the thermal mask using the intersect tool.

## 2) Clean glacier-ice mapping

In this step, the band ratio technique was used to map clean glacier-ice. Several glacier inventories are created using ratio methods (Racoviteanu et al. 2009, Pfeffer et al. 2014). For mapping of clean glacier-ice using ratios of spectral Landsat bands (band 3/band 5 or band 4/band 5) is the most efficient method (Paul 2000). Most accurate results for clean glacier-ice mapping was obtained

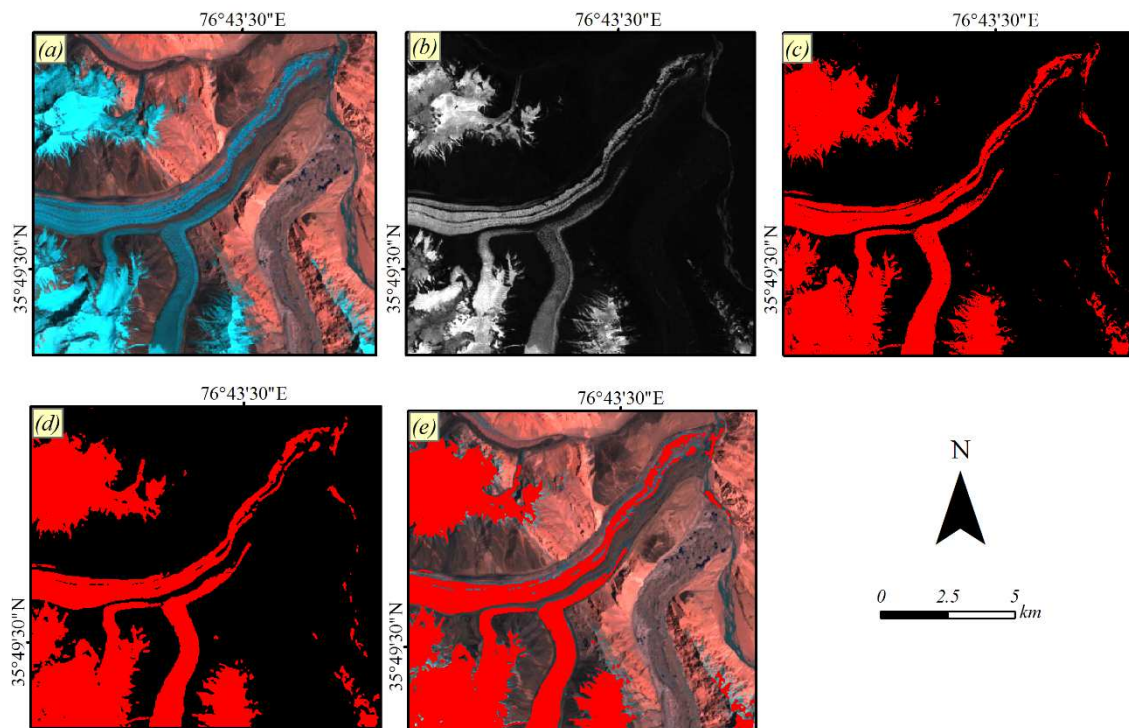


Figure 2.4.6- Examples of clean glacier-ice mapping. (a) Gasherbrum and Urdok glacier terminus region. (b) Band ratio band 4/band 5 image. (c) Binary clean glacier-ice map (in red) derived from thresholding of NIR/SWIR. (d) Median convolution filtering of clean glacier-ice map (image c). (e) The final result of clean glacier-ice map overlaid onto Landsat TM false colour composites image.

from thresholding of a TM band 4 by TM band 5 ratio image based on DN values, in particular on glacier areas in the cast shadow (Paul et al. 2002).

Therefore, in this study, the band ratio based on TM band 4/TM band 5 (Figure 2.4.6.b) was used for clean glacier-ice mapping. The map of clean glacier-ice was generated using threshold of 1.8 because it can optimize minimum clean glacier-ice area (Figure 2.4.6.c). Kernel size  $3 \times 3$  of median convolution filter was used to smooth the resultant image and remove the noise (Figure 2.4.6.d). (Paul 2000). Finally, the result of clean glacier-ice map was converted into a vector polygon map (Figure 2.4.6.e).

### 3) Generation of final glacier outlines using overlay operation

The debris-covered glacier boundaries (Figure 2.4.7.d) are generated from outlines of supraglacial debris derived from a combination of geomorphometric analysis with a thermal mask (Figure 2.4.7.a), merging with clean glacier-ice vector layer (Figure 2.4.7.b). However, some misclassification like turbid water near the glacier tongue and rive channels needs to correct by manually based on Landsat bands composite images (Figure 2.4.7.c and Figure 2.4.8). The glacier outlines separated into individual glaciers based on visual inspection with the hill shade image derived from ASTER GDEM, Landsat false colour composite images and Google Earth™ images. Furthermore, fresh snow covers outside of

the glacier margins removed manually. Moreover, polygons less than 0.02 km<sup>2</sup> were also filtered to eliminate misclassified features like snow patches, rocky surfaces, and shadow areas.

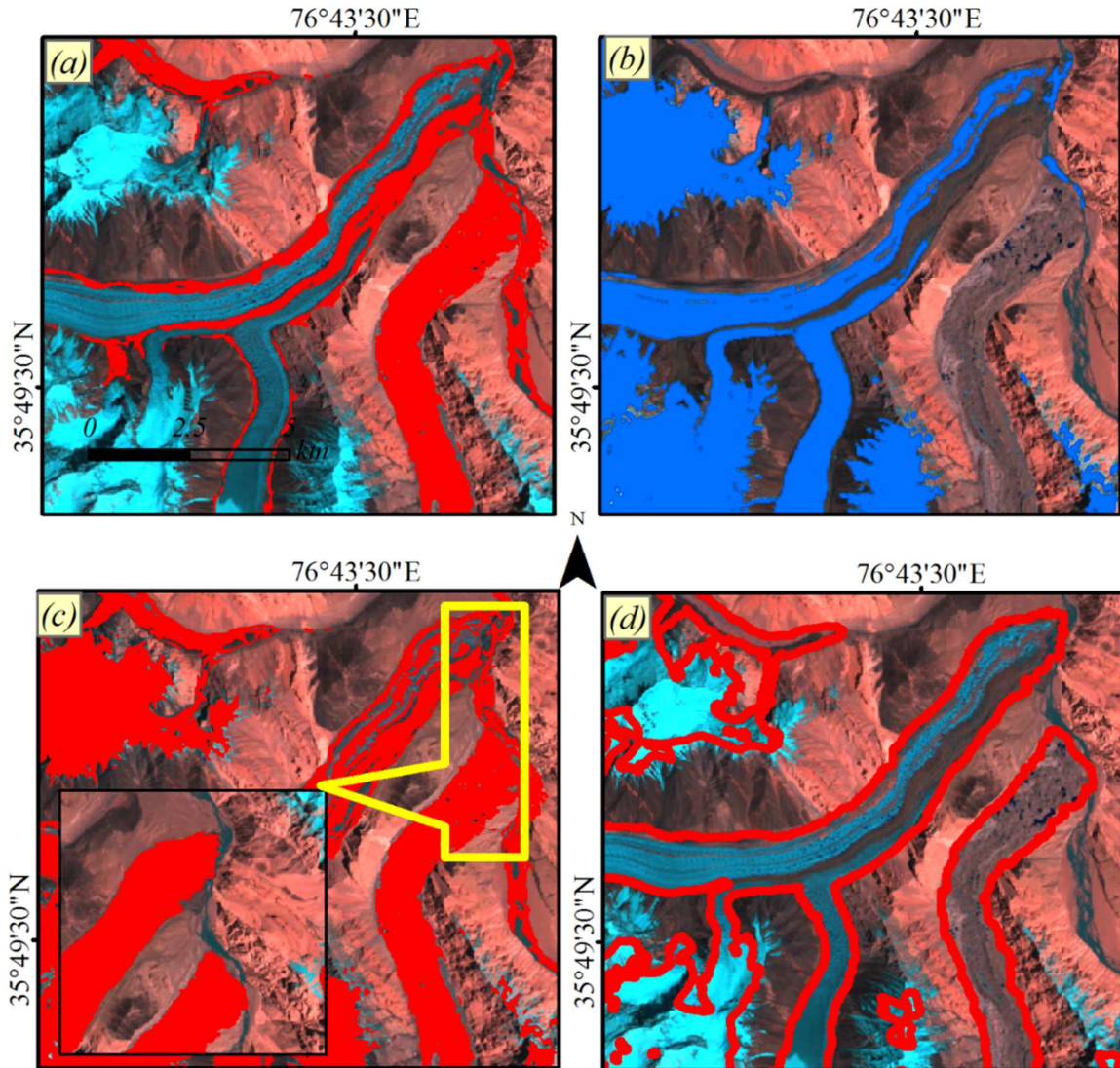


Figure 2.4.7- Examples of overlay operation. (a) Map of supraglacial debris derived from intersection result of the thermal mask and clustering analysis. (b) Map of clean glacier-ice derived from NIR/SWIR band ratio. (c) Map showing the areas of supraglacial debris (a) merged with those of clean glacier-ice map (b); Some river (yellow mark) channel removed manually. (d) The final result of glacier outlines.

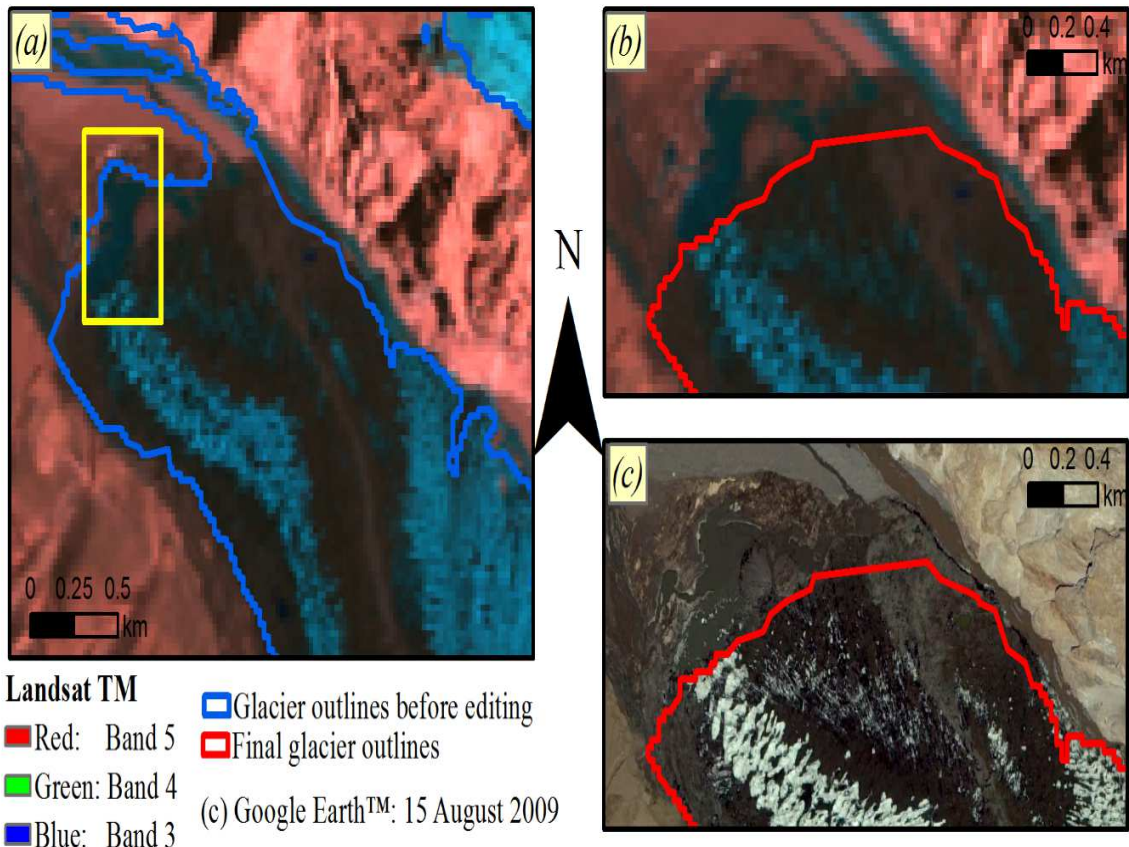


Figure 2.4.8- Examples of manually corrected area such as turbid water near the glacier tongue. (a) Glacier outlines derived from areas of supraglacial debris merged with those of clean glacier-ice map (same in Figure 2.4.7.c). (b) and (c) Closer view of the yellow marked

## **2.5 Results and discussions**

In total, 427 glaciers were mapped with covering an area of 1736.5 km<sup>2</sup> based on the method developed by Bhambri et al. (2011). Table 2.5.1 shows the percentage distribution of glaciers within different size classes. In detail, 70.96% of glaciers are smaller than 1 km<sup>2</sup>, but they contain only 5.37% of the total glacier area. On the other hand, eight largest glaciers are greater than 50 km<sup>2</sup> and smaller than 400 km<sup>2</sup>, covering 62.86% of the total glacierized area. Moreover, nearly 12.41% of the glaciers belonged to debris-covered glacier type, and they contain 72.74% of total glacier area in the study area.

Table 2.5.1- Percentage distribution of glaciers in the Shaksgam Valley derived from this study.

Area (km <sup>2</sup> )	No. of glaciers /%	Area (%)
0.02–1	303/70.96%	5.37%
1–5	83 /19.44%	9.5%
5–10	21 /4.91%	8.25%
10–50	12 /2.81%	14.02%
50–100	4 /0.94%	18.76%
100–400	4 /0.94	44.1%
Total	427 /100%	100%

Glacier area in the SCGI was used to evaluate the glacier area estimated from this study. Comparisons of glacier area (Table 2.5.2) shows that glaciers area derived from this research was less than 1% different in the total area compared with SCGI.

Table 2.5.2 Comparison between glacier areas derived from proposed method and Second Chinese Glacier Inventory (SCGI).

Comparison	TGN (TDGN)	Total GA	Total DG GA	Total CG GA	Min GA	Max GA	Mean GA	SD
This study	427 (52)	1736.57	1248.07	488.5	0.02 3	355.37	4.06	22.51
SCGI	427 (52)	1748.87	1260.57	488.3	0.03	359.05	4.10	22.47

Notes: TGN, total glacier number; TDGN, total debris-covered glacier number; DG, debris-covered glacier; CG, clean glacier-ice GA, glacier area (unit: km<sup>2</sup>); SD, standard deviation.

Specifically, Yangisogat glacier, Teram Kangri glacier, glacier A (G077418E35635N) and glacier B (G077365E35573N) in the reference maps based on SCGI and manual delineation were compared with the calculated area of these glacier using the proposed method. All of the selected glaciers were overlaid onto Google Earth™ images for a visual comparison (Figure 2.5.1).

The clean glacier-ice, glacier B (G077365E35573N) derived based on band ratio

method showed differences in the area by 0.34% and 1.05% comparing with the area measurement from manual digitization and SCGI, respectively (Figure 2.5.1.c and Table 2.4.3). The comparison of results shows that clean glacier-ice which derived by band ratio approach was as accurate as manual digitization (Paul et al. 2013).

Similarly, the glacier A (debris-covered glacier) (G077418E35635N) derived from proposed method differs in the area by 1.95 % and 1.68% compared to reference data sets (Figure 2.5.1.d and Table 2.5.3). Mapped area of Teram Kangri glacier (debris-covered glacier) based on proposed method varies by 1.83% with respect to manual delineation and 0.51% compared to SCGI (Figure 2.5.1.b and Table 2.5.3). The differences occurred probably attribute to the small area of debris covered ice located at the terminus of the glacier (glacier A) and presence of turbid water.

For the area of Yangisogat glacier (debris-covered glacier) differs by 2.74% and 1.41% compared with reference data sets, respectively (Figure 2.5.1.a and Table 2.5.3). However, the completely debris covered terminus part which was covered by a thick debris layer (Shi et al. 2008) was not mapped accurately with this approach. Also, the similar result obtained from the other glaciers such as Muzta glacier. This inaccuracy might cause by coarse resolution of Landsat thermal band (120 m resolution) which only used for detection of supraglacial debris is

limited to a certain thickness of the overlying material (Ranzi et al. 2004).

Overall glacier outlines derived from the combination of morphometric parameters from ASTER GDEM, thermal characteristic and band ratio method from Landsat TM imagery, has shown good agreement and high similarity when comparing with SCGI. The high similarity of two results, between the present study and SCGI, is probably due to the glaciers outlines were derived from similar date of Landsat images and band ratio technique (Guo et al. 2015).

Table 2.5.3 Comparison of selected three different glacier areas measured from this study, Second Chinese Glacier Inventory (SCGI) and manual delineation of Google Earth™ images (glacier area unit: km<sup>2</sup>).

Glacier name	This study	SCGI	Google Earth™
Yengisogat	353.96	359.05	363.92
Teram Kangri	110.96	110.40	113.03
Glacier A	10.64	10.82	10.44
Glacier B	6.99	6.92	6.97

In this study, ASTER GDEM V2 was used to generate the key parameters: slope, plan, and profile curvature to achieve the aim of this study was of good quality. However, the spatial resolution of ASTER GDEM (30 m) still limits to identify the transition between glacierized and ice-free terrain is flat or lateral moraines (i.e.: Yengisogat glacier terminus) are not represented in the DEM (Bolch and

---

Kamp 2006).

The temperatures of debris-covered ice, snow, clean ice, and surrounding moraine materials vary widely because of their internal structure and chemical properties (Mihalcea et al. 2006). Therefore, the results of the thermal mask created from thresholding of the Landsat TM thermal band shows that misclassification occurred for higher elevation (Figure 2.5.1.f), shadowy bedrock areas (Figure 2.5.1.d), and sand surfaces near the glacier terminus (Figure 2.5.1.g). However, overlay the thermal mask with the result of clustering of the morphometric parameters can correct this misclassification. Nevertheless, the result was not satisfactory in the case of Yangisogat glacier (Figure 2.5.2.a and e-f) and Muzta glacier. The only used of coarse resolution of the thermal band (120 m) was unable to separate periglacial debris from supraglacial debris because of the presence of thick debris layer. Thus, manual correction is necessary to improving these glacier outlines.

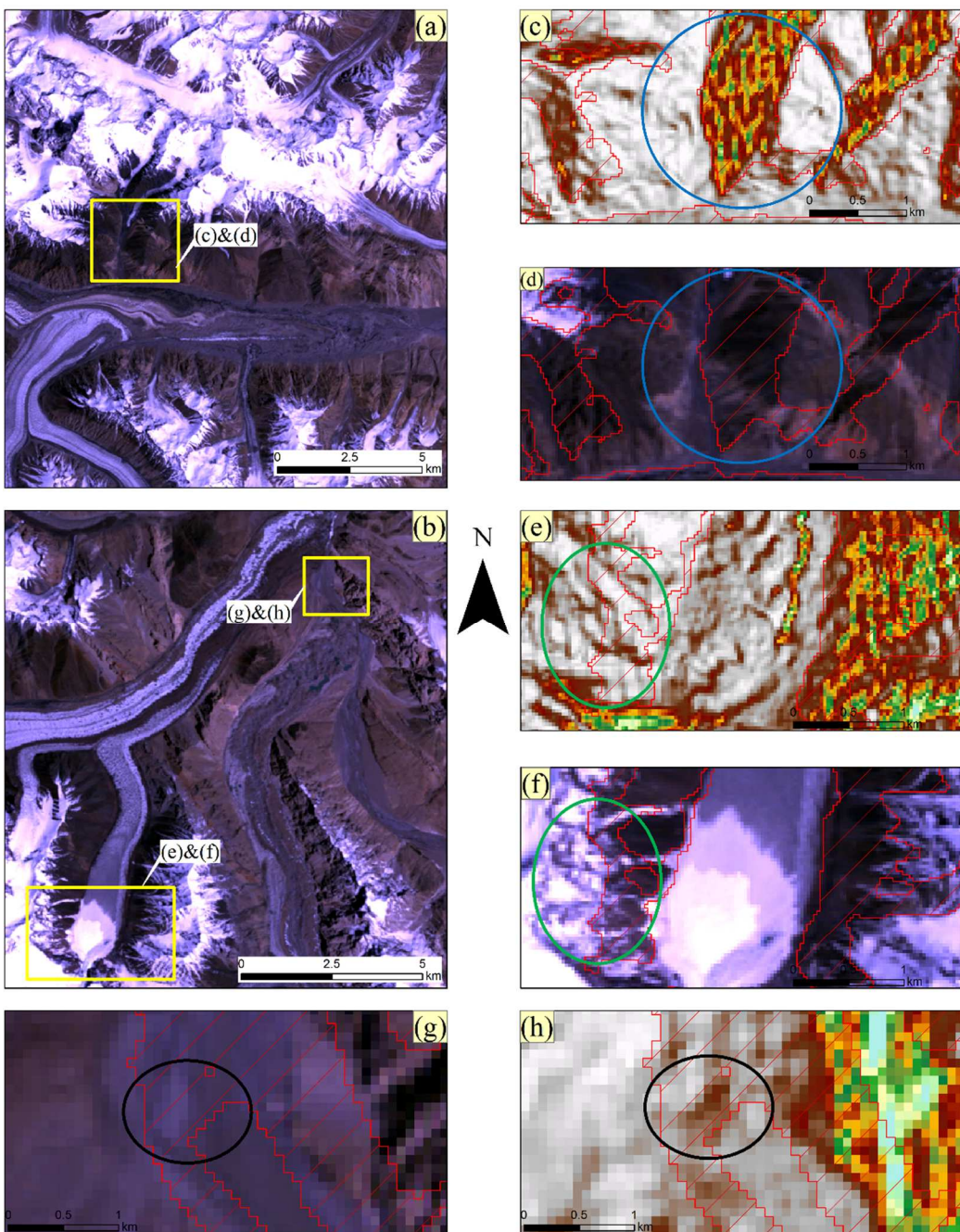


Figure 2.5.1- Examples of misclassification area derived from thermal mask. (a) and (b) True colour composite image (band 3-2-1) of Landsat TM. (c), (e) and (h) Shaded relief image generated by DEM using specified the sun elevation angle and sun azimuth angle from the Landsat data (coloured area representing the shaded area). (d) Misclassified shadowed bedrock. (f) Misclassified some part of higher elevation area. (h) Misclassified sandy river bed.

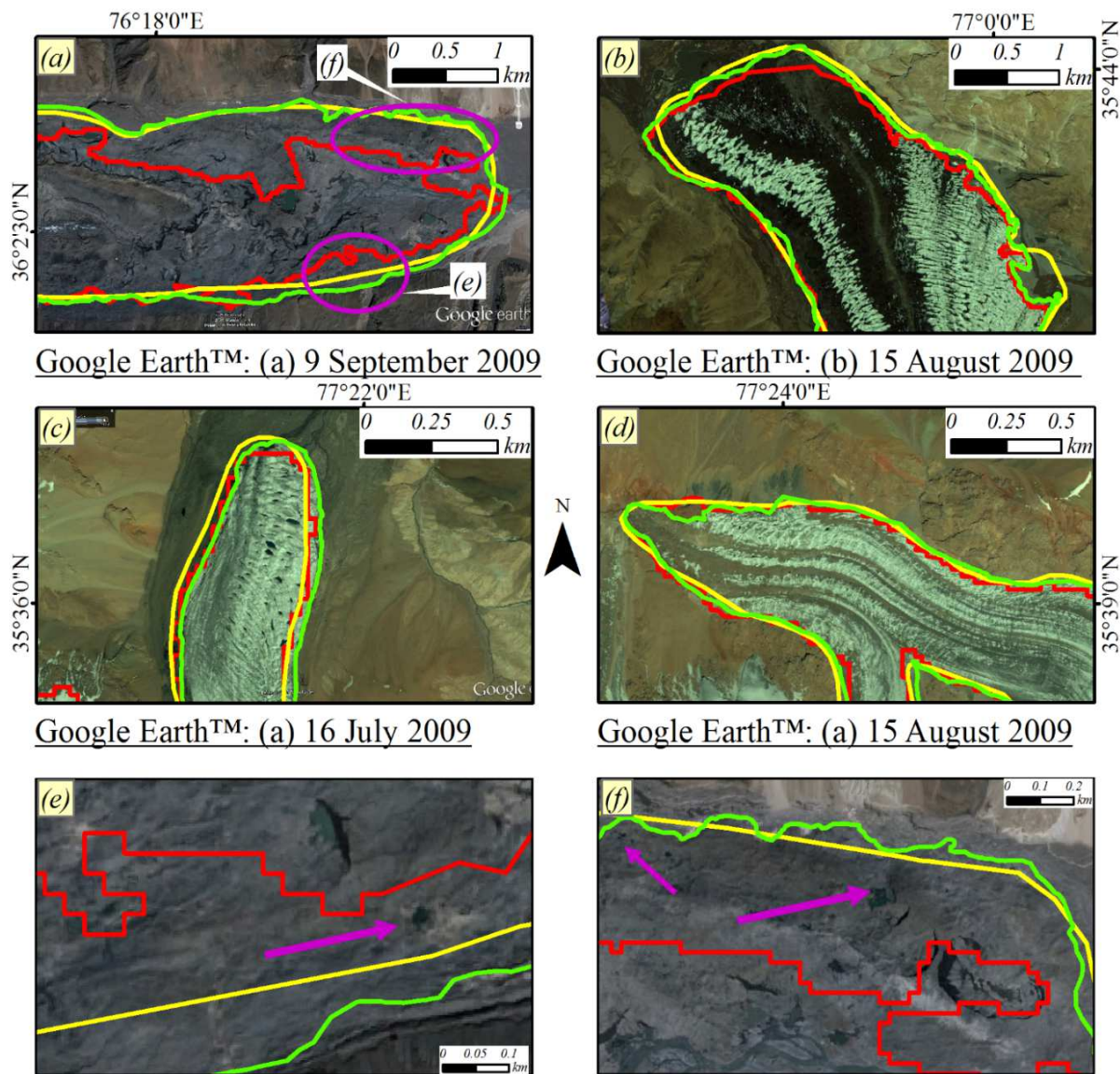


Figure 2.5.2- Comparisons of glacier outlines from different sources. (a) Yengisogat glacier terminus region. b) Teram Kangri glacier terminus region. (c) Glacier B (G077365E35573N) terminus region. (d) Glacier A (G077418E35635N) terminus region. (e) and (f) Closer view of the marked areas in (a) and undetected glacier area by proposed method in this chapter (red). Pink pointed areas (supraglacial lakes) are evidence of glacier ice under the debris. (Red = glacier outlines produced in this study, Green = glacier outlines manually delineating from Google Earth™ images, Yellow = glacier outlines based on the SCGI.

## **2.6 Limitation of method**

The same approach was applied to map debris-covered glaciers in the Garhwal Himalayas using ASTER images (Bhambri et al. 2011). In this study, geomorphometric parameters derived from DEMs generated using ASTER pair images. Similarly, with this study, some approaches were used to map the debris-covered glaciers (Bolch et al. 2007, Bhardwaj et al. 2014, Veettil et al. 2014).

Studies such as that conducted by Bolch et al. (2007) combined ASTER's thermal information with geomorphometric parameters derived from ASTER DEM, which generated from stereo-models to the automated delineation of the debris-covered glaciers in the Khumbu Himal region. Veettil et al. (2014) calculated the land surface temperature from the Landsat TM thermal band (band 6) and combined with the slope of the terrain to map the debris-covered glaciers in the southern Karakoram Range. Similar work was performed by Bhardwaj et al. (2014), based on a combination of geomorphometric parameters which extracted from ASTER GDEM (same parameters used in our study) and land surface temperature values obtained from Landsat TM/ETM+ thermal band to map two debris-covered glaciers in the western Himalayas.

However, ASTER images, which are the primary data used in studies described

above (Bolch et al. 2007, Bhambri et al. 2011). Therfore, appling the method (Veetttil et al. 2014) to a large glacierized region was challenging because the SWIR sensor was inoperative in 2008 and most of the debris-covered glaciers have different slope values. For our studies, we used freely available Landsat TM images and ASTER GDEM to map glaciers in the large glacierized region with acceptable accuracy.

The most significant limitation of our studies is the threshold values used, which might differ when applied to other region or other datasets. Glacier ice under the deeply shaded areas was another of a major problem attributable to the reflectance of these areas, which has similar values to those of rocky areas. Another limitation of this study is ASTER GDEM, which generated from many pairs of ASTER images acquired during different periods. Because of the unavailability of high-quality multi-temporal DEM which represented the glacier terrain properties in that time series, we assumed that glacier geometry and boundary conditions remained unchanged during that specified period.

## **2.7      Conclusions**

The primary objective of this study was achieved. A combination of morphometric parameters, thermal characteristics, and band ratio technique was applied for mapping of glaciers (debris-covered and clean glacier-ice) in Shaksgam Valley.

Results of the multi-criteria method were used to present an accurate layout of debris-covered glaciers covered by thin debris cover or lateral moraine. Less than 3% discrepancy found between the mapped glacier area and the reference glacier area from SCGI and manual delineation. Minor misclassification occurred with turbid water areas, high-elevation periglacial debris, shadowy bedrock areas, and sand surfaces near the glacier terminus.

Furthermore, the multi-criteria method (cluster analysis + (NIR/SWIR) + TIR) was challenging when mapping glaciers that were entirely covered by thick debris cover and where glacier terminus has a gentle slope. As one example, terminus region of Yengisogat glacier area was unable to be mapped using this approach. Therefore, it is necessary to develop a new method for mapping the debris-covered glaciers covered by thick debris layer and where glacier terminus has a gentle slope.

## **Chapter 3 Early stage of the new method for mapping of debris-covered glaciers — Based on the combination of [TIR/(NIR/SWIR)] band ratio image and slope**

---

### **3.1 Introduction**

Yengisogat glacier terminus region was unable to be mapped accurately using an existing method (chapter 2). From literature review as well as practical application further confirmed that current methods have difficulty when applied for delineating the debris-cover glaciers covered by thick debris layer ( $> 40$  cm) (Ranzi et al. 2004, Mihalcea et al. 2006, Mihalcea et al. 2008, Reznichenko et al. 2010 and Collier et al. 2015) and when debris-covered glacier terminus region transition to unglaciated region is gentle. Therefore, in an attempt to solve the above problems, the new approach was proposed based on a combination of a newly developed [TIR/(NIR/SWIR)] band ratio technique with slope information to delineate Yengisogat glacier. Furthermore, to examine the transferability of this new technique to other glaciers, additional test area - Koxkar glacier was also delineate using proposed approach.

### **3.2 Study area – Yengisogat glacier and Koxkar glacier**

Yengisogat glacier and Koxkar glacier are selected to examine the proposed approach. The Yengisogat glacier ( $36^{\circ} 4'58.80''\text{N}$ ,  $76^{\circ} 6'10.08''\text{E}$ , Figure 3.2.1.b) lies on the northern slopes of the Chinese Karakoram mountain range. The Koxkar glacier ( $41^{\circ}45'36.00''\text{N}$ ,  $80^{\circ} 6'36.00''\text{E}$ , Figure 3.2.1.a) locates in the Central Tien Shan, China.

The Yengisogat glacier is a valley glacier. It has four branches (Figure 3.2.1.b) and about 42 km long (Shi et al. 2008). According to the glacier inventory of China in the 1970s, Yengisogat glacier has  $379.97 \text{ km}^2$  surface area and has about  $115.89 \text{ km}^3$  of ice volume (Shi et al. 2008). The transition from the terminus region of Yengisogat glacier to the unglaciated area is gentle (Figure 3.2.1.c). Also, entire Yengisogat glacier terminus covered by a thick debris layer (Shi et al. 2008).

The Koxkar glacier is about 25.1 km long and covers an area of  $83.56 \text{ km}^2$  (Han et al. 2010). The Koxkar glacier has a gentle terminus region (Liu et al. 2013) and it is ablation region covered by thick debris layer (less than 0.01 m on the upper reach of the ablation area and more than 3 m near the glacier terminus) (Juen et al. 2014). Thus, Yengisogat glacier and Koxkar glacier are considered as a good test area for examination of our method.

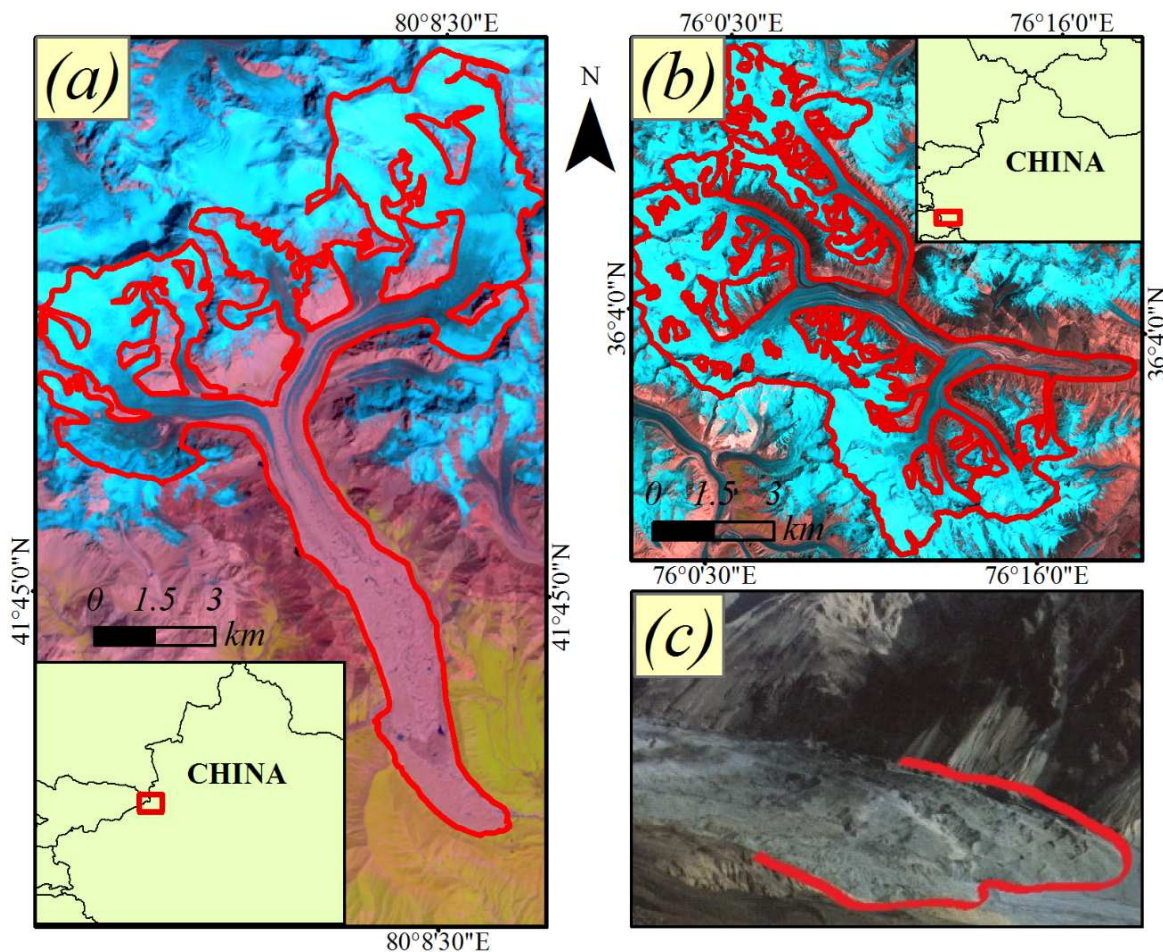


Figure 3.2.1- The overall location of study areas in this chapter. (a) Koxkar glacier with glacier outline (red line) from Randolph Glacier Inventory. (b) Yengisogat glacier with glacier outline (red line) from Glacier Inventory of China). Landsat images are fasle colour composites with R = shortwave infrared band, G = red band, B = green band. (c) Yengisogat glacier tongue (red), taken by John Shen in April 2003 (image source: <http://www.summitpost.org/mount-crown-huangguan/152162>).

### **3.3 Data sources**

For this study, a Landsat-5 Thematic Mapper (TM) image [acquisition time: 4 August 2009, Greenwich Mean Time (GMT): 05:18 (~11:18 am at local time ), Figure 3.2.1.b] was used for mapping the Yengisogat glacier. On the other hand, a Landsat-7 Enhanced Thematic Mapper Plus (ETM+) image [acquisition date: 31 July 2013, Greenwich Mean Time (GMT): 05:16 (~11:16 am at local time ), Figure 3.2.1.a] was used for mapping the Koxkar glacier. Selection of these Landsat images is because of the these images have the similar acquisition dates with available reference datasets and free high-resolution Google Earth™ images.

The Landsat images were acquired at the end of the summer season. No seasonal snow or cloud cover is present in the scenes. The data were freely downloaded from USGS EarthExplorer (USGS EE; <http://earthexplorer.usgs.gov/>). The images have been already orthorectified, and no geometric correction was required. Koxkar glacier is situated in the centre (gap-free area) of Landsat ETM+ footprint which is able to use even after the scan-line correction failure in May 2003 (Figure 3.2.1.a).

The Landsat-5 (TM) has seven bands. Six bands in the visible to the shortwave infrared region which have a spatial resolution of 30-meter. A thermal band has

a 120-meter spatial resolution. On the other hand, the Landsat-7 ETM+ has eight multispectral bands with six bands at 30-meter spatial resolution in the visible to the shortwave infrared region, two bands with 60-meter resolution in the thermal infrared region, and one panchromatic band at 15-meter resolution.

A digital elevation model (DEM) from Shuttle Radar Topography Mission (SRTM) was used to extract the slope information for glacier terrain. The SRTM is a high-resolution digital topographic database of Earth, and it obtained elevation data covers  $\pm$  60-degree latitude. SRTM is a specially modified radar system that flew onboard the Space Shuttle Endeavour during an 11-day mission in February of 2000.

Resampled 90 m resolution of SRTM data is available freely for regions outside the United States. On January 2, 2015, the National Aeronautics and Space Administration (NASA) released NASA SRTM Version 3.0 (SRTMV3) with 30 m resolution, to include coverage over Asia and Australia. The NASA SRTMV3 30 m resolution product is void-filled using elevation data from the Advanced Spaceborne Thermal Emission and Reflection Radiometer Global Digital Elevation Model Version two (ASTER GDEM V2), United States Geological Survey (USGS) Global Multi-resolution Terrain Elevation Data 2010 (GMTED 2010), and USGS National Elevation Dataset (NED). Both 90 m and 30 m resolution of SRTM data can be freely downloaded from NASA's Earth System

Data and Information System (EOSDIS: <http://reverb.echo.nasa.gov/>). In this study, 90 m resolution of SRTM data was downloaded to extract the slope information of the Yengisogat glacier (since analysis of this glacier was done before January 2015) and 30 m of resolution SRTM data was downloaded to extract the slope information of the Koxkar glacier.

The glacier inventory data and a manual delineation using high-resolution Google Earth™ images were used to validate the result of this study. The Yengisogat glacier outline in the Second Chinese Glacier Inventory (SCGI) data was extracted from Landsat series imagery (Guo et al. 2014, detailed description of SCGI available in chapter 2).

Near globally digital glaciers outlines which excluding the Greenland and Antarctic ice sheets are collected for generation of Randolph Glacier Inventory (RGI) (Pfeffer et al. 2014). The RGI Version 4.0 (RGI V4) can be freely downloaded from Global Land Ice Measurements from Space (GLIMS) website (<http://www.glims.org/RGI/index.html>).

The used data sources and method used to extract Koxkar glacier outline from the RGI V4 was unknown. Therefore, high-resolution Google Earth™ images are used to check the Koxkar glacier outline from RGI V4 and also Yengisogat glacier outline from SCGI by visually. The glacier outlines in these reference

datasets showed good agreement compared to our manually delineated glacier boundaries.

Google Earth™ software provide multi-temporal free available high-resolution images. Google Earth™ images which have similar acquisition dates with the Landsat data are used for mapping the Yengisogat glacier (Google Earth™ images acquisition date: 22 August 2009, 9 September 2009, 30 September 2009, 30 October 2009) and Koxkar glacier (Google Earth™ images acquisition date: 29 January 2013, 29 July 2013) in this study.

## 3.4 Method

### 3.4.1 Introducing of the [TIR/(NIR/SWIR)] band ratio image

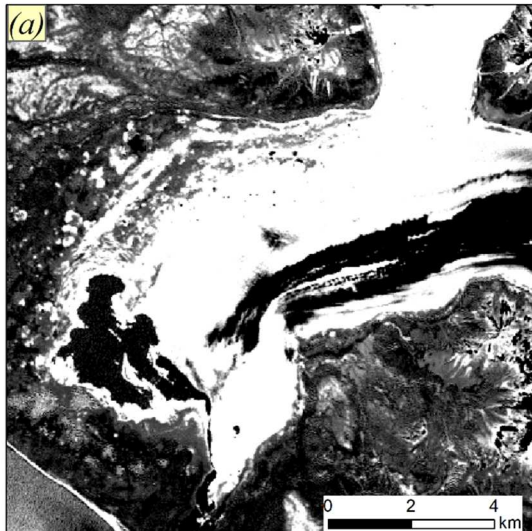
Most of visible light from visible to near-infrared wavelengths (VNIR; 0.4–1.2 μm) is reflected back by clean glacier-ice. In contrast, clean glacier-ice has a very low reflectivity in the shortwave infrared wavelength region (SWIR; 1.4–2.5 μm). The commonly used band ratio images consider Landsat TM or ETM+ bands 2 (green), 3 (red), 4 (NIR) and 5 (SWIR) to take advantage of these spectral differences at different wavelengths and separate clean glacier ice from non-glacier surfaces, for example, band 3/ band 5 (Bolch et al. 2010), band 4/band 5 (Paul et al. 2002), and the normalized difference snow index ((band 2 – band 5)/(band 2 + band 5)) (Silverio and Jaquet 2005) (TM and ETM+ band numbers are the same in these equations). In these conventional ratio images, clean glacier-ice has high reflectance values, on the other hand, supraglacial debris and other nearby non-glacier rocky surfaces have low reflectance values due to supraglacial debris, and the other rocky surfaces have similar spectral responses at these wavelengths. In addition, a temperature difference of different surfaces can be provided by the Landsat thermal band. These thermal difference information can help to separate the supraglacial debris from other rock materials. Temperature data from field measurements as well as from remote sensing techniques studies

indicated that supraglacial debris areas have significantly lower surface temperatures than periglacial debris areas (Taschner and Ranzi 2002, Ranzi et al. 2004, Shukla et al. 2010ab, Karimi et al. 2012).

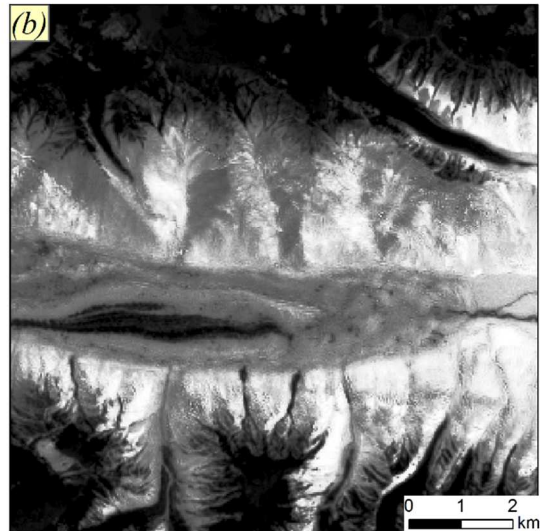
Thus, the idea for [TIR/(NIR/SWIR)] band ratio technique comes out of these characteristics. Low values of supraglacial debris futures in the NIR/SWIR band ratio image (band 4 divided band 5) (pixel 1 and pixel 2 have low values which show in the Figure 3.4.1.2.c and Figure 3.4.1.3.c) can be separated from periglacial debris region when Landsat thermal band (band 6, Figure 3.4.1.2.b and Figure 3.4.1.3.b) divided the result from band 4 divided band 5 ratio image (Figure 3.4.1.2.d and Figure 3.4.1.3.d). For [TIR/(NIR/SWIR)] band ratio, DN value of original bands was used because of a band ratio can minimize the effect of illumination from topography (Crippen 1988, Bayr et al. 1994) and also thresholded NIR/SWIR band ratio from DN values reveals the most efficient method for clean glacier-ice mapping (Paul 2000, Paul et al. 2016). Moreover, the [TIR/(NIR/SWIR)] band ratio can be regenerated from other Landsat images (Figure 3.4.1.1). In this study, the [TIR/(NIR/SWIR)] band ratio image (equation 1) was generated by dividing digital number (DN) values of the thermal band (band 6) by the DN value of NIR band (band 4) divided by SWIR band (band 5), which is presented as follows:

$$[\text{TIR}/(\text{NIR}/\text{SWIR})] \text{ band ratio} = \text{TIR} \div (\text{NIR} \div \text{SWIR}) \quad (1)$$

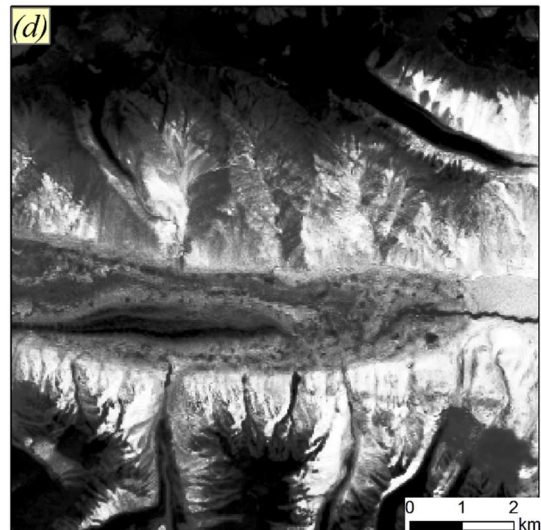
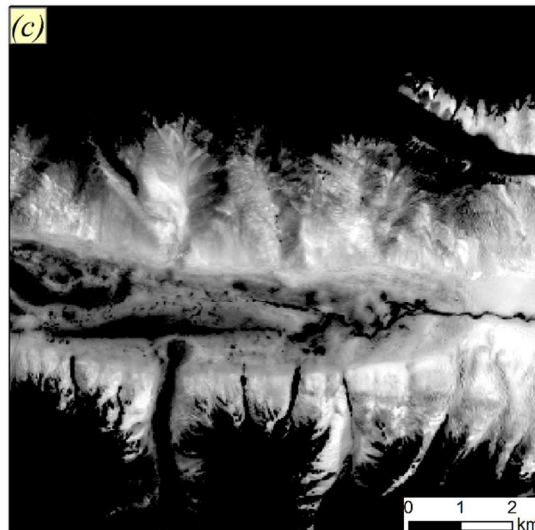
(a) Landsat ETM+ (13 August 2001)



(b) Landsat TM (7 July 1993)



N  
▲



(c) Landsat ETM+ (21 July 2001)

(d) Landsat 8 (5 Jun 2014)

Figure 3.4.1.1- [TIR/(NIR/SWIR)] band ratio images generated by multi-temporal Landsat images. (a) Fairweather glacier terminus region (same area in Figure 4.4.1.2.a). (b)-(d) Yengisogat glacier terminus region (same area in Figure 3.4.1.2.a) (these Landsat data are not used for glacier mapping in this thesis).

As shown in Figure 3.4.1.2.d and Figure 3.4.1.3.d, compared to the conventional band ratio technique, in [TIR/(NIR/SWIR)] band ratio technique the representing the supraglacial debris areas (light gray areas) more distinct from the surrounding non-glacier areas.

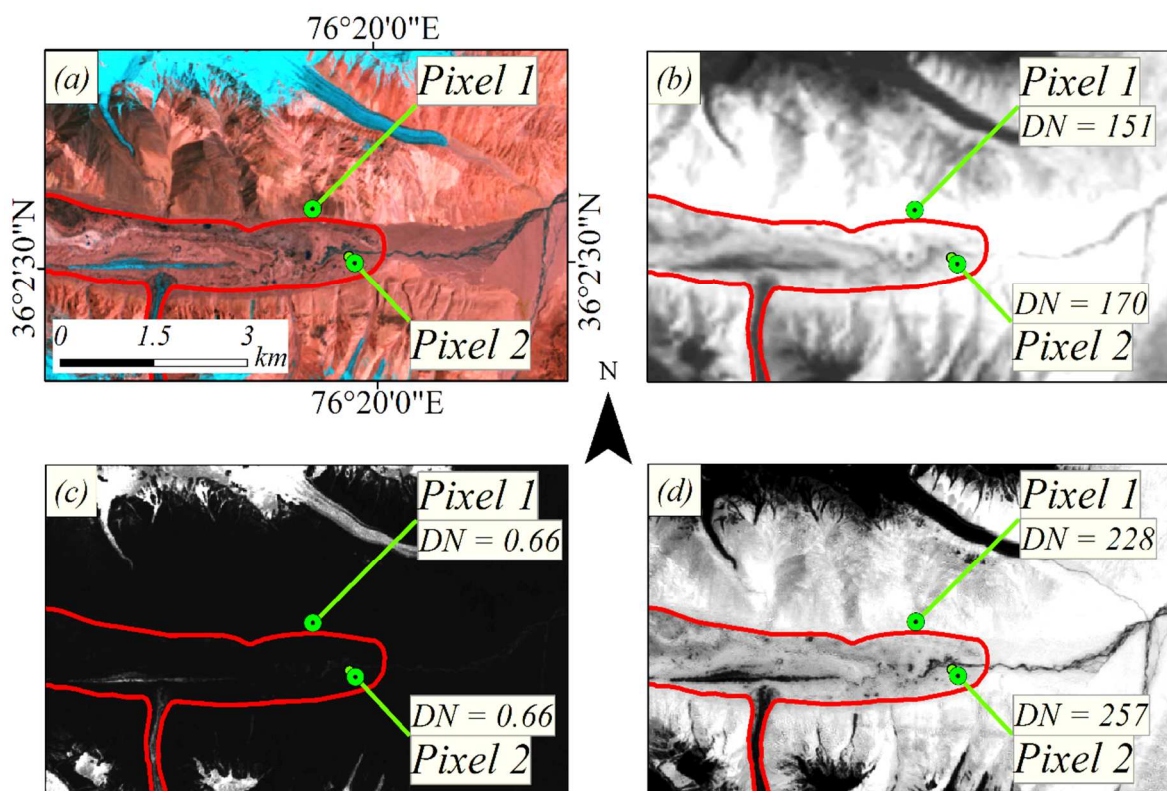


Figure 3.4.1.2- Visual comparisons of Yengisogat glacier terminus region represented by thermal (TIR) band, NIR/SWIR band ratio and [TIR/(NIR/SWIR)] band ratio image. (a) Yengisogat glacier terminus region and location of pixel 1 (periglacial debris region) and pixel 2 (supraglacial debris region) in false colour composite (R = shortwave infrared band, G = red band, B = green band), (b) TIR band (band 6). (c) NIR/SWIR band ratio image. (d) [TIR/(NIR/SWIR)] band ratio image. (Yengisogat glacier outline (red line) from Second Chinese Glacier Inventory).

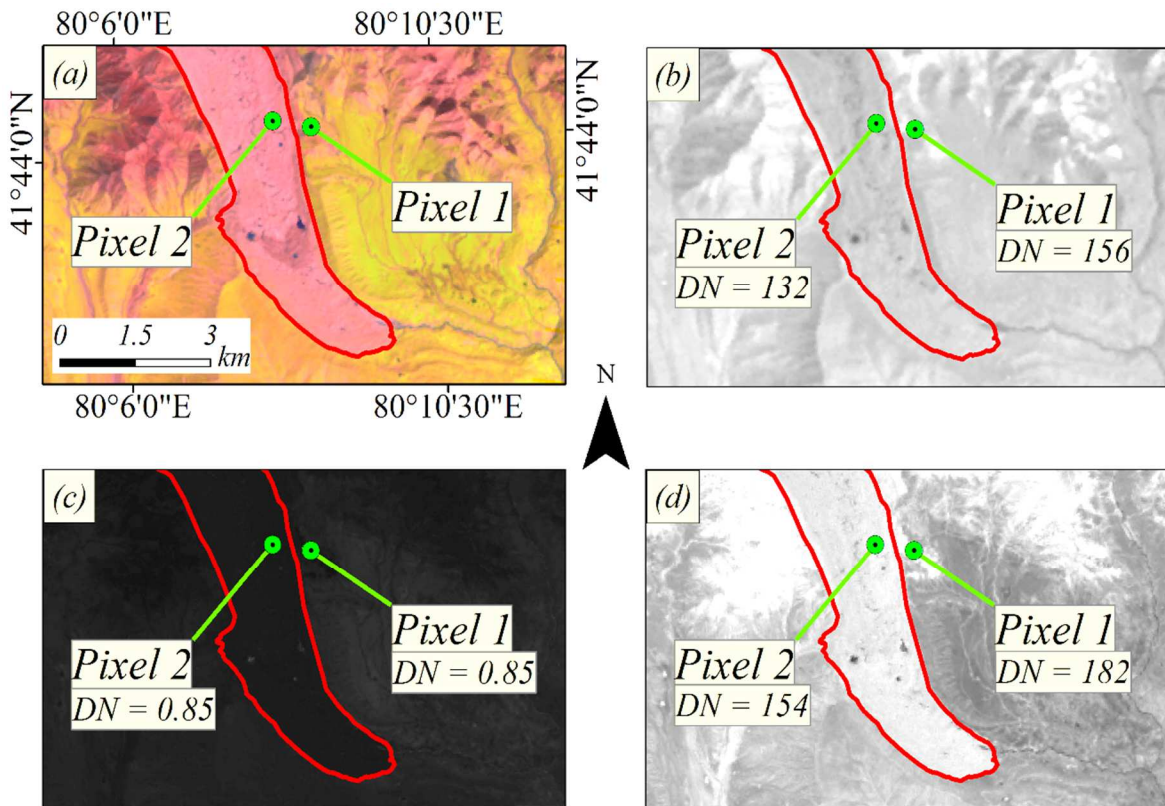


Figure 3.4.1.3- Visual comparisons of Koxkar glacier terminus region represented by thermal (TIR) band, NIR/SWIR band ratio and [TIR/(NIR/SWIR)] band ratio image. (a) Koxkar glacier terminus region and location of pixel 1 (periglacial debris region) and pixel 2 (supraglacial debris region) in false colour composite image (band combination, R = shortwave infrared band, G = red band, B = green band). (b) Koxkar glacier terminus region in the thermal band (band 6\_1). (c) NIR/SWIR band ratio image. (d) [TIR/(NIR/SWIR)] band ratio image. (Koxkar glacier outline (red line) from Randolph Glacier Inventory).

Next, the glaciers were classified by thresholding of the [TIR/(NIR/SWIR)] band ratio imagery. Here, the density slicing method was used to select the threshold ranges for glacier mapping (Meier 1980). The density slicing method is useful when a given surface feature has a unique and narrow set of DN values (Nicholas and Short 1999). Several level slices may be produced, when several features each have different separable DN values (Nicholas and Short 1999). All pixels within a "slice" (i.e. a range) of pixel values are considered to belong to the same information class (i.e. "clean glacier-ice", "supraglacial debris" and "other classes"). The DN values in [TIR/(NIR/SWIR)] band ratio image from 140 to 234 (Figure 3.4.1.4.b) and 137 to 180 (Figure 3.4.1.5.b) were used to mapping the supraglacial debris areas in the Yengisogat glacier and Koxkar glacier.

Figure 3.4.1.4.b and Figure 3.4.1.5.b showed that the result of the density slice contained several inaccuracies for the "supraglacial debris" class`s in areas where bedrock valley walls were located in shade (shaded area was determined by shaded relief image derived from DEM using specified the sun elevation angle and sun azimuth angle from the Landsat data, Figure 3.4.1.4 (ii) is same area in Figure 2.5.1.c-d) and/or higher elevation areas (e.g. figure 3.4.1.4 (i), (ii) and figure 3.4.1.5 (i), (ii)). This misclassification due to the bedrock valley walls in shade area may have a lower temperature than illuminated area. Moreover, spectral information of rocky materials was also reduced in the shaded area. Furthermore, periglacial debris regions near the accumulation zone have low

temperatures due to their locations at higher elevations. However, we found that these classification errors could be removed when combined with slope information.

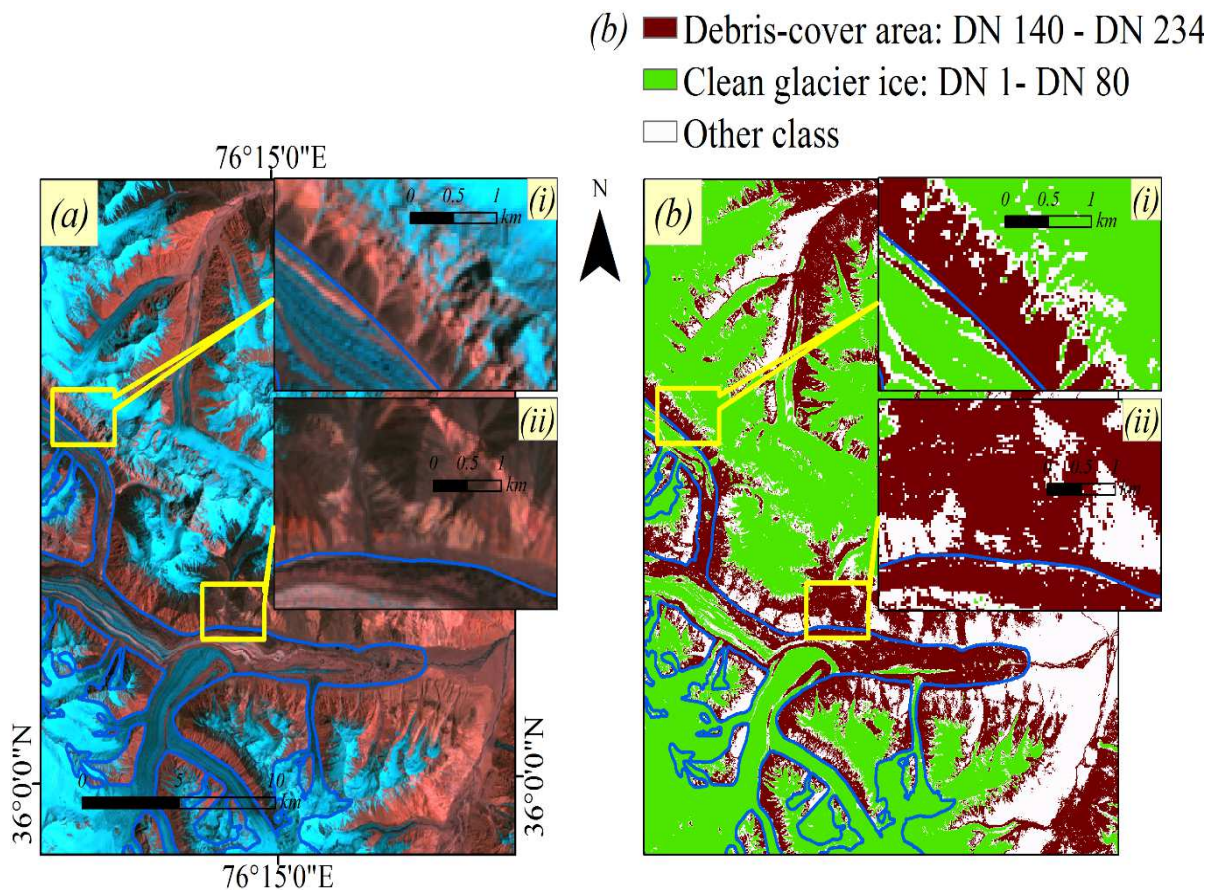


Figure 3.4.1.4- Example of classification map of Yengisogat glacier using [TIR/(NIR/SWIR)] band ratio. (a) Yengisogat glacier ablation region. (b) Thresholding of [TIR/(NIR/SWIR)] band ratio image using density slicing method. (i) and (ii): closer view of misclassified periglacial debris region. (Yengisogat glacier outline (blue line) from Second Chinese Glacier Inventory).

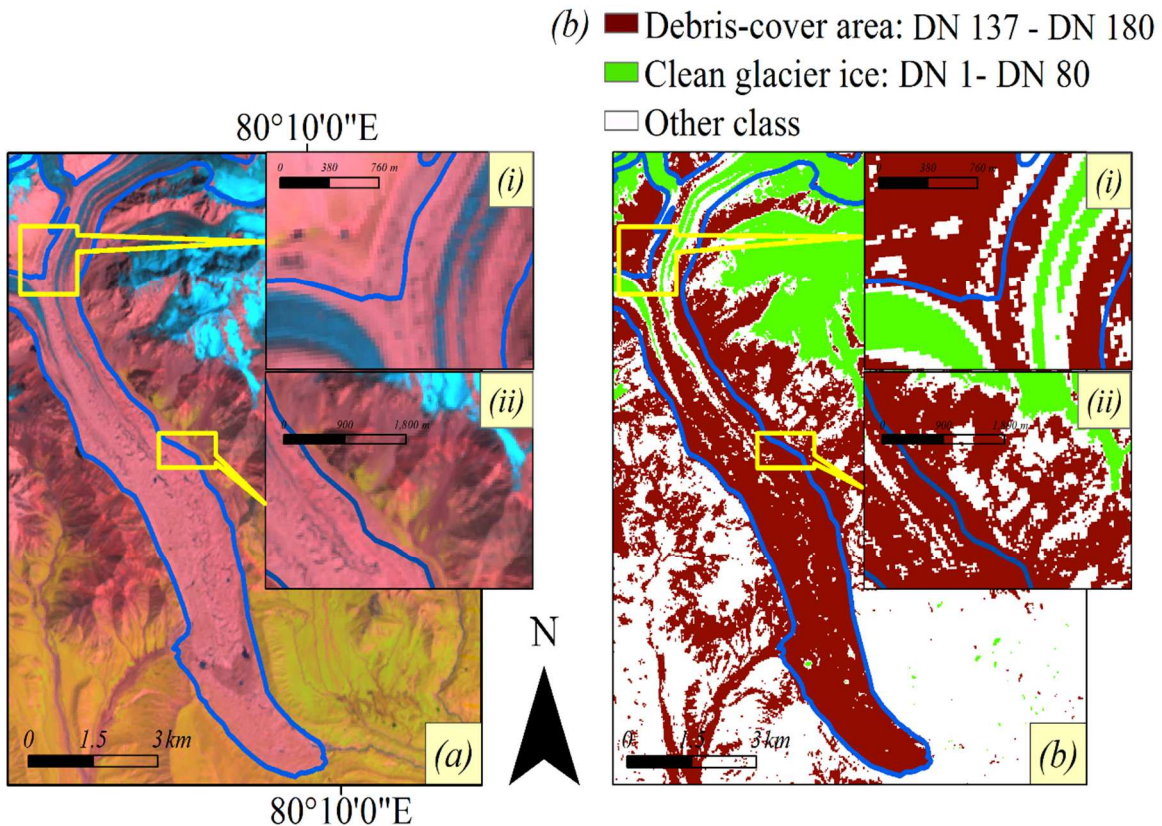


Figure 3.4.1.5- Example of classification map of Koxkar glacier using [TIR/(NIR/SWIR)] band ratio. (a) Koxkar glacier ablation region. (b) Thresholding range of [TIR/(NIR/SWIR)] band ratio image using density slicing method. (i) and (ii) closer view of misclassified periglacial debris region. Koxkar glacier outline (blue line) from Randolph Glacier Inventory.

### **3.4.2 Delineating the final debris-covered glacier boundary by combining classified map with slope information**

In this study, a slope information of glacier was derived from SRTM DEM data.

Several past studies combined morphometric parameters such as slope with other information to delineate the debris-covered glacier boundary (Bishop et al. 2001, Paul et al. 2004, Bolch and Kamp 2006, Shukla et al. 2010b, Bhambri et al. 2011).

Bishop et al. (2001) proposed that the mean of the slope be a key parameter to delineate debris-covered glaciers. The debris is transported by general down-slope movement of a glacier towards terminus (Paul et al. 2004). When glacier surface slope is too steep, debris usually slides on the glacier to further down until a gentler slope allows accumulation (Paul et al. 2004). As a result, some of the glacier termini were covered by debris partly or entirely. Therefore, glacier gradient information can be used to eliminate the other bedrock valley walls from glacier itself. In this study, based on the visual evaluation, less than 12° threshold value was selected to create a binary slope map for both glaciers (Figure 3.4.2.1.a and Figure 3.4.2.2.a).

Result derived from thresholding of the [TIR/(NIR/SWIR)] band ratio image for supraglacial debris classes (Figure 3.4.1.3.b and Figure 3.4.1.4.b) was overlaid onto the binary slope map (Figure 3.4.2.1.a and Figure 3.4.2.1.b), as shown in Figure 3.4.2.1.c and Figure 3.4.2.2.c. Some areas such as river channel (Figure

3.4.2.1.c (i)) connected with glacier tongue and vegetation area (Figure 3.4.2.2.c (i)) need to be deleted manually. Final debris-covered glacier boundaries were generated by combining the result from supraglacial debris map with the clean glacier-ice map derived from threshold values DN range from 1 to 80 for both glaciers (Figure 3.4.1.3.b and Figure 3.4.1.4.b with green, 3.4.2.1.d and Figure 3.4.2.2.d with blue).

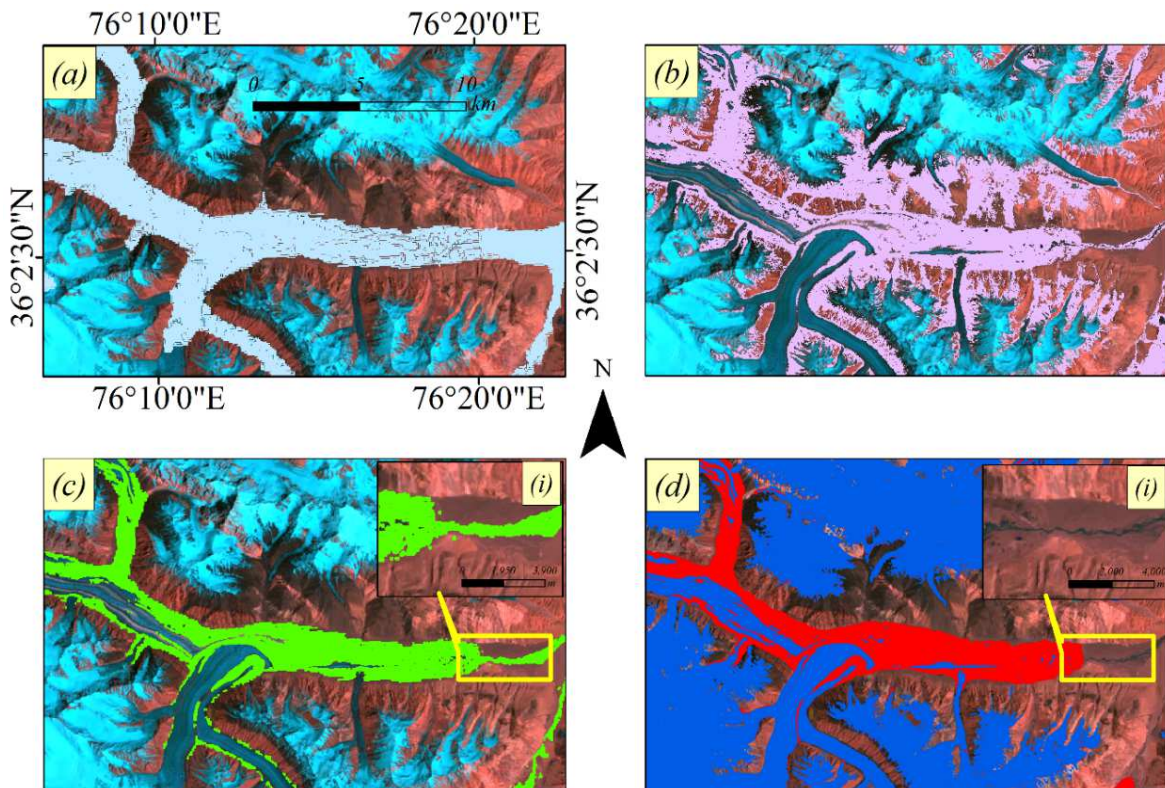


Figure 3.4.2.1- Generation of final Yengisogat glacier outline. (a) Binary slope ( $< 12^\circ$ ) map. (b) Map derived from thresholding of [TIR/(NIR/SWIR)] band ratio image. (c) Map of supraglacial debris derived from the intersection of the map (a) and map (b). (d) Map showing areas of supraglacial debris (in red) merged with those of clean glacier ice (in blue). (i): closer view of some river channel needed to remove manually.

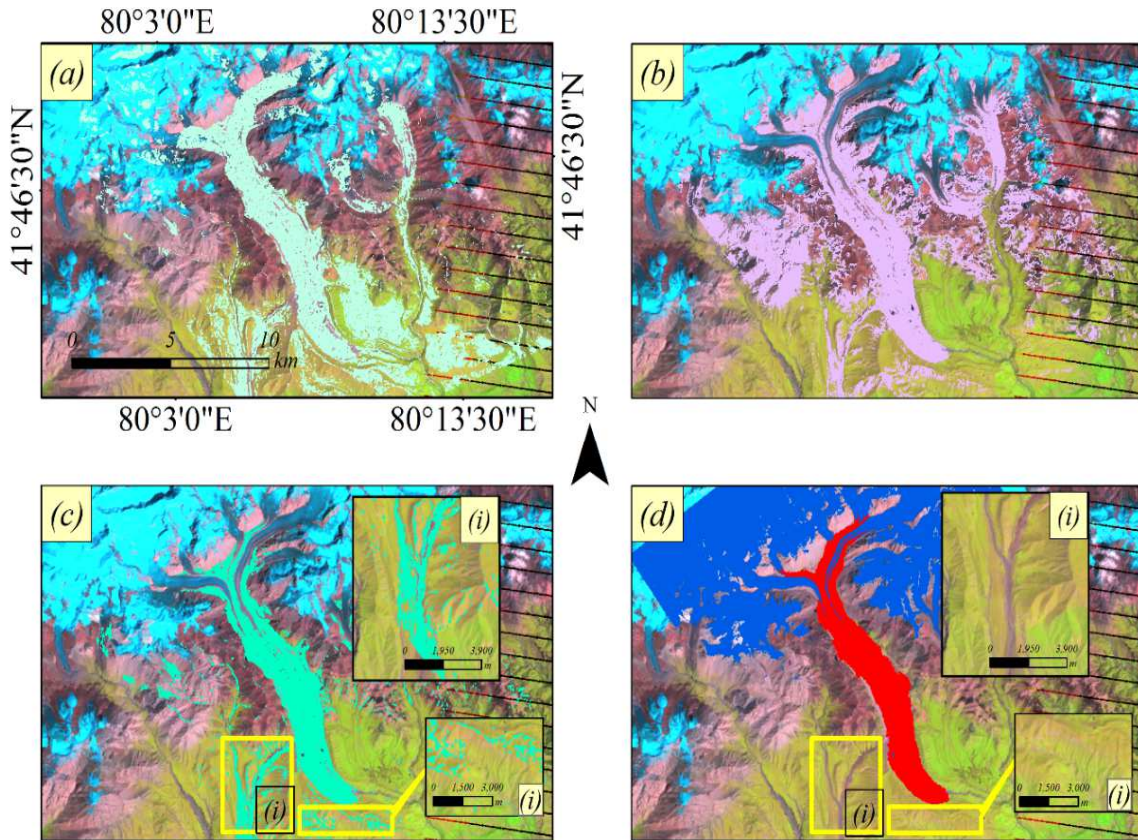


Figure 3.4.2.2- Generation of final Koxkar glacier outline. (a) Binary slope ( $< 12^\circ$ ) map. (b) Map derived from thresholding [TIR/(NIR/SWIR)] band ratio image. (c) Map of supraglacial debris derived from the intersection of the map (a) and map (b). (d) Map showing areas of supraglacial debris (in red) merged with those of clean glacier ice (in blue). (i): closer view of some vegetation area needed to remove manually.

### **3.5 Accuracy assessment**

In this study, to evaluate the final glacier outlines derived from a combination of [TIR/(NIR/SWIR)] band ratio and slope, the RGI 4V, SCGI and manual delineation of the high-resolution Google Earth™ images were used. Specifically, the area of the Koxkar glacier (Figure 3.5.1.a and b) and Yengisogat glacier (Figure 3.5.1.c and d) calculated using the proposed method was compared with the glacier area on the reference maps. Then, the visual comparison was carried out through the vector maps of the glacier from proposed method, and reference maps were overlaid onto Google Earth™ images (Figure 3.5.1).

In detail, in order to deeply analyzing the accuracy of result derived from proposed method compared to reference data sets, overall Yengisogat glacier and Koxkar glacier outlines were separated into three regions. An example:

- 1) Terminus part which completely cover by debris
- 2) The middle part which mixed with exposed ice and debris
- 3) The upper part mainly consists of snow and ice.

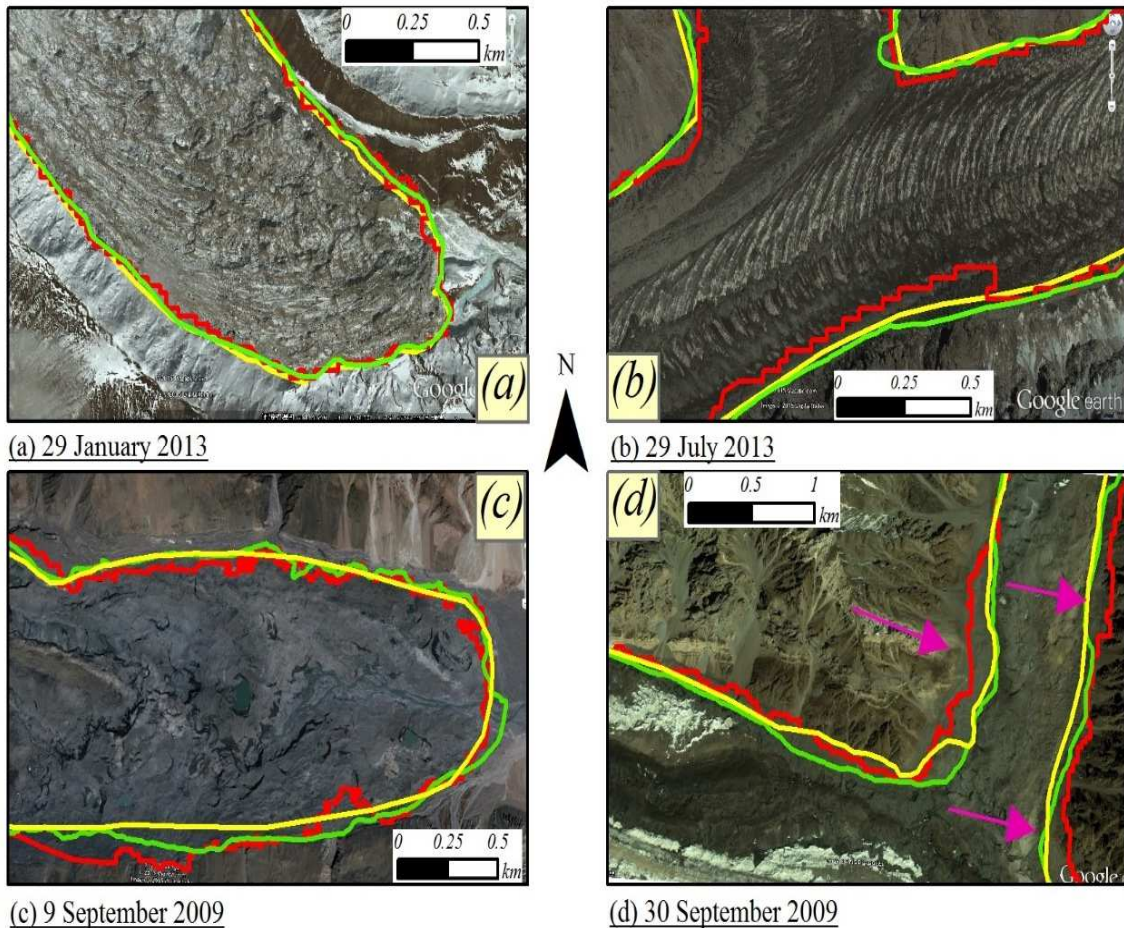


Figure 3.5.1- Comparisons of the results for the delineation of glaciers using the different methods. (a) and (b): yellow = Koxkar glacier boundary based on RGI, red = Koxkar glacier boundary based on the result of this study, green = Koxkar glacier boundary manually delineated from Google Earth™ images. (c) and (d): yellow = Yengisogat glacier boundary according to SCGI, red = Yengisogat glacier boundary base on the result of this study, green = Yengisogat glacier boundary manually delineated from Google Earth™ images, pink point mark shows the overestimated supraglacial debris area. Images: screenshots from Google Earth™.

### **3.6 Results and discussions**

The validation result showed that the glacier boundary derived from the combination of the [TIR/(NIR/SWIR)] band ratio image with the binary slope image was quite similar to the inventory data and manual delineation (Figure 3.5.1). Specifically, there was just a 0.34% difference in the overall Koxkar glacier area measurements between proposed method ( $62.607 \text{ km}^2$ ) and glacier area from the RGI V4 ( $62.821 \text{ km}^2$ ), and 2% difference in area measurements from manual delineation ( $63.886 \text{ km}^2$ ). In the case of Yengisogat glacier, the glacier area calculated by the proposed method ( $362.1 \text{ km}^2$ ) has 2% difference in overall glacier area measurements between the reference data sets ( $363.92 \text{ km}^2$  and  $359.05 \text{ km}^2$ ), respectively.

Accuracy assessment results (Table 3.6.1 and Figure 3.5.1.d) showed that the Yengisogat glacier extent produced by proposed method was slightly overestimated in middle part of supraglacial areas. This was likely caused by slope image which derived from 90 m resolution spatial resolutions of the SRTM data and Landsat thermal band (120 m resolution) were not good enough to reflect the complex glacier terrain features, especially in the glacier margin side.

EARLY STAGE OF THE NEW METHOD FOR MAPPING OF DEBRIS-COVERED GLACIERS — BASED ON THE COMBINATION OF [TIR/(NIR/SWIR)] BAND RATIO IMAGE AND SLOPE

---

Table 3.6.1 Comparisons of separated each part of Yengisogat glacier derived from this study and reference data sets (Glacier area unit: km<sup>2</sup>).

Yengisogat glacier	This study (A)	SCGI (B)	Google Earth™ (C)	A-B (%)	A-C (%)
Terminus	8.82	8.51	8.89	+3.5	-0.79
Middle	32.04	29.64	30.33	+7.5	+5.3
Upper	321.24	320.9	324.7	+0.1	-1

Notes: Positive and negative value showing the percentage of differences in the area was larger (+) or smaller (-) than the reference area.

Table 3.6.2 Comparisons of separated each part of Koxkar glacier derived from this study and reference data sets (Glacier area unit: km<sup>2</sup>).

Koxkar glacier	This study (A)	RGI (B)	Google Earth™ (C)	A-B (%)	A-C (%)
Terminus	13.636	12.992	13.139	+2.5	+3.6
Middle	37.748	38.648	39.397	-2.3	-4
Upper	11.23	11.18	11.35	+0.45	-1

Notes: Positive and negative value showing the percentage of differences in the area was larger (+) or smaller (-) than the reference area.

The previous glacier mapping methods failed when applied to glaciers covered by thick debris and when the glacier terminus region transition to the unglaciated

area was gentle (Bishop et al. 2001, Taschner and Ranzi 2002, Ranzi et al. 2004, Bolch and Kamp 2006, Bolch et al. 2008). In chapter 2, an approach proposed by Bhambri et al. (2011) (combined result derived from clustering of slope, plan curvature and profile curvature with thermal mask and band ratio band 4 divided band 5) was applied to map the glaciers in the Shaksgam Valley using same Landsat images and the digital elevation model. As a result, Yengisogat glacier terminus region was unable to map precisely using Bhambri et al. (2011) approach. Terminus region of Yengisogat glacier had to be manually mapped as the post-processing step (Figure 3.6.1).

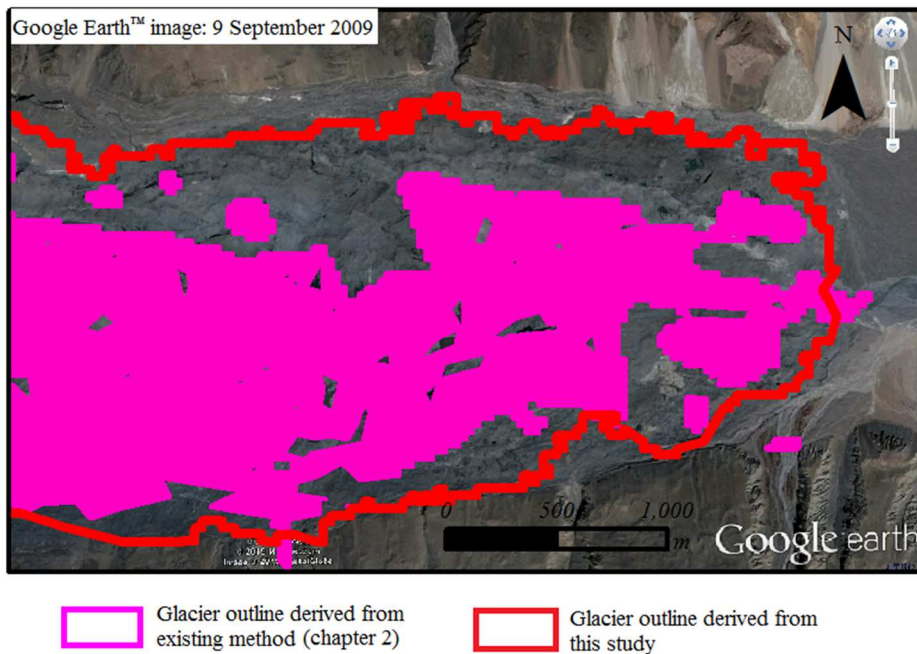


Figure 3.6.1- Comparison of the results derived from existing method (chapter 2) and method described in this chapter.

In Bhambri et al. (2011) approach, supraglacial debris area was delineated based on a combination of result derived from geomorphometric analysis with thermal mask generated from TIR band (Chapter 2, Figure 2.4.1). In this approach, the accurate delineation of supraglacial debris mostly depended on TIR band. Unfortunately, the low resolution of TIR band unable to recognized some part of supraglacial debris which covered by thick debris layer. This happened due to supraglacial debris where covered with thick debris layer have insignificant thermal differences with surrounding periglacial debris.

In contrast with proposed method in this chapter, [TIR/(NIR/SWIR)] band ratio image can take the advantages of both optical and thermal sensors. As a part of the equation, the NIR/SWIR band ratio helps to recognize the clean glacier-ice, on the other hand, TIR band contributes to distinguishing supraglacial debris from surrounding periglacial debris region.

Another point to consider is the most of the supraglacial and periglacial debris have subtle differences or same values in the NIR and SWIR band ratio image (Figure 3.6.2-3) (Casey et al. 2012). Particularly, subtle spectral differences of two classes may cause by different debris materials. Such as vary in debris size (fine to coarse) and sources of debris cover from surrounding the valley, near glacier terminus or flow down from higher elevation area or may transmit by the englacial process (Casey et al. 2012). Moreover, the moister content of debris

cover may be another reason for caused small differences in VNIR to SWIR region (Liang 2005, Casey et al. 2012). However, this little difference can be enhanced when TIR band (use of thermal differences, Figure 3.6.4) divided the NIR/SWIR band ratio (Figure 3.6.5). As a result, the range of difference between supraglacial and periglacial debris features was widening and allowed to separate from each other. However, valley bed in dark shadow and at higher altitude are still misclassified as supraglacial debris due to they have same spectral and thermal properties (Figure 3.6.5). Nevertheless, slope image has used for remove theses error.

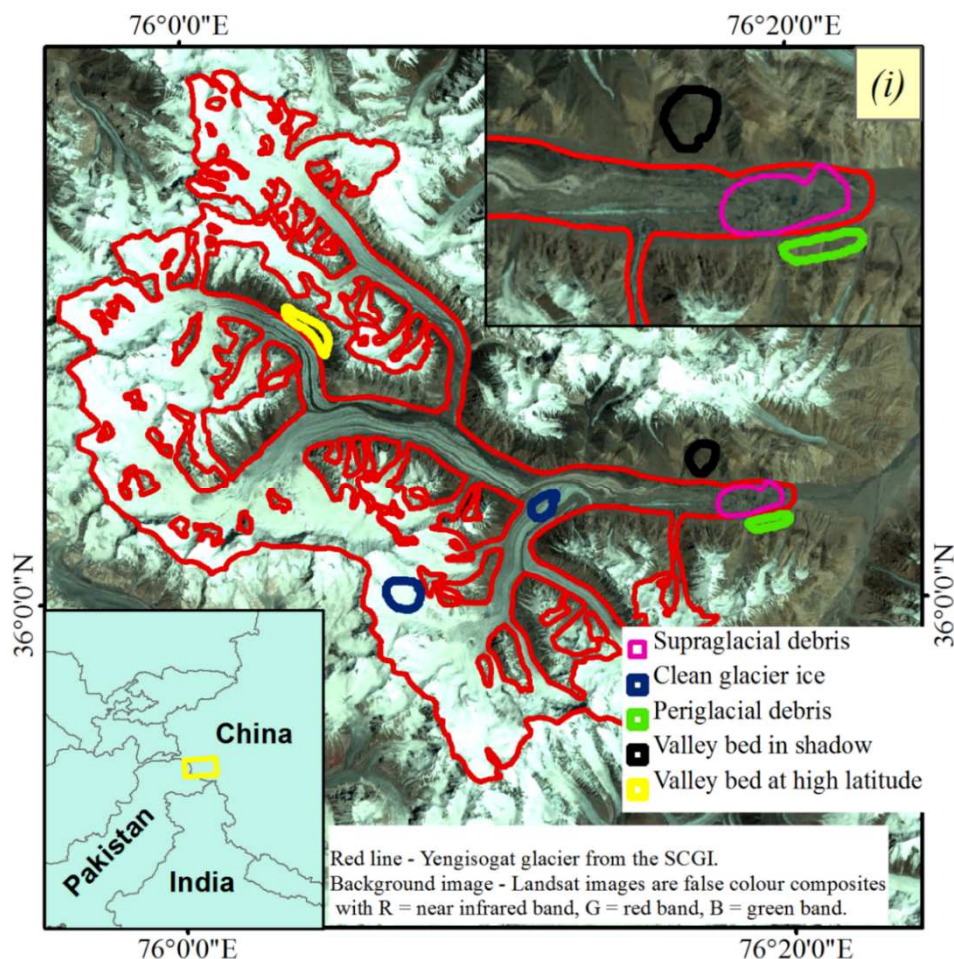


Figure 3.6.2- Yengisogat glacier and five classes which described in Figure 3.6.3-6.

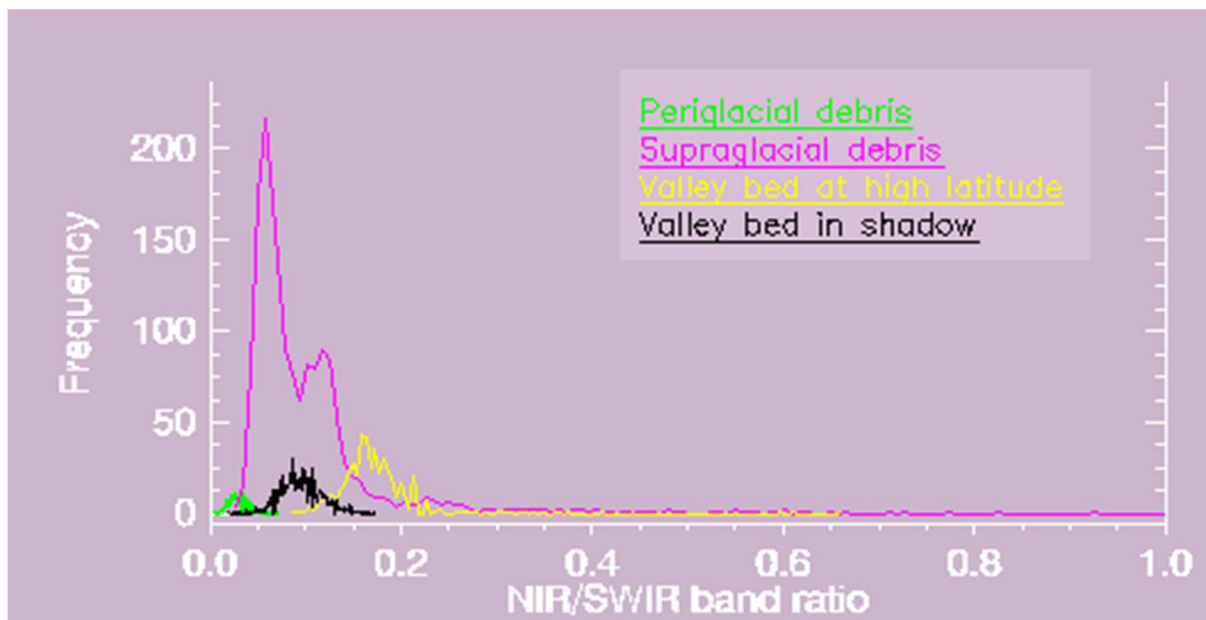


Figure 3.6.3- Normalized histogram showing frequency of each class in the (NIR/SWIR) band ratio derived from Landsat TM data. Corresponding images of the five classes are shown in the Figure 3.6.2.

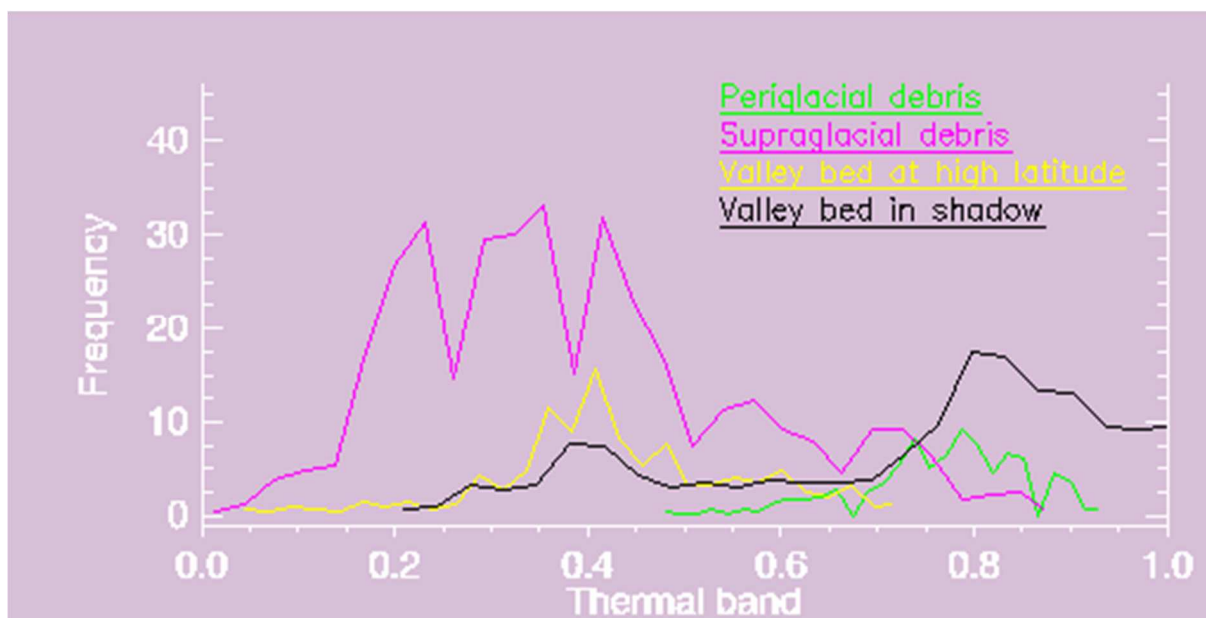


Figure 3.6.4- Normalized histogram showing frequency of each class in the thermal band from Landsat TM data. Corresponding images of the five classes are shown in the Figure 3.6.2.

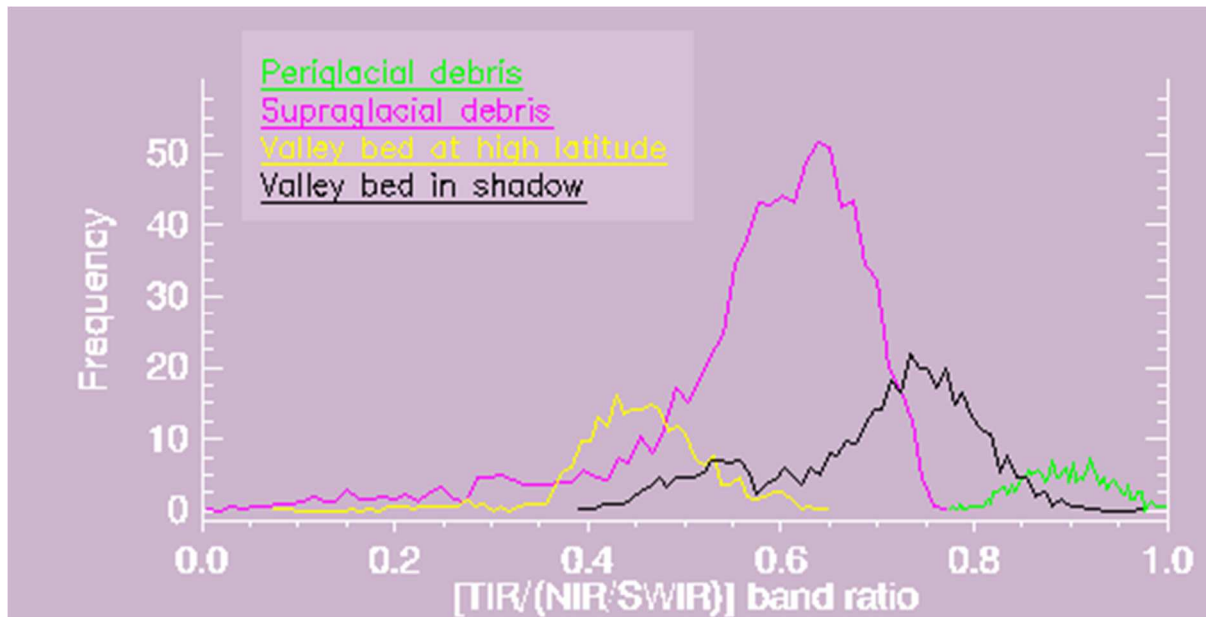


Figure 3.6.5- Normalized histogram showing frequency of each class in the [TIR/(NIR/SWIR)] band ratio derived from Landsat TM data. Corresponding images of the five classes are shown in the Figure 3.6.2.

### **3.7 Limitation of method**

There are several limitations in the presented method, which are:

1. Defining the efficient threshold value is a critical step to delineate the debris-covered glacier accurately. Therefore, before applying threshold values, it necessary to check threshold values by visually overlaying the resultant maps onto Landsat composite images and free high-resolution Google Earth™ images if available.
2. In the present study, threshold values range for supraglacial debris region was chosen because these range values can clearly separate the supraglacial debris in glacier terminus region from the unglaciated area. However, a threshold value for supraglacial debris may be different when work on other glacier area and other images.
3. Moreover, due to the fact that most of the glacier slope facet has different slope values. Therefore, slope threshold values need to be modified, when to apply the current version of the proposed new method to other glaciers. However, the present method can be implemented to map other glaciers when selecting suitable slope threshold value which can reflect that glacier terrain surface.

### **3.8 Conclusions**

In this chapter, the proposed method, which involved combining a [TIR/(NIR/SWIR)] band ratio image with slope information, was able to successfully delineate the Yengisogat glacier and Koxkar glacier with less than 8% discrepancy between the mapped glaciers' areas and the reference glaciers' areas. However, the coarse resolution of the thermal band cannot separate the spectral similarity of supraglacial and periglacial debris in some shaded and high elevation areas. Therefore, additional information (slope) was combined with [TIR/(NIR/SWIR)] band ratio imagery. The result of the approach is promising to map the glaciers in the study areas. The result of Koxkar glacier outlines shows that the 30 m resolution of SRTM V3 data allowed for higher accuracy than previous SRTM (90 m). Nevertheless, supraglacial debris area of Yengisogat glacier was overestimated (Figure 3.5.1.d, pick point mark) because the SRTM data (90 m resolution) was not good enough to reflect the gradient information from the periglacial debris region to the supraglacial debris region. Hence, manual editing was required to improve the result. However, the inclusion of additional information, such as more morphometric parameters (e.g. plan curvature and profile curvature) may further improve the accuracy of the debris-covered glacier mapping and allow the method to be applied to large glaciated regions.

## **Chapter 4    Final stage of the new method for mapping of debris-covered glaciers — Based on the combination of [TIR/(NIR/SWIR)] band ratio and geomorphometric parameters**

---

### **4.1      Introduction**

In chapter 3, the early stage of developed approach ([TIR/(NIR/SWIR)] band ratio image combined with slope) was able to map the debris-covered glaciers covered by thick debris layer and in areas the glaciers where the glacier terminus region transition to the unglaciated area is gentle. However, the slope was the only geomorphometric parameter considered, which resulted in the extent of part of Yengisogat glacier area being overestimated. Another limitation of the early stage of work was that it has difficulty mapping the glaciers in the large region. Therefore, the primary goal of this chapter is to advance the work based on Chapter 3, by using optical and thermal remote sensing data in combination with additional geomorphometric parameters such as plan curvature and profile curvature and to test the method by applying it to larger glacierized regions. Thus, in this study, all threshold range values are defined based on spectral characteristics and terrain features of all of the glaciers in the study areas.

## 4.2 Study area – Shaksgam Valley and Glacier Bay

The glaciers mapped in this chapter are located in the Shaksgam Valley (detailed description of the study area is available in chapter 2) and Glacier Bay National Park and Preserve of Alaska: Fairweather glacier, Desolation glacier, Lituya glacier, Crillon glacier, and Cascade glacier (Figure 4.2.1).

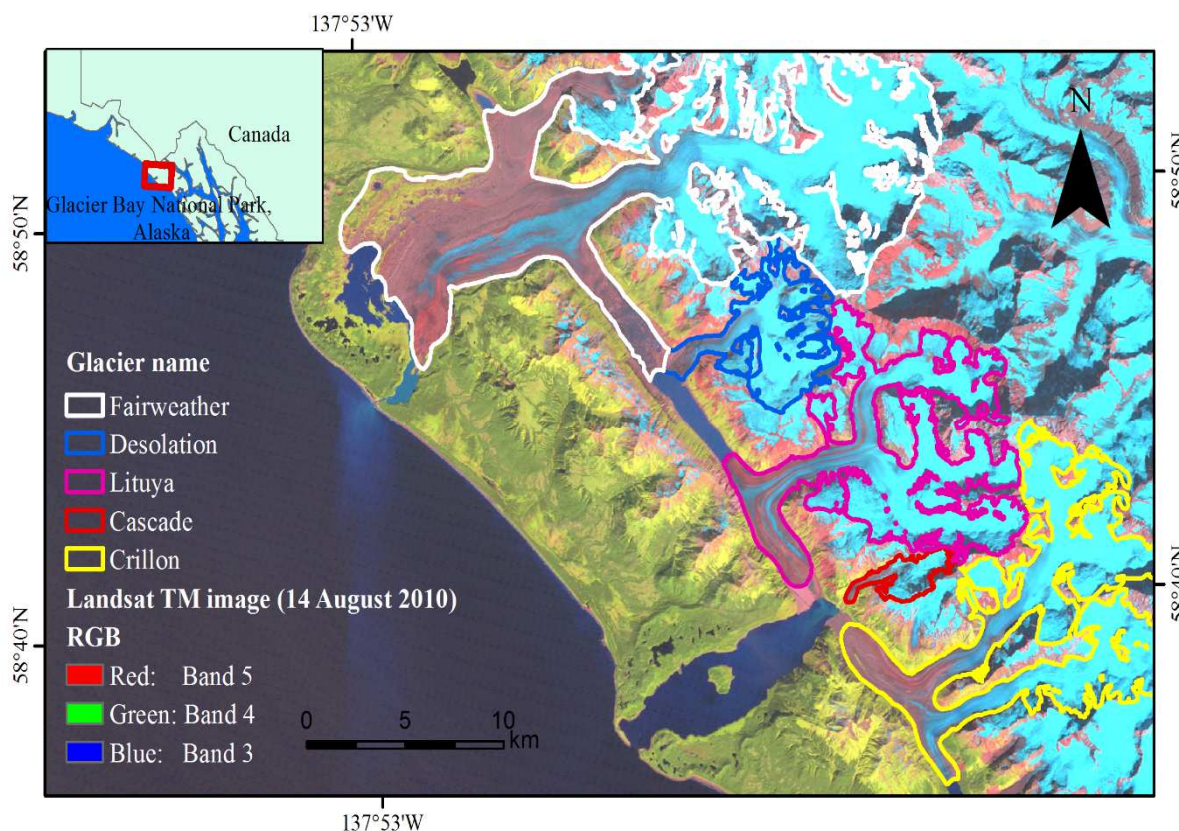


Figure 4.2.1. Studied glaciers which are located in Glacier Bay National Park, Alaska.

The reason for high interest in Glacier Bay, Alaska region is that all have former tidewater or potential tidewater properties (Molnia 2008). Tidewater glaciers can suddenly discharge significant amounts of ice into nearby waters, when some have advanced/retreated (Mertie 1933, Ritchie et al. 2008, Mcnabb and Hock 2014), thereby creating potential hazards to shipping traffic and raising the sea level (Solomon et al. 2007). Therefore, the prompt creation of glacier outline in this region is useful for monitoring their potential hazard activities. Glaciers studied in Glacier Bay region are flowed from the heights of the Fairweather Range (3635–4664 m above sea level) to the Pacific Ocean. Fairweather glacier and Desolation glacier originate from high on the flanks of Mount Fairweather. Reportedly, the Fairweather glacier extended about 4 km beyond the former coast sometimes in the recent past (Field and Collins 1975). Lituya glacier and Crillon glacier are T-shaped glaciers for which the respective glacier termini are flowing in northward and southward directions (Figure 4.2.1). Cascade glacier is a small hanging glacier, descending from above 2,000 m elevation nearly to sea level (Molnia 2008). These glacier surfaces are covered by large terminal moraine and tree-covered stagnant glacier ice (Goldthwait 1963).

In this chapter, in order to examine the applicability of the final stage of developed method to large glacierized regions, glaciers in Shaksgam and Glacier Bay are selected to mapping by the different date of images and digital elevation models.

### **4.3 Data sources**

Landsat TM images [acquisition date: 4 August 2009, Greenwich Mean Time (GMT): 05:18 (~11:18 am at local time)] and ASTER global digital elevation model version two (GDEM V2) data were used to delineate the glaciers in Shaksgam Valley. For mapping glaciers in Glacier Bay, Alaska, Landsat TM data [acquisition date: 14 August 2010, Greenwich Mean Time (GMT): 20:19 (~11:19 am at local time)] and DEMs generated from Interferometric Synthetic Aperture Radar (IFSAR) were used.

The Landsat images, ASTER GDEM V2 and IFSAR DEMs data were downloaded from USGS EarthExplorer (USGS EE; <http://earthexplorer.usgs.gov/>). The Landsat images were already orthorectified prior to distribution, and no seasonal snow and cloud cover were present in the study area.

The 3 m vertical accuracy of IFSAR DEMs derived from airborne X-band data obtained over northwestern Alaska during 14 August through 8 September 2012 (<http://ifsar.gina.alaska.edu/>). For Shaksgam Valley, DEM data from the Shuttle Radar Topography Mission (SRTM) was also available. However, the SRTM 1 Arc-Second Global elevation void filled data (SRTM data tiles that contain no data, which occurs due to bad radar scatter and rough topography) was still contained voids. Therefore, ASTER GDEM V2 and IFSAR DEMs were used to

generate the geomorphometric parameters (slope, plan curvature and profile curvature) which were necessary for glacier mapping in this study.

The vector maps from the SCGI, RGI, manual digitization of selected glaciers from the panchromatic band of ALOS PRISM (2.5 m resolution) and free available high-resolution Google Earth™ images were used for a qualitative validation of results from this study. Also, glacier velocity maps provided by Rankl et al. (2014) were used to evaluate the results of this study by visual comparison.

$\pm 30$  m accuracy of glacier boundaries from SCGI (Guo et al. 2014) and manual digitization of selected glaciers by ALOS PRISM and free available high-resolution Google Earth™ images were used to evaluate results from Shaksgam Valley. RGI and manual delineation of the glacier from Google Earth™ image (only for terminus region of Lituya glacier) were used to validate the glacier outlines derived from Alaska region.

High-resolution images exceedingly support discrimination of glacier ice from seasonal snow and surrounding periglacial debris. In this study, ALOS PRISM and Google Earth™ images were used for manual digitization of selected glaciers (Table 4.3). Acquisition dates of these high-resolution images [August 22, 2009, September 9, 2009, September 30, 2009, October 30, 2009 (Shaksgam Valley) and, 23 July 2011 (Alaska region)] are similar to the Landsat TM data which used

to mapping glaciers in this study. Visual interpretation of debris-covered glacier was by identifying distinctive glacier terrain features such as exposed ice from debris, supraglacial ponds, ice cliffs, and the outlets of subglacial streams, which are connected with the glacier terminus region.

Table 4.3 Manual delineation of selected glaciers for validation purpose.

Glacier name	Region	Type	Data used for delineation
Yengisogat	Shaksgam Valley	Debris-covered	Google Earth™ images
Teram Kangri	Shaksgam Valley	Debris-covered	ALOS PRISM
Kyagar	Shaksgam Valley	Clean glacier ice	ALOS PRISM
Kulqin	Shaksgam Valley	Debris-covered	ALOS PRISM
Small clean glacier-ice	Shaksgam Valley	Clean glacier	ALOS PRISM
Small debris-covered	Shaksgam Valley	Debris-covered	Google Earth™ image
Lituya	Alaska	Debris-covered	Google Earth™ image

Also, Yengisogat glacier outline was visually evaluated by comparing with glacier velocity maps (Figure 4.5.1) which generated using offset intensity tracking on multi-temporal synthetic aperture radar (SAR) satellite images (from 1992 to 2012) provided by Rankl et al. (2014). Glacier velocity maps can be used for detecting the actual glacier margins under the debris cover (Fischer et al. 2014, Kääb et al. 2014, Luckman et al. 2014). However, detecting glacier motion using SAR processing techniques can be challenging due to extreme topography and problems of low coherence (Strozzi et al. 2002, Luckman et al. 2014). Furthermore, SAR processing techniques cannot efficiently detect significant movement of the glacier, if some part of the glacier has motionless or lower speed during the estimated time period (Strozzi et al. 2002, Luckman et al. 2014). However, experienced motion part of the debris-covered glacier still contributes valuable information to verify the results of the proposed method.

## **4.4 Method**

In the final stage of developed method, the debris-covered glaciers outlines were generated from three main processing steps which are thresholding of [TIR/(NIR/SWIR)] band ratio imagery, geomorphometric analysis, and overlay operation.

### **4.4.1 Thresholding of [TIR/(NIR/SWIR)] band ratio imagery**

The [TIR/(NIR/SWIR)] band ratio was created based on different characteristics (spectral and thermal) of supraglacial debris in the conventional band ratio image (TM b4/TM b5) and thermal band (TM b6) to better distinguish from surrounding rocky materials. The glaciers (supraglacial debris and clean glacier) were classified using thresholding of [TIR/(NIR/SWIR)] band ratio imagery (Figure 4.4.1.1 and Figure 4.4.1.2). The classified results (i.e. clean ice part of the debris-covered glacier, supraglacial debris) contained several inaccuracies for the supraglacial debris where the periglacial debris in the shaded area, in higher elevation area and vegetated area. This might be caused by periglacial debris may have lower temperatures and same spectral properties (Figure 4.4.1.1 and Figure 4.4.1.2). Moreover, water body near glacier tongue also misclassified as glacier

ice (Figure 4.4.1.1.d and Figure 4.4.1.2.c). Therefore, additional information from geomorphometric parameters (i.e. slope) was integrated with [TIR/(NIR/SWIR)] band ratio imagery in the early stage of the developed method with its original form (see in Chapter 3). However, resulted in the extent of part of Yengisogat glacier area being overestimated because of the slope was the only considered geomorphometric parameter. Another limitation of the previous work (Chapter 3) is that it is hard to map the glaciers in the vast region.

Fortunately, many of these errors can be removed when inclusion of additional geomorphometric parameters such as slope, plan curvature, and profile curvature. Alos, additional geomorphometric parameters might further improve the accuracy of the debris-covered glacier delineation and allow the method to be applied to large glaciated regions.

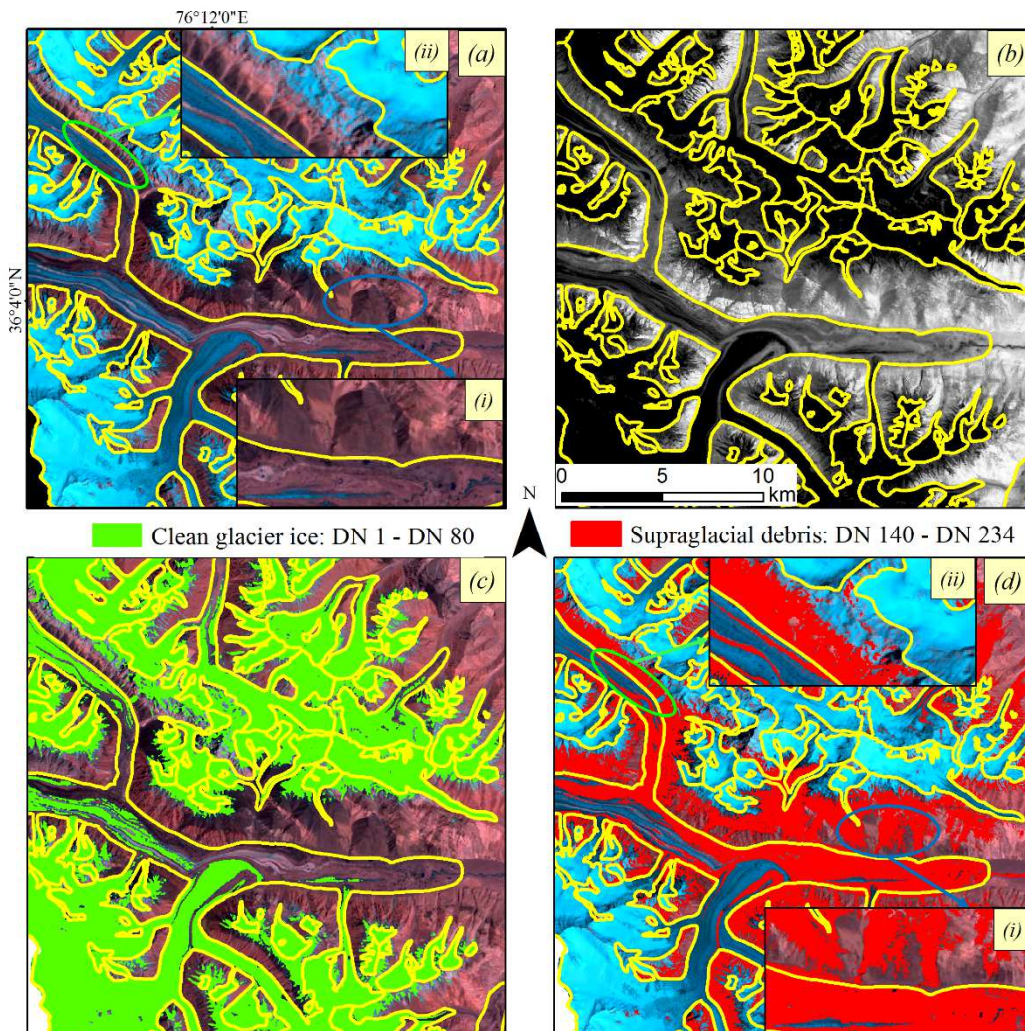


Figure 4.4.1.1- Examples of thresholding of [TIR/(NIR/SWIR)] band ratio. (a) Glaciers in Shaksgam Valley represented by a false colour composite image (R = shortwave infrared band, G = near infrared band, B = red band). (b) [TIR/(NIR/SWIR)] band ratio image. (c) Clean glacier ice (in green) map derived from the thresholding of [TIR/(NIR/SWIR)] band ratio image. (d) Map of supraglacial debris derived the thresholding of [TIR/(NIR/SWIR)] band ratio image. (i) and (ii) Showing the misclassifications area such as valley bed under deep shadow (blue cycle) and periglacial debris area in higher elevation (green cycle). Glacier outlines (yellow) are based on SCGI.

FINAL STAGE OF THE NEW METHOD FOR MAPPING OF DEBRIS-COVERED GLACIERS — BASED ON THE COMBINATION OF [TIR/(NIR/SWIR)] BAND RATIO AND GEOMORPHOMETRIC PARAMETERS

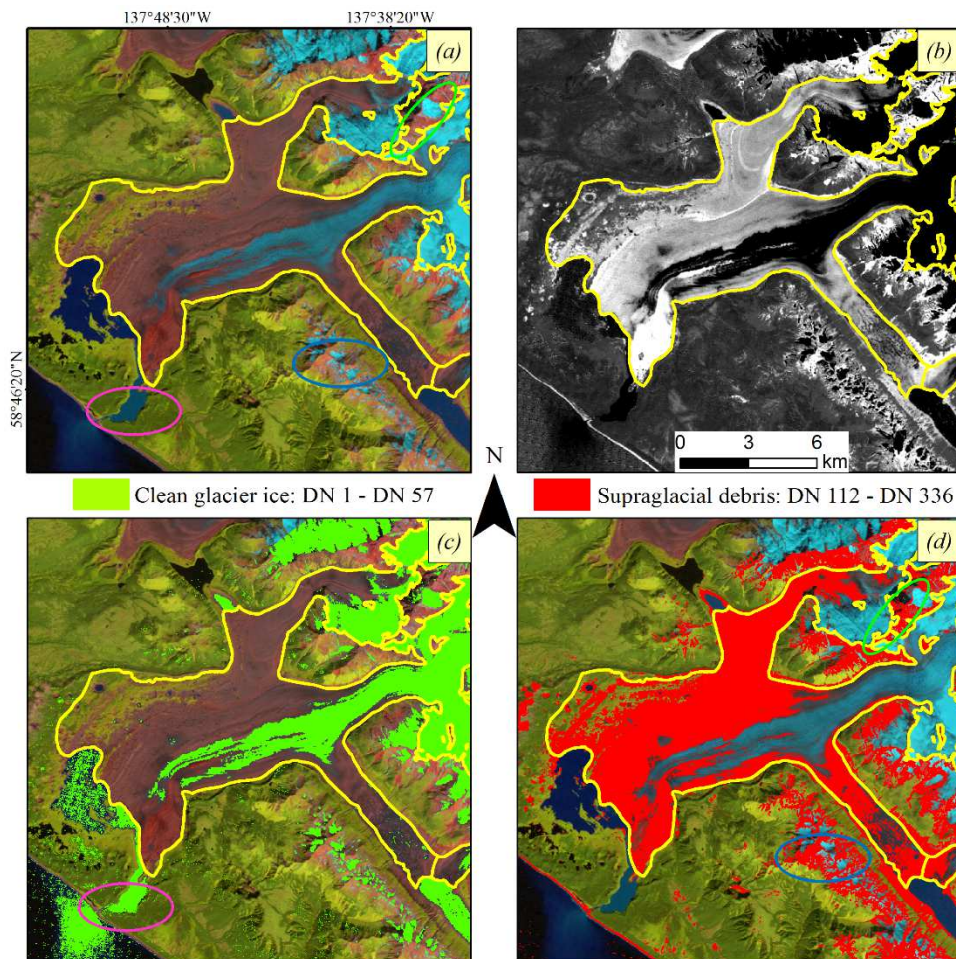


Figure 4.4.1.2- Examples of thresholding of [TIR/(NIR/SWIR)] band ratio. (a) Glaciers in Glacier Bay represented by a false colour composite image ( $R$  = shortwave infrared band,  $G$  = near infrared band,  $B$  = red band). (b) [TIR/(NIR/SWIR)] band ratio image. (c) Clean glacier ice (in green) map derived from the thresholding of [TIR/(NIR/SWIR)] band ratio image. (d) Map of supraglacial debris derived the thresholding of [TIR/(NIR/SWIR)] band ratio image. Marked areas such as pink cycle in (a, c), green cycle in (a, d) and blue cycle in (a,d) are misclassified areas of the water body, valley bed in higher elevation and vegetated area. Glacier outlines (yellow) are based on RGI.

#### **4.4.2 Geomorphometric Analysis**

Geomorphometric parameters, specifically, such as slope, plan curvature, and profile curvature, were computed from the ASTER GDEM V2 and IFSAR DEMs data. These parameters can reflect the unique morphological properties of glacier terrain. Thus, those parameters would be helpful to identify the supraglacial debris margin more accurately. Debris-covered glaciers are always orientated on the gradual slope faces, whereas steep slope faces do not allow for the accumulation of snow which necessary for glacier formation (Waldfinger 1999). Debris materials on the glacier surface are deposited from the surrounding steep valley by the processes of volcanic ash, snow, and rock avalanches (Shroder et al. 2000). Therefore, slope gradient information (such as mean of slope) can be used to define the glacier boundary from the surrounding valley bed (Bishop et al. 2001). On the other hand, plan curvature enhances the crests of ridges (Figure 4.4.2.1.b and Figure 4.4.2.2.b in blue) and alpine-basin valley bottoms ridges (Figure 4.4.2.1 and Figure 4.4.2.2). Whereas, profile curvature highlights the convexity associated with lateral moraines ridges (Figure 4.4.2.1.d and Figure 4.4.2.2.d in yellow) (Bishop et al. 2001). Thus, concave and convex terrain proprieties information from curvature image can be useful for differentiating glacier surfaces from non-glacier surfaces (Bishop et al. 2001). Therefore, a

combination of these three parameters should be able to determine the debris-covered glacier margin more efficiently.

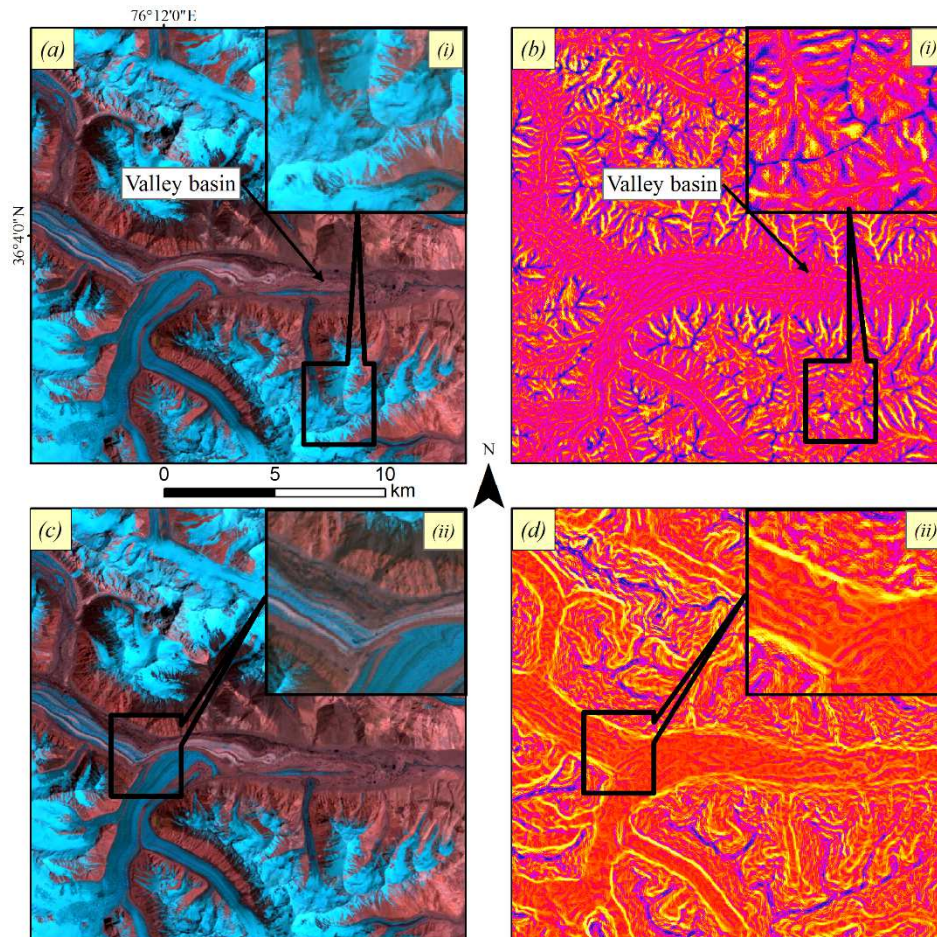


Figure 4.4.2.1- Examples of Plan and profile curvature image computed from ASTER GDEM V2. (a) and (c) Supraglacial debris region of Yengisogat glacier. (b) Plan curvature image and same location with (a) and (c). (d) Profile curvature image and same location with (a) and (c). (i) Closer view of enhanced crests of ridges (blue). (ii) Closer view of highlighted convexity associated with the lateral moraines (yellow).

FINAL STAGE OF THE NEW METHOD FOR MAPPING OF DEBRIS-COVERED GLACIERS — BASED ON THE COMBINATION OF [TIR/(NIR/SWIR)] BAND RATIO AND GEOMORPHOMETRIC PARAMETERS

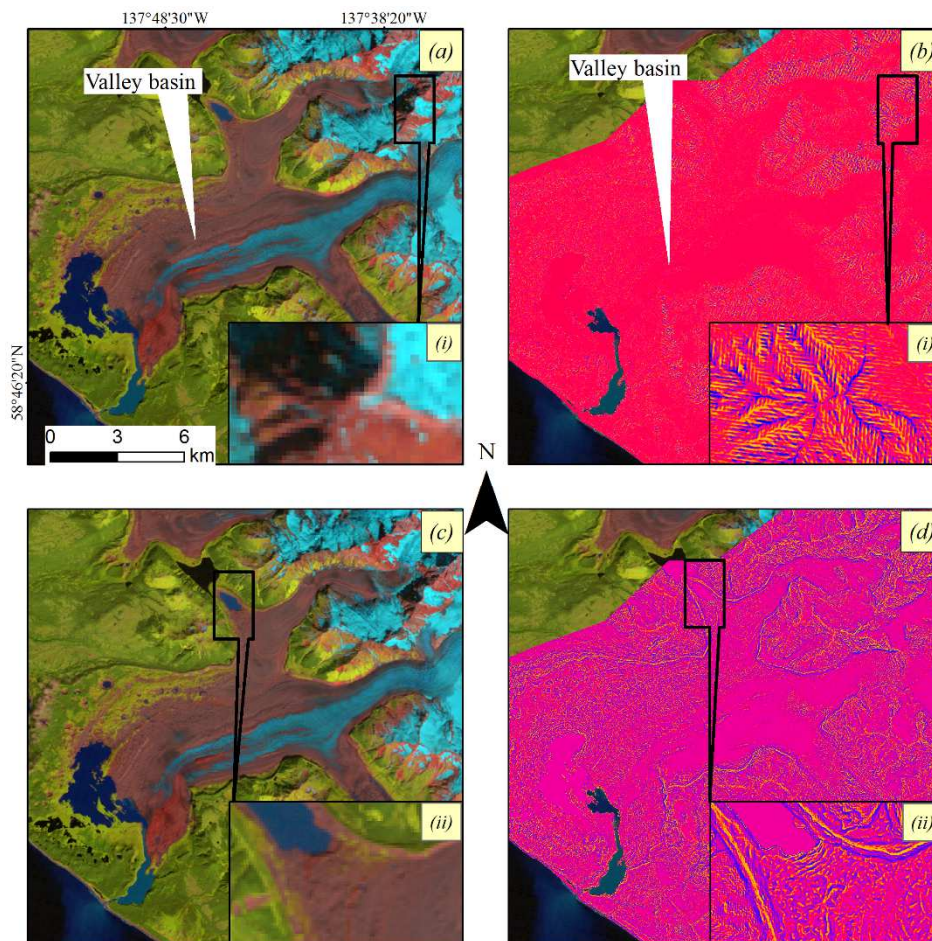


Figure 4.4.2.2- Examples of Plan and profile curvature image computed from IFSAR DEMs.

(a) and (c) Supraglacial debris region of Fairweather glacier. (b) Plan curvature image and same location with (a) and (c). (d) Profile curvature image and same location with (a) and (c).

(i) Closer view of enhanced crests of ridges (blue). (ii) Closer view of highlighted convexity associated with the lateral moraines (yellow).

In the geomorphometric analysis step, first, plan curvature, and profile curvature information were combined using the iterative minimum distance statistical clustering technique (Forgy 1965) implemented into the SAGA software (SAGA-GIS: <http://www.sagagis.uni-geottingen.de/html/index.php>).

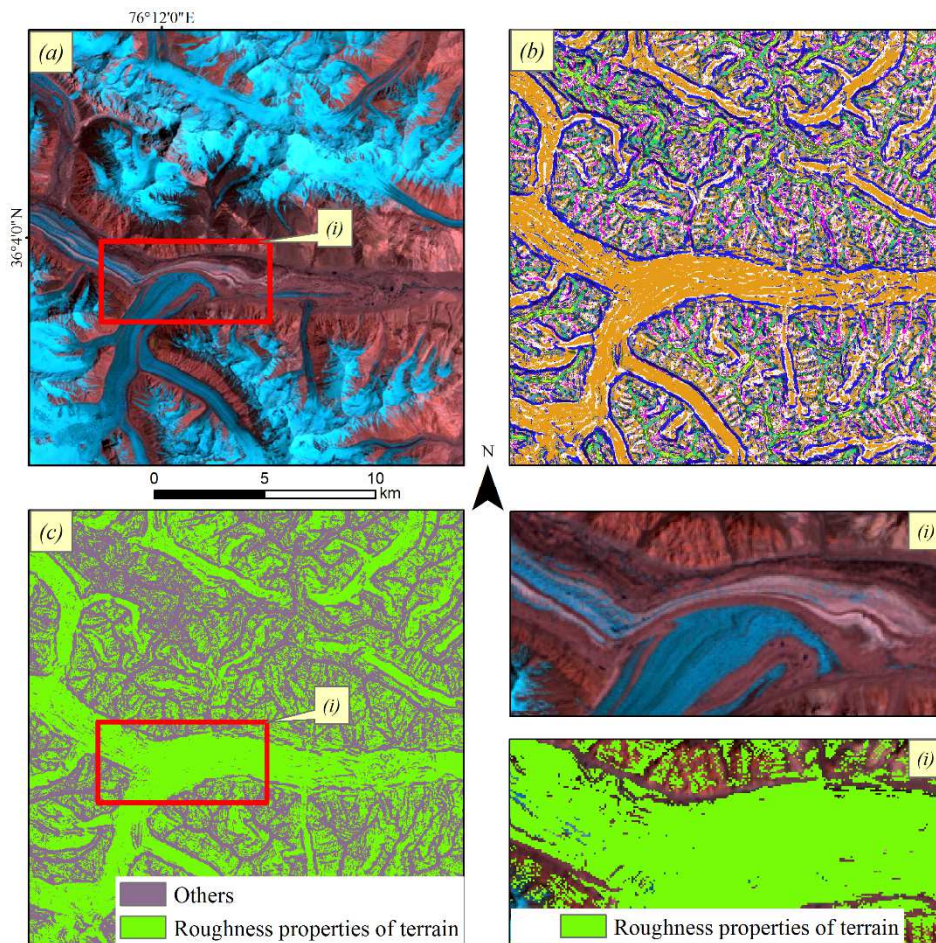


Figure 4.4.2.3- Examples of clustering of plan curvature and profile curvature. (a) Supraglacial debris region of Yengisogat glacier. (b) Clustering plan and profile curvature in ten initial classes. (c) Reclassify clustering result from (b) into two classes. (i) Closer view of “Roughness properties of terrain” derived from (c) and (i) upper image is the same location with (i) below image.

FINAL STAGE OF THE NEW METHOD FOR MAPPING OF DEBRIS-COVERED GLACIERS — BASED ON THE COMBINATION OF [TIR/(NIR/SWIR)] BAND RATIO AND GEOMORPHOMETRIC PARAMETERS

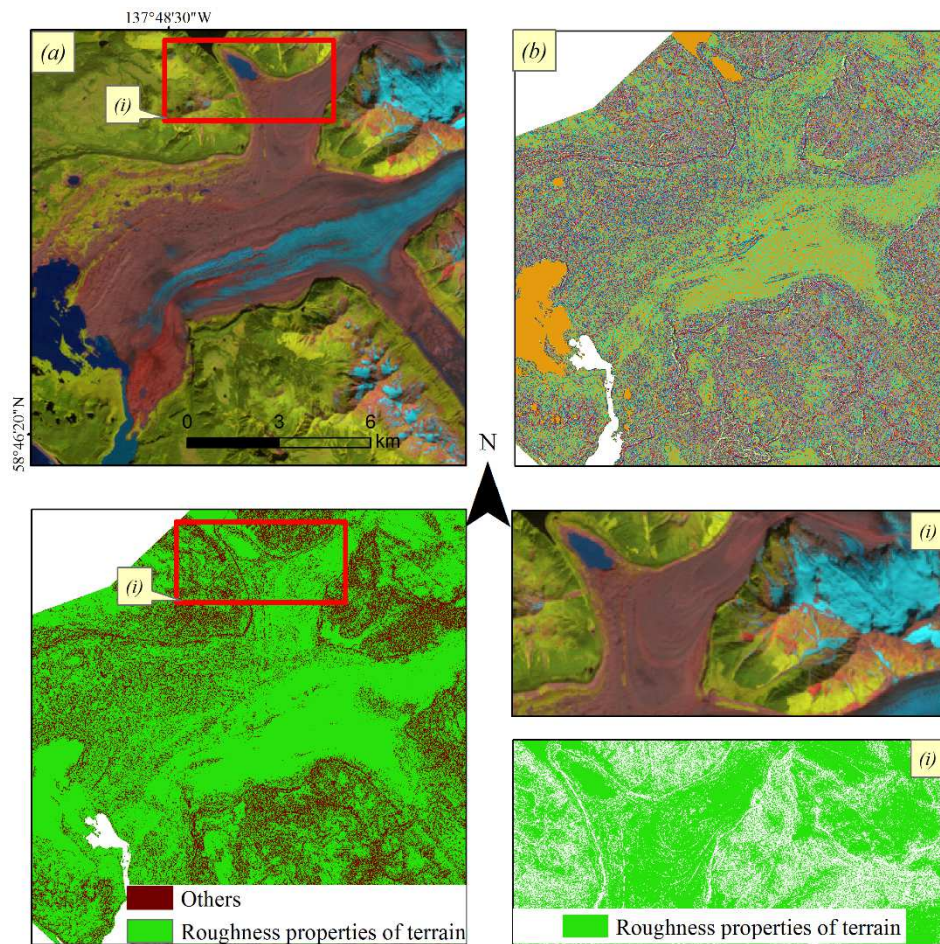


Figure 4.4.2.4- Examples of clustering of plan curvature and profile curvature. (a) Supraglacial debris region of Fairweather glacier. (b) Clustering plan and profile curvature in ten initial classes. (c) Reclassify clustering result from (b) into two classes. (i) Closer view of “Roughness properties of terrain” derived from (c) and (i) upper image is the same location with (i) below image.

For this clustering process, in each iteration, all samples are assigned to existing cluster centers, and then new means values for each class (i.e., cluster centers) are calculated (Ball and Hall 1965). The optimal number of classes is usually unknown (Richards and Jia 1999). Therefore, it is suggested to use a conservatively high number of clusters, analyze the resulting clusters, and then rerun the function or reclassify again with a reduced number of classes (Richards and Jia 1999).

In this study, as a first step, plan curvature, and profile curvature were clustered into ten primary classes (Figure 4.4.2.3.b and Figure 4.4.2.4.b). Then, these ten classes were reclassified into two categories: “Roughness properties of terrain” and “Others” which are showing in Figure 4.4.2.3.c-i and Figure 4.4.2.4.c-i.

Next, a mean of slope threshold values (Figure 4.4.2.5 and Figure 4.4.2.6) were defined for all glaciers in study areas based on statistics from the slope image and visual comparison of Landsat false color composite image. This threshold values selected because of slope value could represent the most of the glaciers terrain, in entire Shaksgam Valley ( $< 28^\circ$ ) and Glacier Bay ( $< 18^\circ$ ). However, the resultant mean of slope image also includes other valley bed, which has a similar slope (Figure 4.4.2.5.a and Figure 4.4.2.6.a). Therefore, the mean of slope image was converted to a vector map (Figure 4.4.2.5.b and Figure 4.4.2.6.b), and then, polygons which covered the glacier terrain was selected manually (Figure

4.4.2.5.c and Figure 4.4.2.6.c). The selected vector map was converted back into the raster format (Figure 4.4.2.5.d and Figure 4.4.2.6.d). For determining the debris-covered glacier margin more pricey, converted raster map (Figure 4.4.2.5.d and Figure 4.4.2.6.d) was combining with the result derived from the clustering of plan curvature and profile curvature (Figure 4.4.2.5.e and Figure 4.4.2.6.e), using raster calculator in ArcMap software.

The final result (Figure 4.4.2.5.f and Figure 4.4.2.6.f) derived from combining the mean of the slope, plan curvature and profile curvature can clearly distinguish the supraglacial debris region from the periglacial debris area in the glacier margin side. Nevertheless, it also showed that using geomorphometric information alone could not be separated terminus region of debris-covered glaciers (i.e.: Yengsiogat glacier in Figure 4.4.2.5.f; Fairweather glacier in Figure 4.4.2.6.f) from the nonglacier region. However, this can be overcome when the final result of the geomorphometric analysis is integrated with the thresholded TIR/NIR/SWIR band ratio image, which is described in next.

FINAL STAGE OF THE NEW METHOD FOR MAPPING OF DEBRIS-COVERED GLACIERS — BASED ON THE COMBINATION OF [TIR/(NIR/SWIR)] BAND RATIO AND GEOMORPHOMETRIC PARAMETERS

---

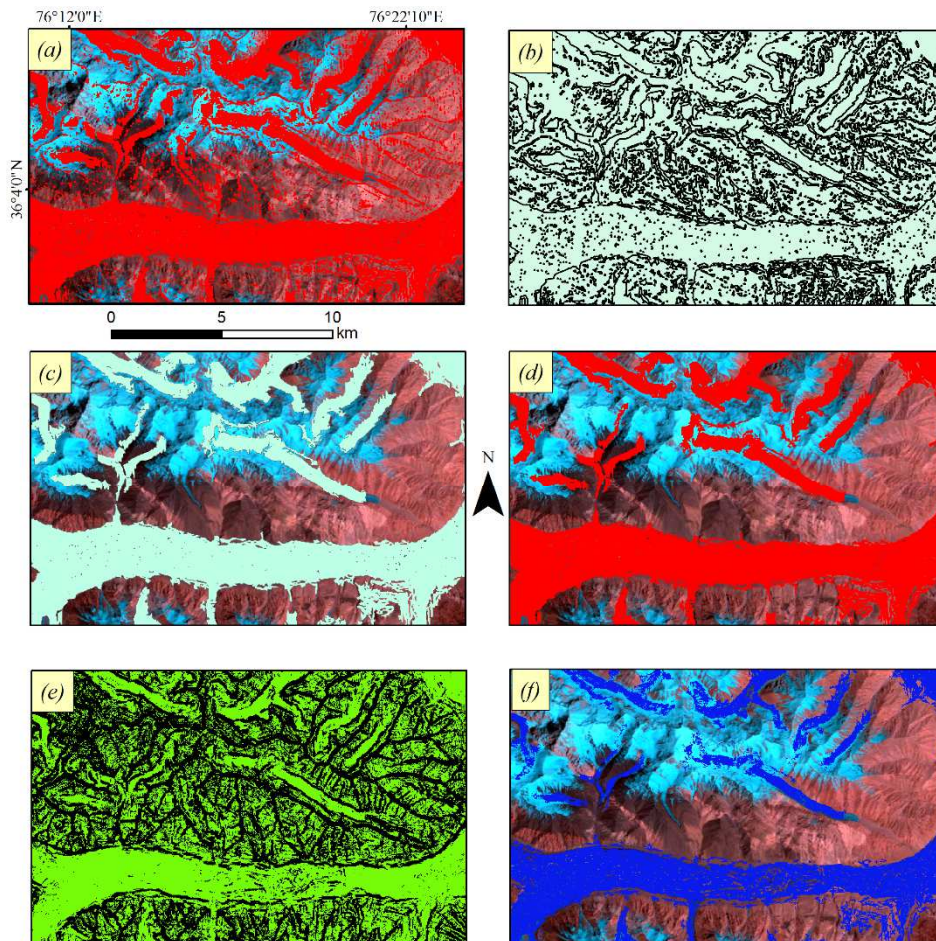


Figure 4.4.2.5- Examples of combining the mean of the slope, plan curvature, and profile curvature. (a) Mean of slope ( $\leq 28^\circ$ ) map for Shaksgam Valley. (b) Vectorization of the mean of slope map. (c) Glacier slope faces selected manually from (b). (d) Raster map converted from (c). (e) Glacier with flat valley basin area derived from clustering analysis. (f) The final result of geomorphometric analysis derived from combining map (d) and map (e) using ``AND`` operation (map (d) red area AND map (e) green area).

FINAL STAGE OF THE NEW METHOD FOR MAPPING OF DEBRIS-COVERED GLACIERS — BASED ON THE COMBINATION OF [TIR/(NIR/SWIR)] BAND RATIO AND GEOMORPHOMETRIC PARAMETERS

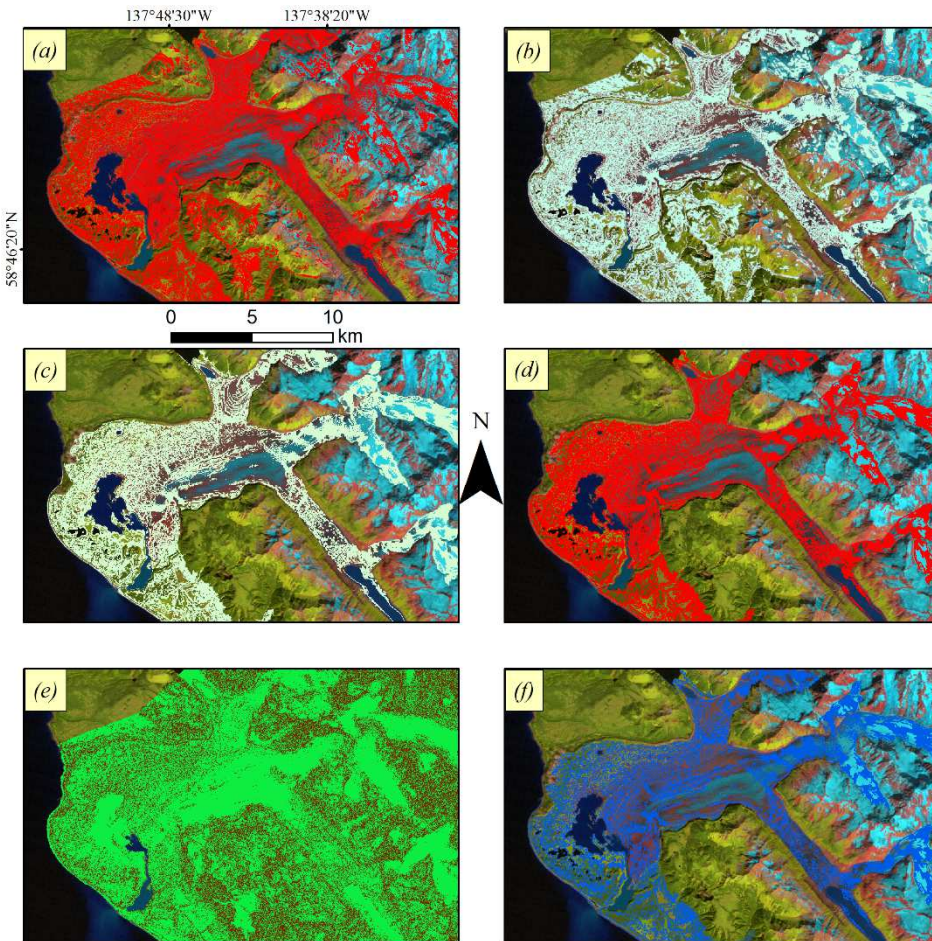


Figure 4.4.2.6- Examples of combining the mean of the slope, plan curvature, and profile curvature. (a) Mean of slope ( $\leq 18^\circ$ ) map for Glacier Bay. (b) Vectorization of the mean of slope map. (c) Glacier slope faces selected manually from (b). (d) Raster map converted from (c). (e) Glacier with flat valley basin area derived from clustering analysis. (f) The final result of geomorphometric analysis derived from combining map (d) and map (e) using ``AND`` operation (map (d) red area AND map (e) green area).

#### **4.4.3 Overlay operation**

In the overlay operations step, the supraglacial debris regions of glaciers were mapped by integrating the results derived from the geomorphometric analysis with “supraglacial debris class” obtained from thresholding of [TIR/(NIR/SWIR)] band ratio image, as shown in Figure 4.4.3.1 and Figure 4.4.3.2. Then, raster maps (Figure 4.4.3.1.c and Figure 4.4.3.2.c) of supraglacial debris regions of glaciers were converted into vector maps for manually remove some areas, such as isolated areas smaller than  $0.2 \text{ km}^2$  that are outside of the main body of the glacier (Bolch et al. 2007, Bhambri et al. 2011) and river channels, which are connected with glacier tongue, vegetated area.

Finally, the final glacier outlines (Figure 4.4.3.1.d and Figure 4.4.3.2.d) were generated by merging the vector map of the supraglacial debris region (Figure 4.4.3.1.d and Figure 4.4.3.2.d in red) with the map of clean glacier-ice (Figure 4.4.3.1.d and Figure 4.4.3.2.d in blue) derived from thresholding of [TIR/(NIR/SWIR)] band ratio image.

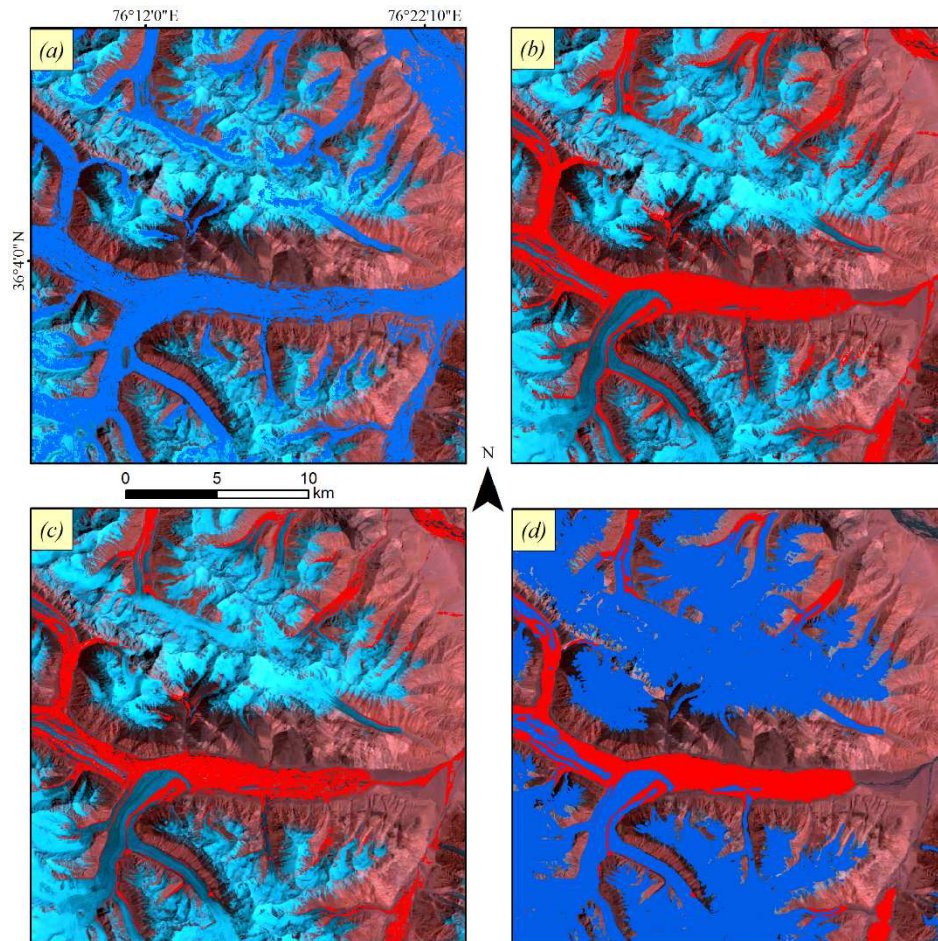


Figure 4.4.3.1 – Examples of final glaciers outlines generation in Shaksgam Valley by combining the results from thresholding of [TIR/(NIR/SWIR)] band ratio and geomorphometric analysis. (a) Result derived from the geomorphometric analysis. (b) Supraglacial debris map of Yengisogat glacier derived from thresholding of [TIR/(NIR/SWIR)] band ratio image. (c) Combining map (a) and map (b) using “AND” operation [map (a) blue area and map (b) red area]. (d) Final Yengisogat glacier map (supraglacial debris in red; clean glacier ice in blue) after editing process.

FINAL STAGE OF THE NEW METHOD FOR MAPPING OF DEBRIS-COVERED GLACIERS — BASED ON THE COMBINATION OF [TIR/(NIR/SWIR)] BAND RATIO AND GEOMORPHOMETRIC PARAMETERS

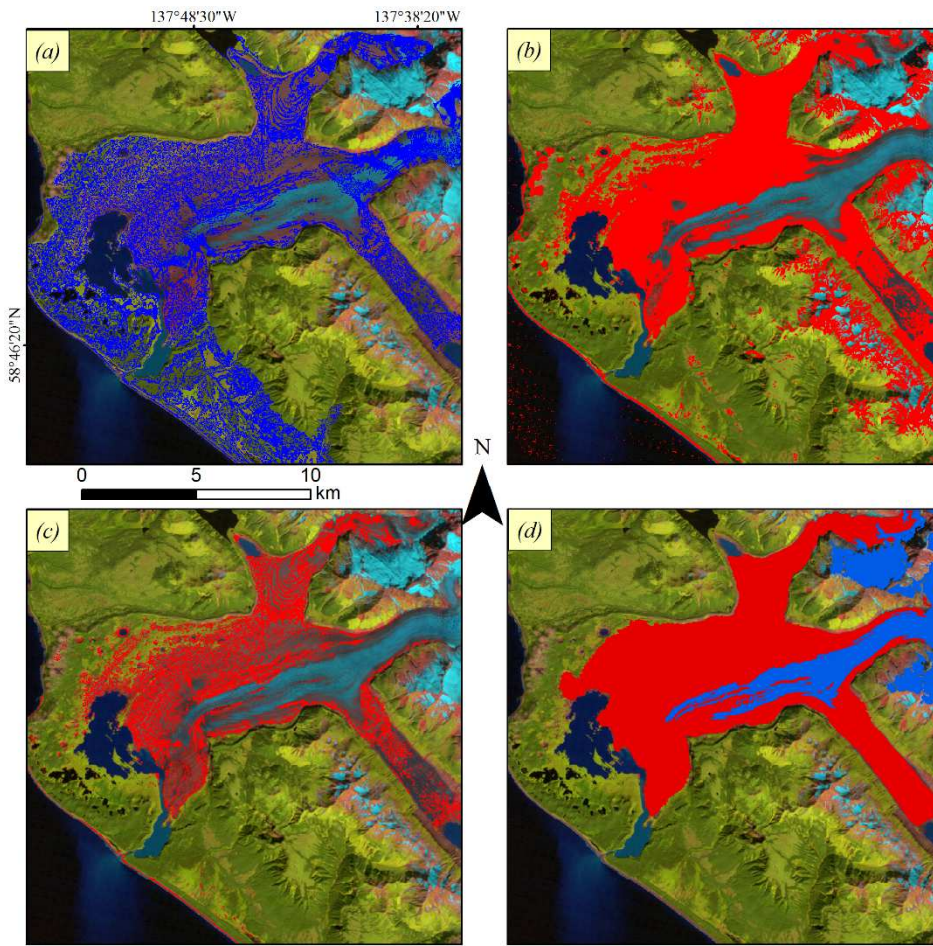


Figure 4.4.3.2- Examples of generating of final glaciers outlines in Glacier Bay by combining the results from thresholding of [TIR/(NIR/SWIR)] band ratio and geomorphometric analysis.

(a) Result derived from the geomorphometric analysis. (b) Supraglacial debris map of Yengisogat glacier derived from thresholding of TIR/NIR/SWIR band ratio image. (c) Combining map (a) and map (b) using “AND” operation [map (a) blue area and map (b) red area]. (d) Final Yengisogat glacier map (supraglacial debris in red; clean glacier ice in blue) after editing process.

## **4.5 Accuracy assessment**

To evaluate the final glacier outlines (for Shaksgam Valley) derived from proposed method, glacier outlines based on SCGI (Guo et al. 2015), manual delineation of selected glaciers based on the high-resolution images from ALOS PRISM and Google Earth™, and velocity maps of Yengisogat glacier estimated from SAR images (Rankl et al. 2014) were used. In the case of the Glacier Bay, glacier outlines based on RGI and manual delineation of Lituya glacier using the high-resolution Google Earth™ images were used for validation of final glacier outlines.

All of the vector maps of the glacier (for Shaksgam Valley) were overlaid onto and ALOS PRISM and Google Earth™ images (Figure 4.5.1-3), and glacier velocity maps (Figure 4.5.2) to allow for visual comparisons. Specifically, the area extent of selected glaciers from SCGI and manual delineation of ALOS PRISM and high-resolution Google Earth™ images were compared with the glacier area calculated from the proposed method. In detail, in order to more detailed analysing accuracy of results derived from proposed method, selected glacier outlines (results and reference datasets) were separated into three regions which are terminus part which mostly covered by debris, middle part where mixed between exposed ice and debris, and, upper part which contains snow and

ice (Figure 4.5.1-3 and Table 4.5.1-5). Also, total glacier area of Shaksgam Valley which derived from proposed method are separated to five sub-regions to compared with glacier area from SCGI (Figure 4.5.4-8 and Table 4.5.6).

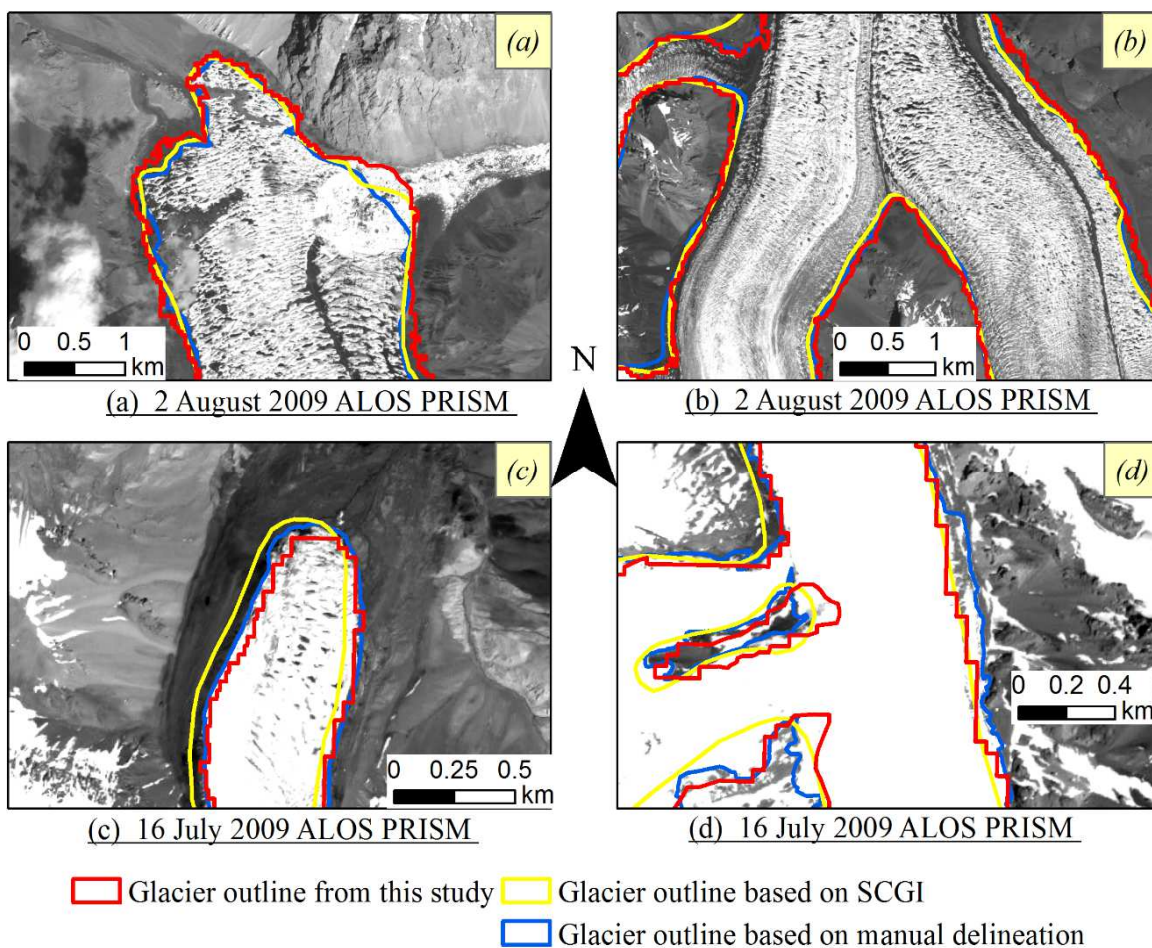


Figure 4.5.1- Comparisons of the selected clean glacier-ice outlines derived from proposed method with reference datasets. (a) and (b) Kyagar glacier. (c) and (d) Small clean glacier-ice.

**FINAL STAGE OF THE NEW METHOD FOR MAPPING OF DEBRIS-COVERED GLACIERS — BASED ON THE COMBINATION OF [TIR/(NIR/SWIR)] BAND RATIO AND GEOMORPHOMETRIC PARAMETERS**

---

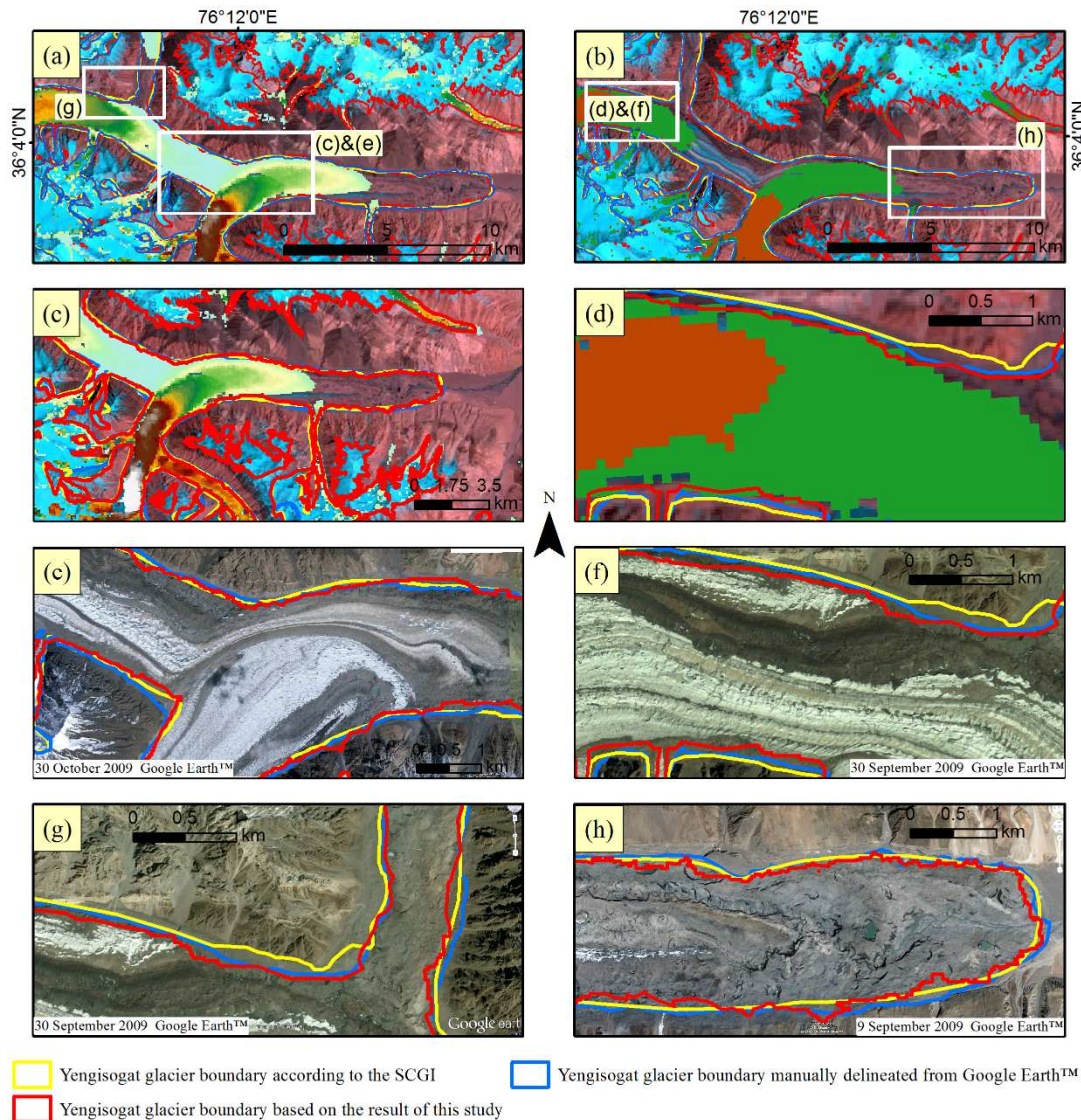


Figure 4.5.2- Comparisons of the Yengisogat glacier outlines derived from proposed method with reference datasets. (a) Yengisogat glacier outlines overlaid on glacier velocity map derived from SAR data during 2007 to 2011 which provided by Rankl et al. (2014). (b) Yengisogat glacier outlines overlaid on glacier velocity map derived from TerraSAR-X SM image pairs (16 June 2009 to 12 September 2009 and 24 December 2009 to 15 January 2010) provided by Rankl et al. (2014). (c) and (e) Closer view of the map (a). (d) and (f) Closer view of the map (b).

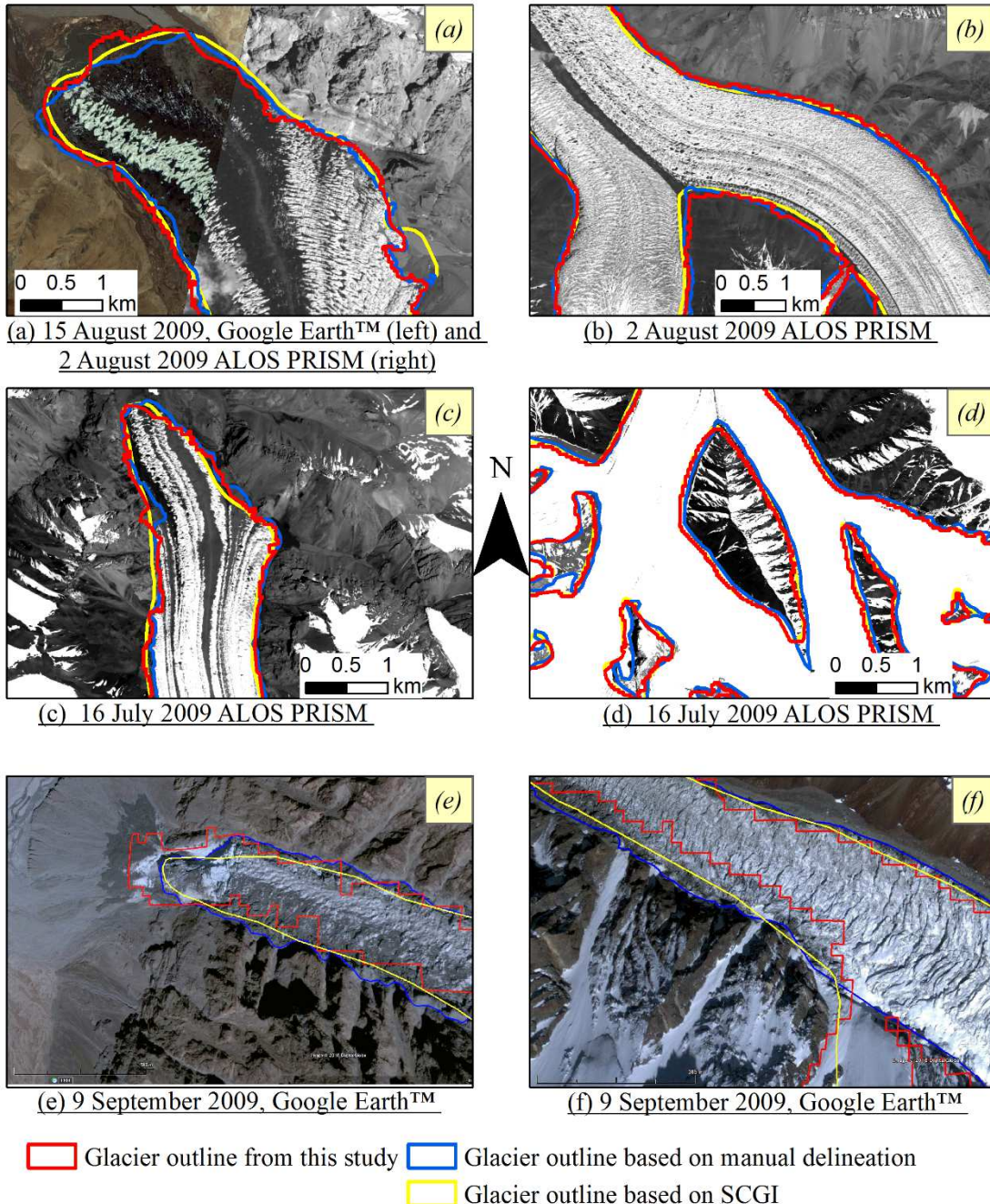


Figure 4.5.3- Comparisons of the selected debris-covered glaciers outlines derived from proposed method with reference datasets. (a) and (b) Teram Kangri glacier. (c) and (d) Kulqun glacier. (e) and (f) Small debris-covered glacier.

FINAL STAGE OF THE NEW METHOD FOR MAPPING OF DEBRIS-COVERED  
GLACIERS — BASED ON THE COMBINATION OF [TIR/(NIR/SWIR)] BAND  
RATIO AND GEOMORPHOMETRIC PARAMETERS

---

Table 4.5.1 Comparisons of Yengisogat glacier area derived from this study, Second Chinese Glacier Inventory (SCGI) and manual delineation of Google Earth™ images.

Yengisogat glacier	This study (A) km <sup>2</sup>	SCGI (B) km <sup>2</sup>	Google Earth™ (C) km <sup>2</sup>	(A-B)	(A-C)
Overall	361.75	359.05	363.92	+0.75	-0.6
Terminus	8.54	8.51	8.89	+0.35	-3.9
Middle	30.35	29.64	30.33	+2.3	+0.07
Upper	322.86	320.9	324.7	+0.6	-0.56

Notes: Positive and negative value showing the percentage of differences in the area was larger (+) or smaller (-) than the reference area.

Table 4.5.2 Comparisons of Teram Kangri glacier area derived from this study, Second Chinese Glacier Inventory (SCGI) and manual delineation of ALOS PRISM images.

Teram Kangri glacier	This study (A) km <sup>2</sup>	SCGI (B) km <sup>2</sup>	ALOS PRISM (C) km <sup>2</sup>	(A-B)	(A-C)
Overall	110.91	110.4	114.27	+0.5	-3
Terminus	8.473	8.46	8.22	+0.2	+3
Middle	10.297	10.2	10.43	+0.9	-1.3
Upper	92.14	91.74	95.62	+0.43	-3.6

Notes: Positive and negative value showing the percentage of differences in the area was larger (+) or smaller (-) than the reference area.

FINAL STAGE OF THE NEW METHOD FOR MAPPING OF DEBRIS-COVERED GLACIERS — BASED ON THE COMBINATION OF [TIR/(NIR/SWIR)] BAND RATIO AND GEOMORPHOMETRIC PARAMETERS

---

Table 4.5.3 Comparisons of Kulqin glacier area derived from this study, Second Chinese Glacier Inventory (SCGI) and manual delineation of ALOS PRISM images.

Kulqin glacier	This study (A) km <sup>2</sup>	SCGI (B) km <sup>2</sup>	ALOS PRISM (C) km <sup>2</sup>	(A-B) %	(A-C) %
Overall	39.85	39.55	39.6	+0.75	+0.63
Terminus	2.3	2.26	2.32	+1.74	-0.9
Middle	3.7	3.79	3.81	-2.4	-2.8
Upper	33.85	33.5	33.47	+1	+1.1

Notes: Positive and negative value showing the percentage of differences in the area was larger (+) or smaller (-) than the reference area.

Table 4.5.4 Comparisons of Small debris-covered glacier area derived from this study, Second Chinese Glacier Inventory (SCGI) and manual delineation of Google Earth™ images.

Small debris-covered	This study (A) km <sup>2</sup>	SCGI (B) km <sup>2</sup>	Google Earth™ (C) km <sup>2</sup>	(A-B) %	(A-C) %
Overall	3.30	3.42	3.65	-3.5	-9.5
Terminus	0.426	0.4	0.43	+6.1	-0.9
Middle	0.78	0.88	0.92	-11	-15
Upper	2.094	2.14	2.3	-2.1	-8.9

Notes: Positive and negative value showing the percentage of differences in the area was larger (+) or smaller (-) than the reference area.

FINAL STAGE OF THE NEW METHOD FOR MAPPING OF DEBRIS-COVERED  
GLACIERS — BASED ON THE COMBINATION OF [TIR/(NIR/SWIR)] BAND  
RATIO AND GEOMORPHOMETRIC PARAMETERS

---

Table 4.5.5 Comparisons of clean glacier-ice area derived from this study, Second Chinese Glacier Inventory (SCGI) and manual delineation of Google Earth™ images.

Clean glacier-ice	This study (A) km <sup>2</sup>	SCGI (B) km <sup>2</sup>	Google Earth™ (C) km <sup>2</sup>	(A-B)	(A-C)
Kyagar	94.86	94.45	92.2	+0.43	+2.8
Small clean glacier-ice	6.94	6.93	7.09	+0.2	-2.1

Notes: Positive and negative value showing the percentage of differences in the area was larger (+) or smaller (-) than the reference area.

Table 4.5.6 Comparisons between glacier areas derived from proposed method and SCGI  
(glacier area unit: km<sup>2</sup>).

Regions	This Study	SCGI	Area difference (%)
1	238.83	240.42	-0.66
2	322.76	334.67	-3.5
3	243.21	245.1	-0.77
4	716.21	705.62	+1.48
5	226.41	223.06	+1.47
Total	1747.42	1748.87	-0.1

Notes: Positive and negative value showing the percentage of differences in the area was larger (+) or smaller (-) than the reference area.

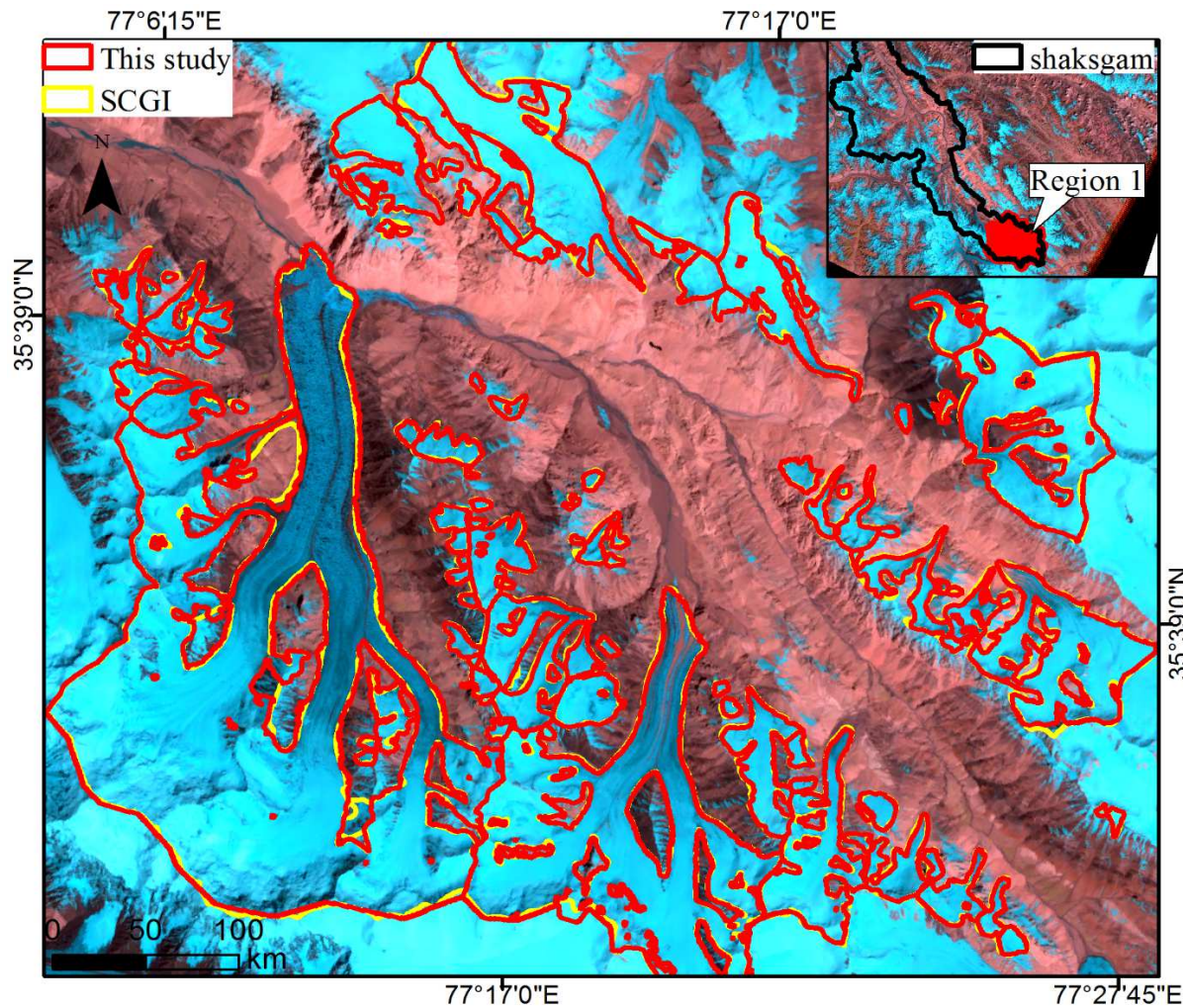


Figure 4.5.4- Comparison between glacier outlines derived from proposed method and SCGI in the case of the region (1). Landsat images: R = shortwave infrared band, G = red band, B = green band were acquired from 4 August 2009. Total glacier area of the region (1) from proposed method and SCGI are given in Table 4.5.6.

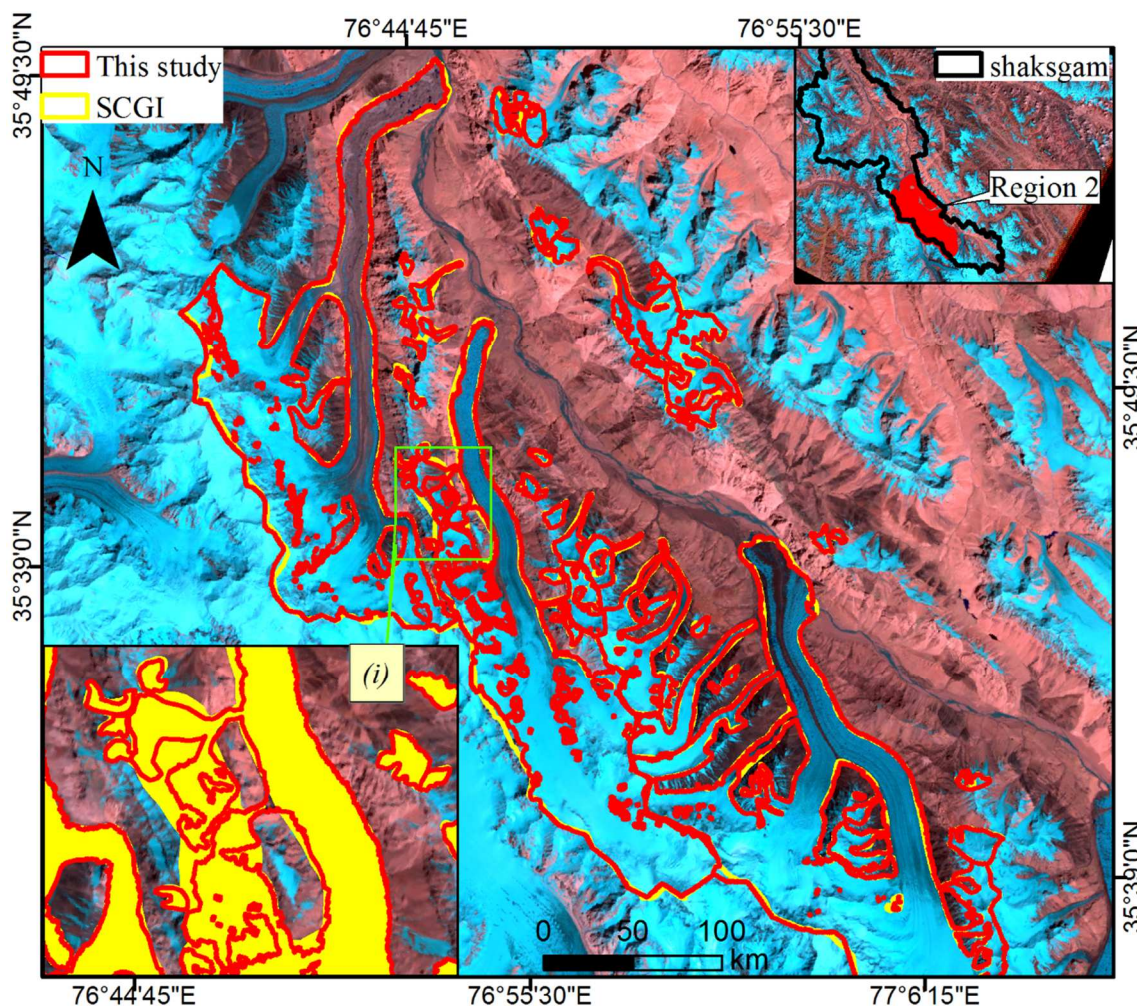


Figure 4.5.5- Comparison between glacier outlines derived from proposed method and SCGI in the case of the region (2). Landsat images: R = shortwave infrared band, G = red band, B = green band were acquired from 4 August 2009. Total glacier area of the region (2) from proposed method and SCGI are given in Table 4.5.6. (i) showing the main area difference between result from proposed method and SCGI.

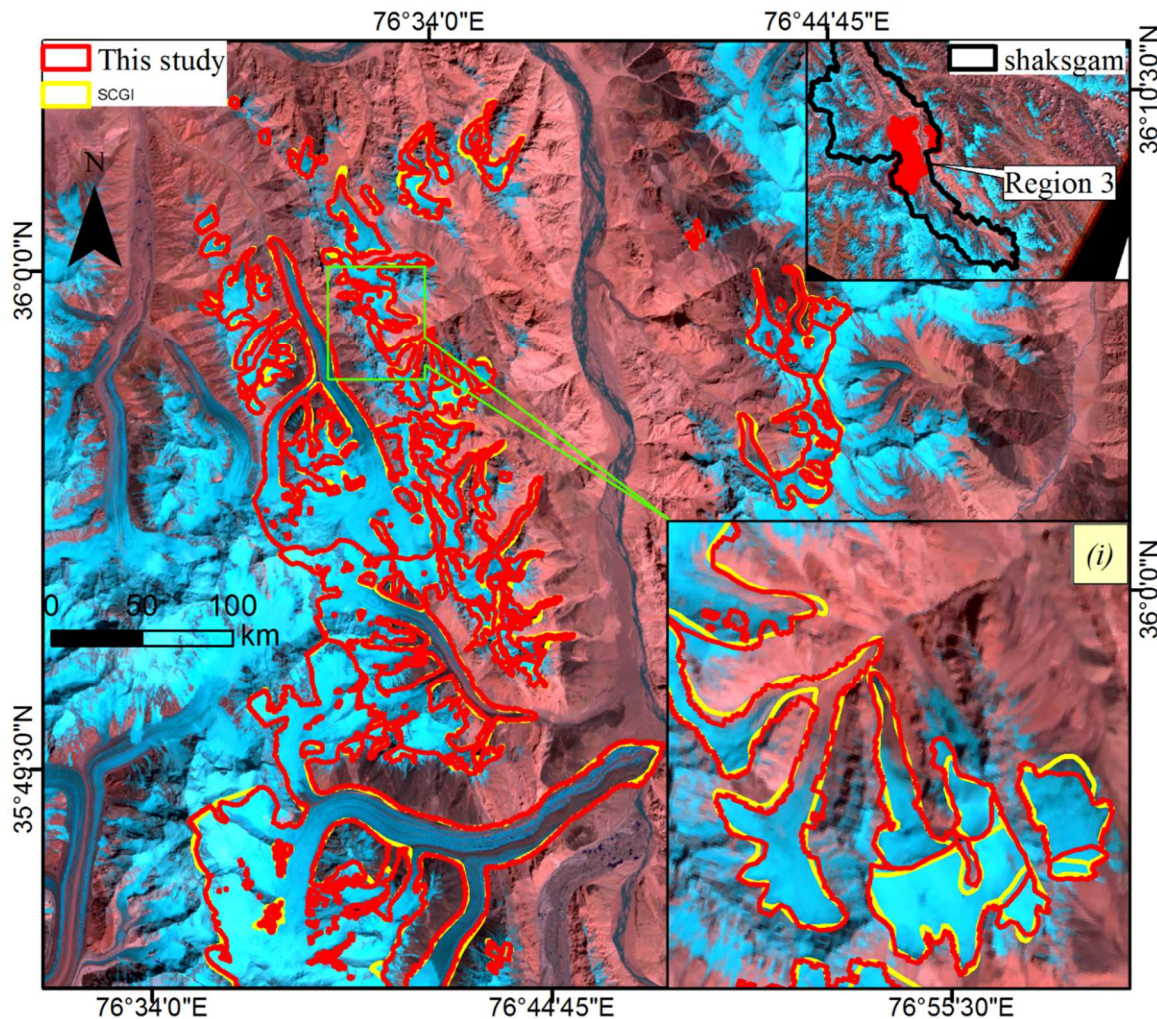


Figure 4.5.6- Comparison between glacier outlines derived from proposed method and SCGI in the case of the region (3). Landsat images: R = shortwave infrared band, G = red band, B = green band were acquired from 4 August 2009. Total glacier area of the region (3) from proposed method and SCGI are given in Table 4.5.6. (i) Closer view of selected area (green mark).

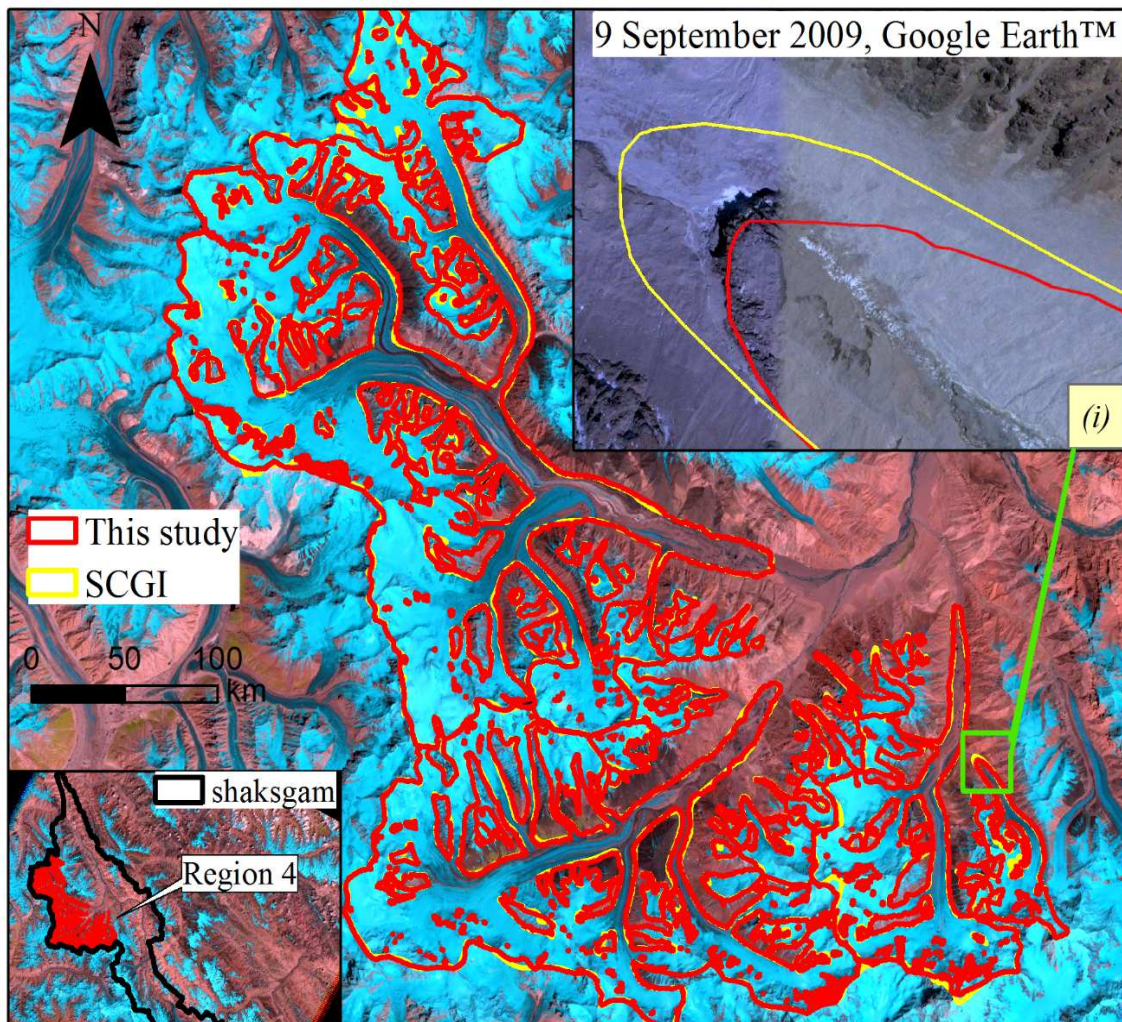


Figure 4.5.7- Comparison between glacier outlines derived from proposed method and SCGI in the case of the region (4). Landsat images: R = shortwave infrared band, G = red band, B = green band were acquired from 4 August 2009. Total glacier area of the region (4) from proposed method and SCGI are given in Table 4.5.6. (i) showing the main area difference between result from proposed method and SCGI.

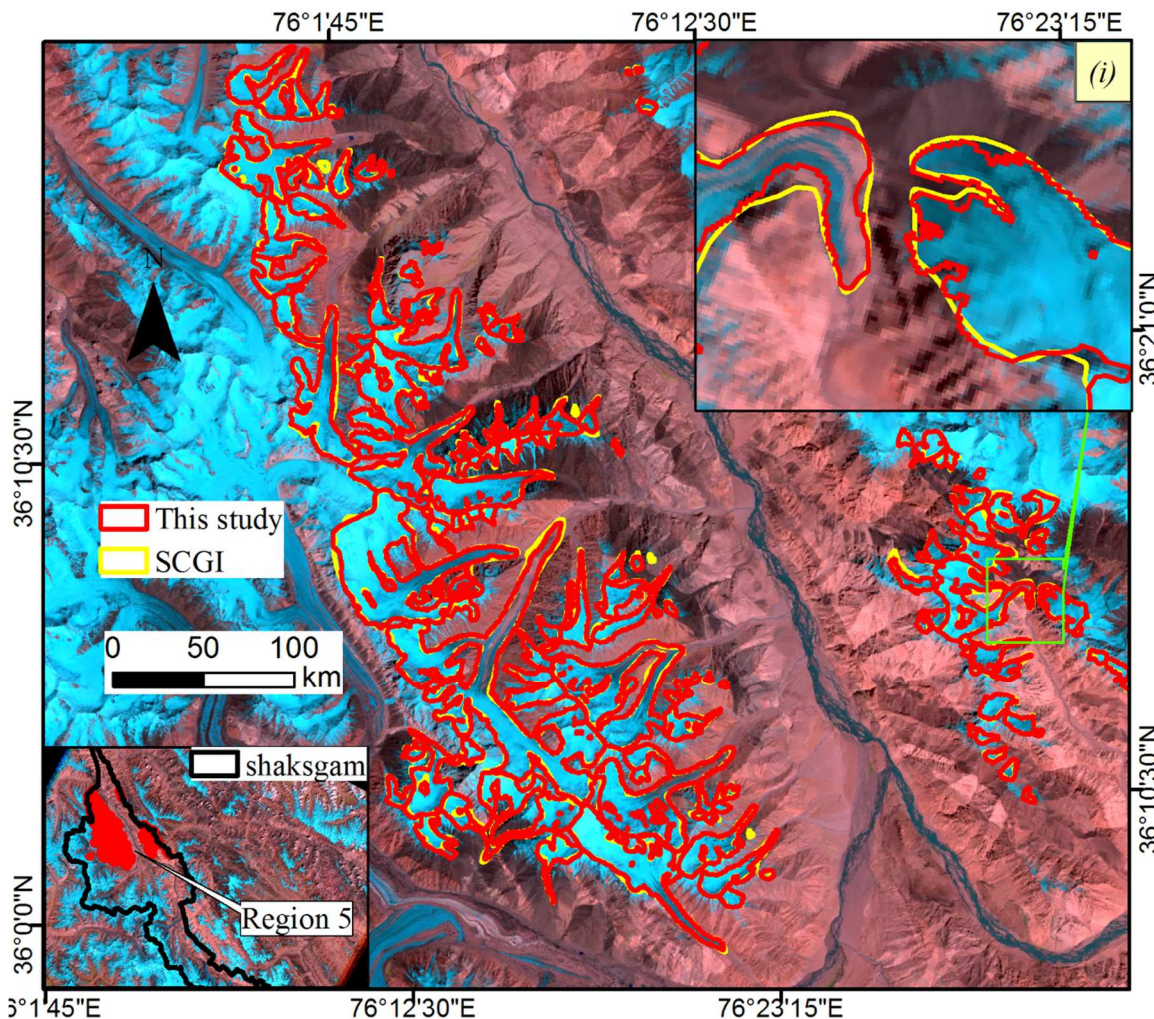


Figure 4.5.8- Comparison between glacier outlines derived from proposed method and SCGI in the case of the region (5). Landsat images: R = shortwave infrared band, G = red band, B = green band were acquired from 4 August 2009. Total glacier area of the region (5) from proposed method and SCGI are given in Table 4.5.6. (i) Closer view of selected area (green mark).

Similarly, glacier outlines based on RGI (Pfeffer et al. 2014) and manual delineation of Lituya glacier using high-resolution Google Earth™ image (similar data with Landsat images are only available for terminus part of Lituya glacier, Figure 4.5.10.d) were used to validate the results from Glacier Bay. Glacier outlines (results and reference data sets) were separated into three regions which are terminus part, middle part, and upper part for more detailed comparisons (Figure 4.5.9 and Figure 4.5.10, Table 4.5.7-12).

Table 4.5.7 Comparisons of Fairweather glacier area derived from this study and Randolph Glacier Inventory (RGI) (Figure 4.5.9 a-b), (glacier area unit: km<sup>2</sup>).

Fairweather glacier	This study (A)	RGI (B)	A-B (%)
Overall	203.7	211.5	-3.6
Terminus	51.29	53.60	-4.3
Middle	54.46	56.30	-3.2
Upper	97.95	101.60	-3.5

Table 4.5.8 Comparisons of Desolation glacier area derived from this study and Randolph Glacier Inventory (RGI) (Figure 4.5.9 c-d), (glacier area unit: km<sup>2</sup>).

Desolation glacier	This study (A)	RGI (B)	A-B (%)
Overall	26.5	27.3	-2.9
Terminus	1.76	1.83	-3.8
Middle	3.76	3.91	-3.8
Upper	20.98	21.56	-2.6

Notes: In Table 4.5.8-9, positive and negative value showing the percentage of differences in the area was larger (+) or smaller (-) than the reference area.

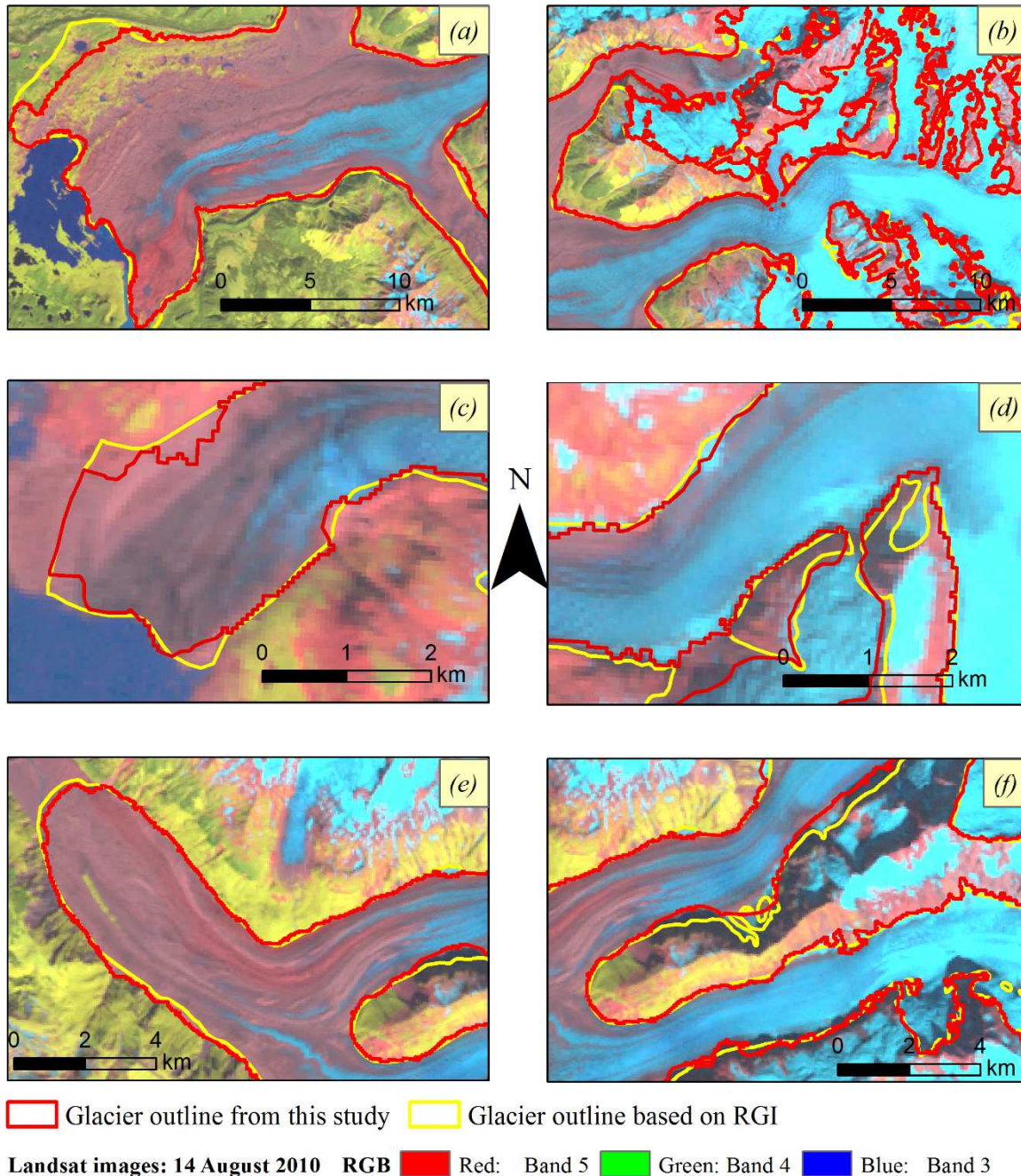


Figure 4.5.9- Comparisons of the Fairweather, Desolation and Crillon glacier outlines (Glacier Bay, Alaska) derived from proposed method with reference datasets. (a) and (b) Fairweather glacier. (c) and (d) Desolation glacier. (e) and (f) Crillon glacier.

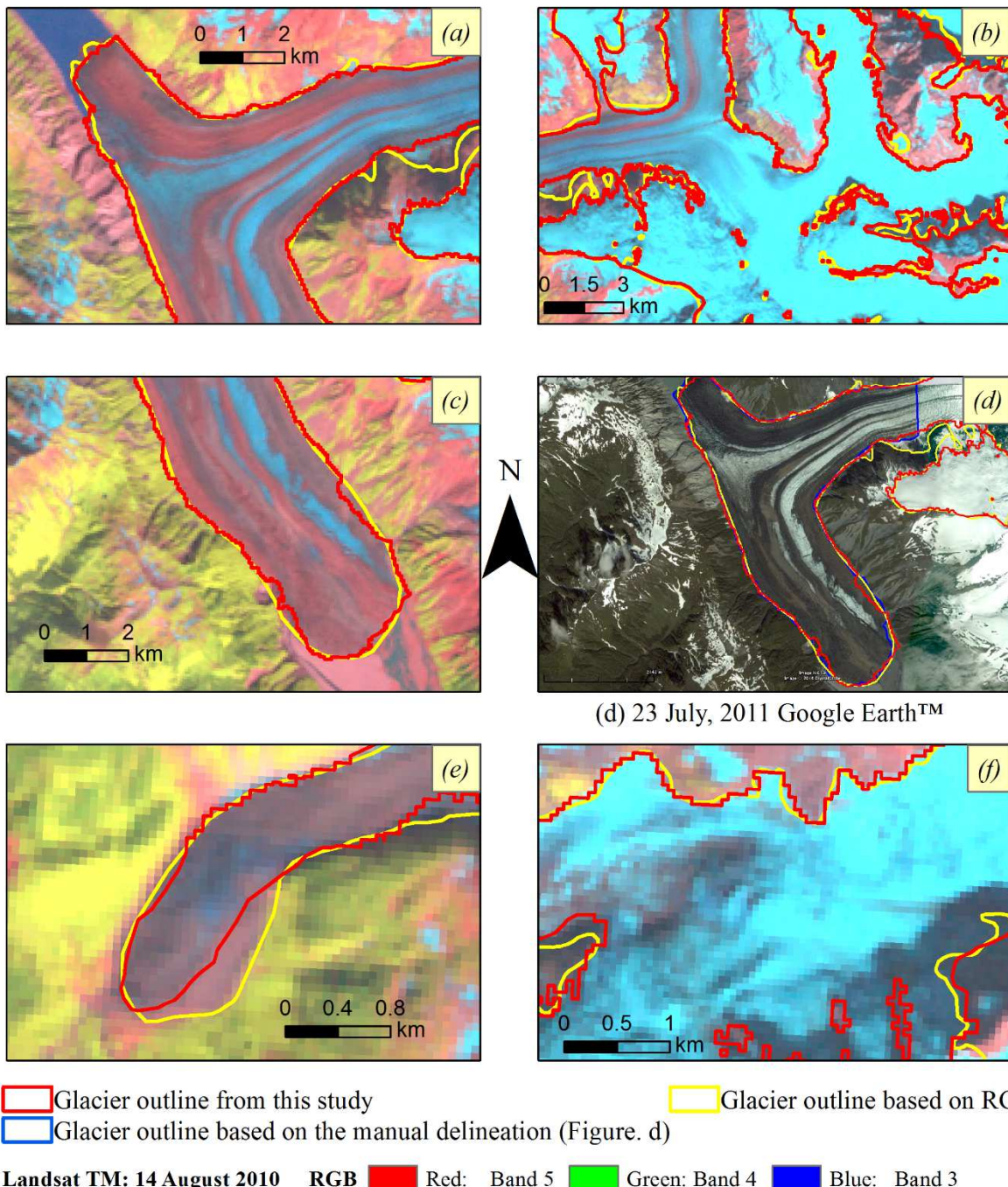


Figure 4.5.10- Comparisons of the Lituya and Cascade glacier outlines (Glacier Bay, Alaska) derived from proposed method with reference datasets. (a)-(d) Lituya glacier. (e) and (f) Cascade glacier.

FINAL STAGE OF THE NEW METHOD FOR MAPPING OF DEBRIS-COVERED  
GLACIERS — BASED ON THE COMBINATION OF [TIR/(NIR/SWIR)] BAND  
RATIO AND GEOMORPHOMETRIC PARAMETERS

---

Table 4.5.9 Comparisons of Crillon glacier area derived from this study and Randolph Glacier Inventory (RGI) (Figure 4.5.9 e-f), (glacier area unit: km<sup>2</sup>).

Crillon glacier	This study (A)	RGI (B)	A-B (%)
Overall	88.6	87.28	+1.5
Terminus	13.31	13.09	+1.65
Middle	10.19	10.69	-4.4
Upper	65.1	63.5	+2.4

Table 4.5.10 Comparisons of Lituya glacier area derived from this study, Randolph Glacier Inventory (RGI) and Google Earth images™ (Figure 4.5.10 a-d), (glacier area unit: km<sup>2</sup>).

Lituya glacier	This study (A)	RGI (B)	Google Earth™ (C)	A-B (%)	A-C (%)
Overall	76.65	76.62	\	+0.03	\
Terminus	11.89	11.99	11.96	-0.8	-0.6
Middle	6.1	6.37	\	-4.2	\
Upper	58.66	58.26	\	+0.7	\

Table 4.5.11 Comparisons of Cascade glacier area derived from this study and Randolph Glacier Inventory (RGI) (Figure 4.5.10 e-f), (glacier area unit: km<sup>2</sup>).

Cascade glacier	This study (A)	RGI (B)	A-B (%)
Overall	5.7	6.09	-6.5
Terminus	0.39	0.48	-11
Middle	1.36	1.47	-7
Upper	3.95	4.14	-4.5

Notes: In table 4.5.9-11, positive and negative value showing the percentage of differences in the area was larger (+) or smaller (-) than the reference area.

## **4.6 Results and discussions**

In this section, the accuracy of the glacier outlines derived from the proposed method is reported and discussed. Visual comparisons with the glacier inventories (SCGI and RGI), high-resolution ALOS PRISM and Google Earth™ images and the velocity maps showed that the glacier boundaries derived from the presented method had high similarity to the reference data sets (Figure 4.5.1-10).

### **Glacier outlines derived from presented method — Shaksgam Valley**

Area measurement of selected glacier outlines derived from presented method had less than 9.5% area differences compared to the glacier area estimated from SCGI and manual delineation, respectively (Figure 4.5.1-3 and Table 4.5.1-5).

Specifically, in the case of Yengisogat glacier, there was a 0.75% (larger) difference between the glacier area (overall glacier area) measurement from the proposed method and the SCGI measurement and a 0.6% (smaller) difference in the area compared to the manual delineation (Figure 4.5.2 and Table 4.5.1). Less than 2.5% area difference was found comparing the result with reference data sets in separated regions within the Yengisogat glacier (Table 4.5.1).

Similarly, Teram Kangri glacier derived from proposed method differs in the area (overall glacier area) by 0.5 % (larger) and 3% (smaller) compared to SCGI and

manual delineation (Figure 4.5.3.a-b and Table 4.5.2). There is less than 3.6% area difference in separated regions of Teram Kangri glacier derived from proposed method and reference data sets (Table 4.5.2).

Mapped area (overall glacier area) of Kulqin glacier based on proposed method varies by 0.63% (larger) with respect to manual delineation and by 0.75% (larger) compared to SCGI (Figure 4.5.3.c-d and Table 4.5.3). In carefully analyzing of separated regions of Kulqin glacier derived from proposed method and reference data sets, less than 2.8% area differences were found (Table 4.5.3).

In the case of the small debris-covered glacier, largest area (overall glacier area) discrepancy (9.5% smaller) was found between the mapped glacier area and the reference glacier area (Figure 4.5.3.e-f and Table 4.5.4). In detail, less than 15% area differences (separated regions within glacier) were measured from result comparing with reference data sets (Table 4.5.4).

On the other hand, one of the selected clean glacier ice- Kyagar glacier has 2.8% (larger) and 0.43 % (smaller) area differences compared to the reference datasets.

In the case of another one- small clean glacier-ice, 0.2% (larger) and 0.21% (smaller) area discrepancy were found between proposed method with SCGI and manual delineation (Figure 4.5.1 and Table 4.5.5).

Furthermore, total glacier area of Shaksgam Valley was separated to five sub-regions to allow comparing in more detailed scale comparison with SCGI.

Comparisons results based on the total glacier area and glacier area from separated five sub-regions derived from method and SCGI showed the less than 3.5% area differs (Figure 4.5.4-8 and Table 4.5.5).

### **Glacier outlines derived from presented method — Glacier Bay**

The RGI and manual delineation based on the Google Earth™ image (just for Lituya glacier terminus region) were used to evaluate the results obtained from this study. Glacier areas in the reference maps were compared with the areas of the glaciers calculated using the presented method. The accuracy assessment revealed that the glacier boundaries derived from the presented method was quite similar to the reference data (Figure 4.5.9-10 and Table 4.5.7-11). Specifically, less than 6.5%, and 11% differences were found between the glacier area (overall glacier area and separated regions of the glacier) measurements from the presented method and the reference datasets (Figure 4.5.9-10 and Table 4.5.7-11).

Analyzing of the validation results indicated that selected glaciers outlines derived from the presented method are satisfying for clean glacier-ice and larger debris-covered glaciers in both study areas. However, the small differences (less than 4.5%) occurred probably in heavy debris covered terminus regions, and middle part of the debris-covered glacier area. These difference occurred due to reference data sets. Because of reference data were generated from the use of

closer date of images (Landsat and Google Earth™) by different methods with this study. Notably, inaccuracies were increased reaching to the middle part of the glacier, due to the increase of steepness of glacier slope and the very complex topography of the glaciers and their adjacent moraines. These inaccuracies occurred due to coarse resolution of the ASTER GDEM and Landsat TIR data. Especially, resolution of ASTER GDEM is not sufficient to reflect the different crucial surface (such as adjacent moraines in the glacier margin side) characteristics clearly. In the case of glaciers outline results from glacier bay, IFSAR DEMs showed the higher resolution and quality which can able to describing the very complex topography of the glaciers and their surroundings. However, vegetation cover on the surface of glacier terminus (Fairweather glacier, Figure 4.5.9) and near the glacier margin was the main source of inaccuracies in the case of glacier mapping in Glacier Bay. Moreover, critical surface characteristics of the debris-covered glaciers and their adjacent moraines may change in the acquired time of IFSAR DEMs, because of Fairweather Range is notable for large landslides (Post 1967).

The accuracy assessment revealed that the small debris-covered glacier boundaries (in both study areas) derived from the presented method had larger area differences (less than 15%) compared to larger glaciers. This misclassification might be attributed to size effect (resolution of data used in this study). Such as, this type of small glacier is often located in a steep, narrow valley

and resulted formation of the glacier has very narrow-width. For example, the width of Cascade glacier has

approximately 440 m, on the other hand, the width of a small debris-covered

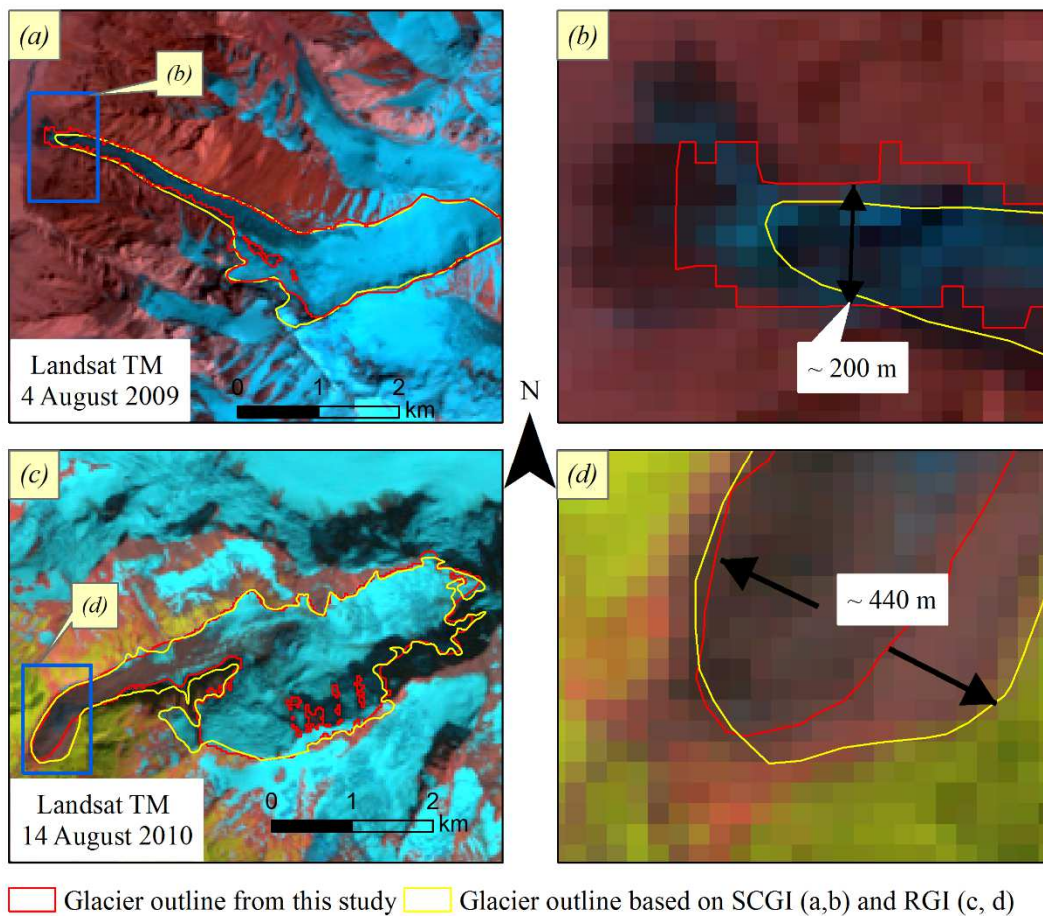


Figure 4.6.1- Small debris-covered glaciers which are studied in this study. (a) Small debris-covered glacier in Shaksgam Valley. (b) Closer view of the blue marked area in (a). (c) Cascade glacier in Glacier Bay. (d) Closer view of the blue marked area in (c).

glacier in Shaksgam Valley has about 200 m (Figure 4.6.1). Thus, only used several pixels' information (6~14 pixels for VNIR-SWIR and 1~4 pixels for TIR) to distinguished supraglacial debris from adjacent rock debris is challenged using

the presented method. A major problem for the presented method for mapping small debris-covered glaciers due to the resolution of Landsat bands (30 m ~ 120 m) too coarse to distinguish these debris moraines from glacier tongue.

Overall glacier outlines derived from presented method showed good agreement and high similarity when compared with SCGI (Figure 4.5.4-8 and Table 4.5.6). High similarity of the two results from the present study and SCGI is probably attributable to the glacier outlines derived from similar dates of Landsat images and band ratio technique (Guo et al. 2015). However, the main differences appeared in the delineation of accumulation region of the glacier (Figure 4.5.5.i). This differences might be caused by the difference of snow cover at observation times. The Landsat images used in SCGI has more fresh snow cover than that used in this study. Furthermore, there has disparity detection of glacier terminus position between result derived from the presented method and SCGI (Figure 4.5.7.i). This area difference may come from the Landsat data (23 August 2010) which was used for digitizing this glacier in SCGI (Figure 4.5.7.i). Glacier terminus region was moved (advanced) in that time period of data used in SCGI, compared to Landsat data employed in this study. However, detailed comparisons of glacier outlines indicated that in the case of some parts of Yengisogat glacier margin derived by the final stage of method is closer to glacier margin derived from high resolution of Google Earth images and velocity maps than SCGI (Figure 4.6.2). This is occurred due to the distinct supraglacial features in these

areas was roughly identifiable by manually interpretation (debris-covered glacier outlines in SCGI were manually delineated based on Landsat images from 2009). On other hand, result from final stage of method was generated based on thermal, spectral and landscape properties of supraglacial debris. Therefore, result from final stage of method gives the relative better result compared to the SCGI in the case of distinct supraglacial features are indistinguishable by manually based on the Landsat images.

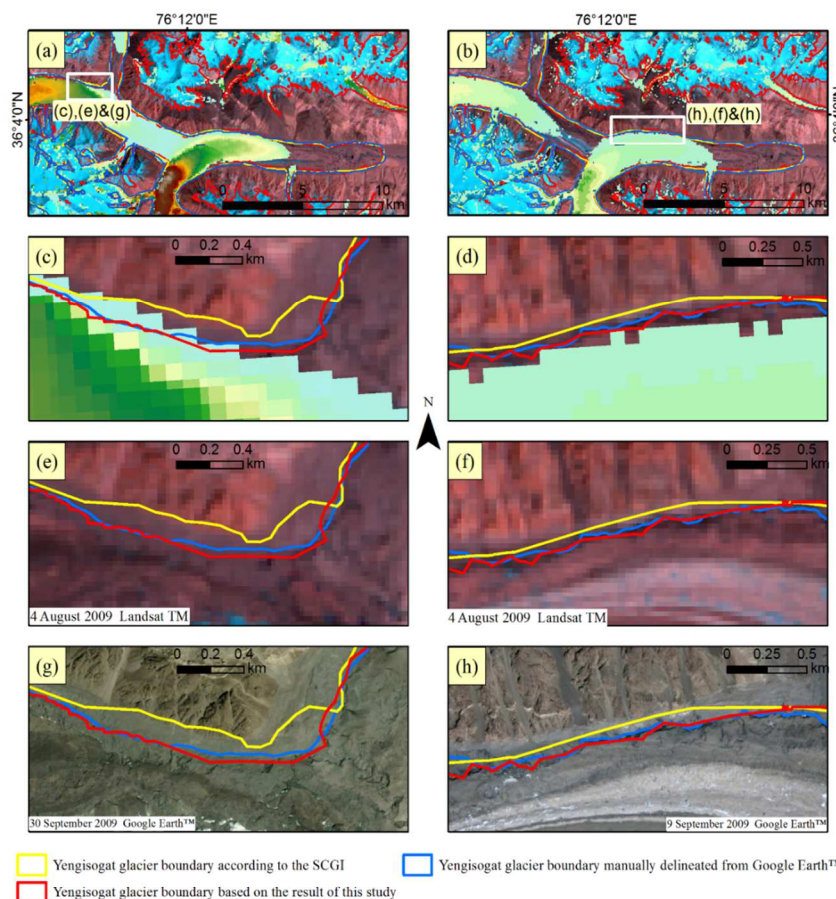


Figure 4.6.2- Examples of differences in Yengisogat glacier outlines. (a) and (c) Yengisogat glacier outlines overlaid on glacier velocity map derived from SAR data during 2007 to 2011 which provided by Rankl et al. (2014). (b) and (d) Yengisogat glacier outlines overlaid on glacier velocity map derived from TerraSAR-X SM image pairs (16 June 2009 to 12 September 2009 and 24 December 2009 to 15 January 2010) provided by Rankl et al. (2014). (e) and (f) Yengisogat glacier outlines overlaid on Lansat images used in this study. (f) and (h) Yengisogat glacier outlines overlaid on high resolution images from Google Earth™.

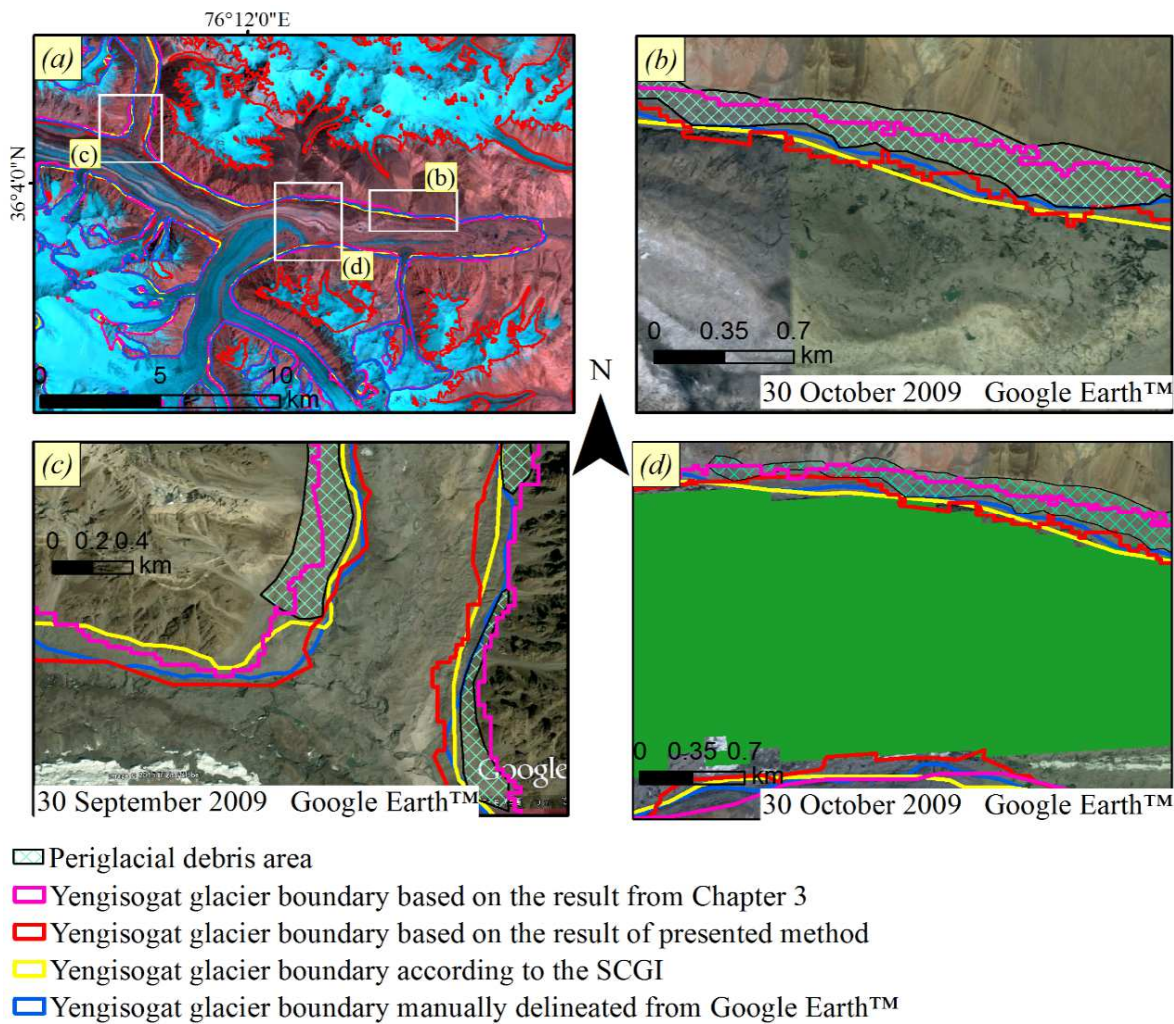


Figure 4.6.3- Examples of overestimated Yengisogat glacier outline reported in Chapter (3) comparing with results derived from presented method and references data sets [(b)–(d)]. (a) The overall location of the image (b)–(d). (d) Glacier velocity map derived from Terra SAR-X SM image pairs (June 16, 2009, to September 12, 2009, and December 24, 2009, to January 15, 2010) provided by Rankl et al. (2014) overlaid on the Google Earth™ image.

Specially, regarding to clarify the presented method is improved from its early stage form (Chapter 3) which involved combining the [TIR/(NIR/SWIR)] band ratio image with slope faces information, Yengisogat glacier outlines derived

from chapter 3, SCGI, manual delineation using Google Earth™ and presented method were comparing each other (Figure.4.6.3). Figure.4.6.3 shows that the Yengisogat glacier margin derived by the presented method is closer to that of SCGI or Google Earth™ than result derived from its early stage form (Chapter 3).

Table 4.6.1 Comparison of Yengisogat glacier area from four different studies

Yengisogat glacier	Chapter 3 (A) km <sup>2</sup>	SCGI (B) km <sup>2</sup>	Google Earth™ (C) km <sup>2</sup>	This study (D) km <sup>2</sup>	(A-B)	(A-C)	(D-B)	(D-C)
Terminus	8.82	8.51	8.89	8.54	+3.5	-0.79	+0.35	-3.9
Middle	32.04	29.64	30.33	30.35	-7.5	+5.3	+2.3	+0.07
Upper	321.24	320.9	324.7	322.86	+0.1	-1	+0.6	-0.56
Overall	362.1	359.0	363.92	361.75	+0.84	-0.5	+0.75	-0.6

Notes: Positive and negative value showing the percentage of differences in the area was larger (+) or smaller (-) than the reference area.

At the same time, comparisons of the areas (overall and separated areas) measurement of Yengisogat glacier (Table 4.6.1) indicated that detection of middle part of glacier outline (which appearing very complex topography of the glaciers and their adjacent moraines) was a significant improvement.

In particular, some of the misclassified areas occurred in the previous approach (Chapter 3) in the area where the terrain of periglacial debris (near the glacier

FINAL STAGE OF THE NEW METHOD FOR MAPPING OF DEBRIS-COVERED GLACIERS — BASED ON THE COMBINATION OF [TIR/(NIR/SWIR)] BAND RATIO AND GEOMORPHOMETRIC PARAMETERS

---

margin side) transitions to the supraglacial debris (due to their have similar slopes) (Figure 4.6.3). Also defined glacier slope faces values derived from 90 m resolution of SRTM limited the method to single glacier (Table 4.6.2). On the other hand, the result of the final stage of the method was improved even used larger slope faces value (derived from 30 m resolution of ASTER GDEM) than early stage of the method, because of curvatures information plays the important role (Table 4.6.2). Like, landscape variation of the periglacial debris area's (glacier margin side) transition to supraglacial debris can be accurately observed from curvature information (Figure 4.4.2.1.d and Figure 4.4.2.2.d, yellow area).

Table 4.6.2 Comparison of data used in the early and final stage of method.

Study	Early stage	Final stage
Data used	Landsat TM	
	SRTM (90 m)	ASTER GDEM (30 m)
Method	[TIR/(NIR/SWIR)] + <b>Slope (&lt;12°)</b>	[TIR/(NIR/SWIR)] + <b>[(Plan + Profile) + Slope (&lt; 28°)]</b>

Therefore, curvature can be of used to eliminated periglacial debris in the glacier margin side and combination with large slope faces allow to the final stage of the method can apply to the larger glaciated region. According to the visual comparison and area measurement (Figure 4.6.3 and Table 4.6.1), the final

Yengisogat glacier boundary derived by the presented method was considered to be more accurate than that derived from its early stage form (Chapter 3).

The band-thresholded of TIR/NIR/SWIR image and the results of the geomorphometric analysis complement each other, as the TIR/NIR/SWIR image could detect the actual glacier terminus, whereas the geomorphometric analysis allowed the glacier margin to be detected more accurately. In addition, in this study, threshold range values are selected based on terrain features and spectral characteristics of all of the glaciers in the study areas. Thus, presented approach able to map glaciers in the larger glacierized region.

There have several advantages of the presented method compared to the existing approaches. As a first, [TIR/(NIR/SWIR)] band ratio image included the spectral and thermal properties of supraglacial debris, whereas in other studies, for only thermal information is used for extraction of supraglacial debris. Secondly, in geomorphometric analysis step, mean slope value is defined (covered the almost all glaciers) as first, then combining with result derived from the clustering of plan curvature and profile curvature. Mean slope map avoids the final supraglacial debris overestimated and essential help for determination of glacier terminus.

In past studies found that supraglacial debris whether in illuminated or shaded areas, it has colder surface temperatures than the periglacial debris regions

(Shukla et al. 2010b, Karimi et al. 2012). However, this result is based on single glacier basin ( $< 200 \text{ km}^2$ ). In contrast, results from this study (larger glacier basin area  $< 4646 \text{ km}^2$ ) showed that some cases such as periglacial debris under the deep shadow and at higher elevation might also have similar surface temperatures as supraglacial debris regions. This similarity might be caused by valley bed under the deep shadow during most of the sunny day and cold temperature in higher elevation. Also, wind circulation such as katabatic winds circulating within a cold glacier valley might be another reason (Hewitt et al. 2014). However, classification errors from these factors can be minimized when combining the [TIR/(NIR/SWIR)] band ratio imagery with results from the geomorphometric analysis.

Glacier velocity maps provided by Rankl et al. (2014), were used to evaluate visually the part of Yengisogat glacier outline derived by the presented method. In terms of the Yengisogat glacier terminus region has a lower motion in the estimated time period which resulted in no clear ice flow information detected by the SAR feature tracking method. However, velocity maps can be considered as a good reference data especially in the parts of the supraglacial debris region that are in motion.

## **4.7 Limitation of method**

There are several limitations in the proposed method, which are following as:

1. [TIR/(NIR/SWIR)] band ratio image misclassified vegetation cover near the glacier tongue as supraglacial debris. This is particularly in the case for debris-covered glacier covered by vegetation.
2. The final glacier outlines were generated from a combination of classified maps derived by thresholding of [TIR/(NIR/SWIR)] band ratio image and geomorphometric analysis. Therefore, defining threshold values is a critical step for delineation of actual debris-covered glacier boundary. Based on our experiences from this study, we recommended that threshold ranges for delineation of supraglacial debris region can be defined using a density slice range of 20 or more, and then, merging the similar classes by comparing density-sliced maps with Landsat composite images.
3. Good quality and higher resolution of DEM was considerable importance to the accurate delineation of debris-covered glacier using the present method. However, as a result of ASTER GDEM resolution is too coarse to reflect the different crucial surface characteristics clearly, such as distinct terrain surface of debris moraine or supraglacial debris were too small or missing in the DEM. In addition, ASTER GDEM was generated from

many pairs of ASTER images acquired during different periods. Hence, the typical debris-covered glacier terrain characteristics are not sufficiently represented, and this limits the accuracy of glacier outlines.

4. Small debris-covered glaciers and rock glaciers are the major limitations of presented method. Especially, in the case of rock glaciers, because of a much smaller size compared to the debris-covered glacier and its overall glacier area entirely covered by rocky materials caused difficult to detection using medium-resolution satellite imagery.
5. Furthermore, manual editing steps are still required in debris-covered glacier mapping method described in this chapter, such as river channel which is connected with glacier tongue and isolate areas that are outside the main body of the glacier.

## **4.8      Conclusions**

In this chapter, we presented an advanced approach to map the glaciers in the Shaksgam Valley and Glacier Bay using optical, thermal images (Landsat TM) and DEMs (ASTER GDEM V2 and IFSAR). Similar to a previous study in Chapter 3, a [TIR/(NIR/SWIR)] band ratio image is used to generate preliminary maps of “supraglacial debris” and “clean ice glacier ice.” However, unlike the previous work (Chapter 3), this map is combined with additional geomorphometric information including mean slope, plan curvature, and profile curvature because these geomorphometric parameters can also help identify distinctive glacier landscape properties. Overall, glacier outlines (larger debris-covered glacier and clean glacier-ice) derived from final stage of method have higher similarity from visual comparision and less than 5% glacier area discrepancy copmared with reference data sets. The proposed method could map the Yengisogat glacier with a higher accuracy than the previous approach. Also, the developed combination method can map the glaciers in the large region. However, mapping of small debris-covered glaciers is still challenged using present method due to their size is much smaller than the resolution of data used for glacier mapping. Nevertheless, the presented method was similar in terms of accuracy and faster than manual delineation despite the final manual corrections still required.

---

## Chapter 5 General conclusions

---

Observations of clean glacier-ice using remote sensing technology have been widely applied in global glacier monitoring programs such as GLIMS (Global Land Ice Measurements from Space). However, the number of studies focused on monitoring of debris-covered glaciers has been sparse compared to the number on clean glacier-ice. Previous studies observing debris-covered glaciers have implemented various methods based on the remote sensing technique, such as debris-covered glacier boundary mapping over limited areas, glacier surface velocity measurement, and debris cover variation over time. One of the main reasons for the small number of studies using remote sensing of debris-covered glaciers is that existing methods have limitations in terms of distinguishing the actual supraglacial debris area from the adjacent valley rock. Moreover, the surged type of supraglacial debris termini cannot be detected by surface velocity measurement methods. Therefore, developing a new approach based on remote sensing will be a useful tool for further understanding of debris-covered glaciers systems. Moreover, since the number of debris-covered glaciers is expected to increase, accurate assessment of debris-covered glaciers and their temporal changes are of vital importance to the understanding of local climate variations, especially planning and management of water resources.

Consequently, this thesis concentrated on exploitation and implementation of new approaches for accurate delineation of debris-covered glaciers based on the spectral, thermal, and terrain properties of the glacier, and testing of an existing approach to assess its effectiveness. The development and examination of proposed new methods in this thesis is intended to highlight the applicability of the new method for monitoring debris-covered glaciers. Thus, the method can be used to complete multi-temporal glacier inventories, which are still lacking for many glacierized regions.

Finally, the results highlight the successes and failures of the new approaches. For example, a method (chapter 3) involving [TIR/(NIR/SWIR)] band ratio images combined with slope information was able to map debris-covered glaciers, which are challenging for existing methods. However, this approach was limited to monitoring of a single glacier or glaciers that have a similar slope; therefore, this method is recommended for observations of a single glacier. In contrast, an approach involving [TIR/(NIR/SWIR)] band ratio images combined with additional geomorphometric parameters allowed mapping of debris-covered glaciers in a larger region with promising accuracy. Nevertheless, inaccuracy was detected for the small debris-covered glaciers, and glacial lateral and terminus moraines were missed on DEM. Also, water bodies such as river channels connected with the glacier tongue and supraglacial lakes are classified as supraglacial debris. Nonetheless, small debris-covered glaciers outlines and river

channels can be improved by manual editing. Importantly, supraglacial debris areas can be mapped precisely by the proposed methods, and both methods possess the advantage of transferability to other regions and other dates. Information on the distribution of supraglacial debris is particularly important for the Himalaya–Karakoram region; in addition, its variations in time can provide essential help for accurate prediction of future water resources and understanding the responses of debris-covered glaciers to climate change.

Overall, the quality of the DEM directly influenced the accuracy of the mapped debris-covered glacier margin. Therefore, in future, it is expected that applying the proposed method using DEMs with high temporal resolution generated from freely available SAR data (such as Sentinel-1) combined with optical data (such as Sentinel-2, which has 10-meter resolution) and thermal data (such as Landsat-8) should further improve the accuracy of mapping debris-covered glaciers.

## References

- Adhikary, S., Nakawo, M., Seko, K., and Shakya, B., 2000, Dust influence on the melting process of glacier ice: experimental results from Lirung Glacier, Nepal Himalayas. IAHS PUBLICATION, pp. 43-52.
- Aggarwal, S., 2004, Principles of remote sensing. Satellite remote sensing and GIS applications in agricultural meteorology, 23.
- Ball, G. H., Hall, D. J., 1965, A Novel Method of Data Analysis & Pattern Classification. Technical Report NTIS AD 699616. Stanford Research Institute, Stanford, CA. pp. 4-31.
- Bayr, K. J., Hall, D. K., and Kovalick, W. M., 1994, Observations on glaciers in the eastern Austrian Alps using satellite data, International Journal of Remote Sensing, 15(9), pp. 1733-1742.
- Benn, D., and Evans, D. J., 2014, Glaciers and glaciation. Routledge.
- Benn, D. I., and Ballantyne, C. K., 1994, Reconstructing the transport history of glaciogenic sediments: a new approach based on the co-variance of clast form indices. Sedimentary Geology, 91(1-4), pp.215-227.
- Bennett, M. M., and Glasser, N. F. (Eds.), 2011, Glacial geology: ice sheets and landforms. John Wiley & Sons.
- Berthier, E., Schiefer, E., Clarke, G. K., Menounos, B., and Rémy, F., 2010, Contribution of Alaskan glaciers to sea-level rise derived from satellite imagery. Nature Geoscience, 3(2), pp. 92-95.
- Bhambri, R., and Bolch, T., 2009, Glacier mapping: a review with special reference to the Indian Himalayas, Progress in Physical Geography, 33(5), pp. 672-704.
- Bhambri, R., Bolch, T., and Chaujar, R. K., 2011, Mapping of debris-covered glaciers in the Garhwal Himalayas using ASTER DEMs and thermal data, International Journal of Remote Sensing, 32(23), pp. 8095-8119.
- Bhambri, R., Bolch, T., Kawishwar, P., Dobhal, D. P., Srivastava, D., and Pratap, B., 2013, Heterogeneity in glacier response in the upper Shyok valley, northeast Karakoram, The Cryosphere, 7(5), pp. 1385-1398.

## REFERENCES

---

- Bhardwaj, A., Joshi, P. K., Singh, M. K., Sam, L., and Gupta, R. D., 2014, Mapping debris-covered glaciers and identifying factors affecting the accuracy, *Cold Regions Science and Technology*, 106, pp. 161-174.
- Bhardwaj, A., Joshi, P. K., Sam, L., Singh, M. K., Singh, S., and Kumar, R., 2015, Applicability of Landsat 8 data for characterizing glacier facies and supraglacial debris. *International Journal of Applied Earth Observation and Geoinformation*, 38, pp. 51-64.
- Bishop, M. P., Hickman, B. L., and Shroder Jr. J. F., 1999, High resolution satellite imagery and neural networks for information extraction in a complex mountain environment, *Geocarto International*, vol. 14, no. 2, pp. 17–26.
- Bishop, M. P., Bonk, R., Kamp Jr, U., and Shroder Jr, J. F., 2001, Terrain analysis and data modeling for alpine glacier mapping. *Polar Geography*, 25(3), pp. 182-201.
- Blain, Bodil Bjerkvik, 2006, Melting markets: the rise and decline of the Anglo-Norwegian ice trade, pp. 1850-1920.
- Bolch, T., and Kamp, U., 2006, Glacier mapping in high mountains using DEMs, Landsat and ASTER data, *Grazer Schriften der Geographie und Raumforschung*, 41, pp. 37-48
- Bolch, T., Buchroithner, M. F., Kunert, A., and Kamp, U., 2007, Automated delineation of debris-covered glaciers based on ASTER data. In *Geoinformation in Europe*. proceedings of the 27th EARSeL Symposium 2007, June (pp. 4-6).
- Bolch, T., Menounos, B., and Wheate, R., 2010, Landsat-based inventory of glaciers in western Canada, 1985–2005. *Remote Sensing of Environment*, 114(1), pp. 127-137.
- Bolch, T., Yao, T., Kang, S., Buchroithner, M. F., Scherer, D., Maussion, F., Huninjes, E., and Schneider, C., 2010, A glacier inventory for the western Nyainqntanglha Range and the Nam Co Basin, Tibet, and glacier changes 1976–2009, *The Cryosphere*, 4, pp. 419-433.
- Bolch, T., 2011, "Debris." *Encyclopedia of Snow, Ice and Glaciers*. Springer Netherlands, pp.186-188
- Bolch, T., Kulkarni, A., Kääb, A., Huggel, C., Paul, F., Cogley, J.G., Frey, H., Kargel, J.S., Fujita, K., Scheel, M., Bajracharya, S., Stoffel, M., 2012, The state and fate of Himalayan glaciers. *Science*, 336(6079), 310-314
- Brenning, A., Peña, M.A., Long, S., and Soliman, A., 2012, Thermal remote sensing of ice-debris landforms using ASTER: an example from the Chilean Andes. *The Cryosphere*, 6(2), pp. 367-382.
- Casey, K. A., Kääb, A., and Benn, D. I., 2012, Geochemical characterization of supraglacial debris via in situ and optical remote sensing methods: a case study in Khumbu Himalaya, Nepal, *The Cryosphere*, 6(1), pp. 85-100.

## REFERENCES

---

- Clement, A. C., and Peterson, L. C., 2008, Mechanisms of abrupt climate change of the last glacial period. *Reviews of Geophysics*, 46(4), pp. 1-39.
- Collier, E., Maussion, F., Nicholson, L. I., Mölg, T., Immerzeel, W. W., and Bush, A. B. G., 2015, Impact of debris cover on glacier ablation and atmosphere–glacier feedbacks in the Karakoram, *The Cryosphere*, 9, pp. 1617-1632.
- Copland, L., Sylvestre, T., Bishop, M. P., Shroder, J. F., Seong, Y. B., Owen, L. A., Bush, A., and Kamp, U., 2011, Expanded and recently increased glacier surging in the Karakoram, Arctic, Antarctic, and Alpine Research, pp. 503-516.
- Crippen, R.E., 1988, The dangers of underestimating the importance of data adjustments in band rationing. *International Journal of Remote Sensing*. 9(4), pp.767-776.
- Dansgaard, W., Johnsen, S. J., Møller, J., and Langway, C. C., 1969, One thousand centuries of climatic record from Camp Century on the Greenland ice sheet. *Science*, 166(3903), pp. 377-380.
- Falaschi, D., Bravo, C., Masiokas, M., Villalba, R., and Rivera, A., 2013, First glacier inventory and recent changes in glacier area in the Monte San Lorenzo Region (47 S), Southern Patagonian Andes, South America. *Arctic, Antarctic, and Alpine Research*, 45(1), pp. 19-28.
- Farmer, G. T., 2015, Modern climate change science: an overview of today's climate change science, pp. 32-34, Springer.
- Field, W. O., and Collins, S. G., 1975, Glaciers of the St. Elias Mountains, in Field, W. O., ed., *Mountain glaciers of the Northern Hemisphere*: Hanover, New Hampshire, U.S. Army Corps of Engineers, Cold Regions Research and Engineering Laboratory, v. 2, pp. 143–297.
- Fischer, M., Huss, M., Barboux, C., and Hoelzle, M., 2014, The new Swiss Glacier Inventory SGI2010: relevance of using high-resolution source data in areas dominated by very small glaciers. *Arctic, Antarctic, and Alpine Research*, 46(4), pp. 933-945.
- Forgy, E., 1965, Cluster Analysis of Multivariate Data: Efficiency versus Interpretability of Classification, *Biometrics* 21 (3), pp. 768-769.
- Gao, J., and Liu, Y., 2001, Applications of remote sensing, GIS and GPS in glaciology: a review. *Progress in Physical Geography*, 25(4), pp.520-540.

## REFERENCES

---

Goldthwait, R.P., 1963, Dating the little ice age in Glacier Bay, Alaska. Det Berlingske Bogtrykkeri, pp. 37–46.

Gruber, S., Fleiner, R., Guegan, E., Panday, P., Schmid, M.-O., Stumm, D., Wester, P., Zhang, Y., and Zhao, L.: Review article: Inferring permafrost and permafrost thaw in the mountains of the Hindu Kush Himalaya region, *The Cryosphere Discuss.*, doi:10.5194/tc-2016-104, 2016.

Gruber, S., and Haeberli, W., 2009, Mountain permafrost. In *Permafrost soils*(pp. 33-44). Springer Berlin Heidelberg.

Gurnell, A. M., 1983, Downstream channel adjustments in response to water abstraction for hydro-electric power generation from alpine glacial melt-water streams. *Geographical Journal*, pp. 342-354.

Guo, W., Liu, S., Xu, J., Wu, L., Shangguan, D., Yao, X., Wei, J., Bao, W., Yu, P., Liu, Q., and Jiang, Z., 2015, The second Chinese glacier inventory: data, methods and results. *Journal of Glaciology*, 61(226), pp. 357-372.

Gleick, P. H., 1993, Water in crisis: a guide to the world's fresh water resources. Oxford University Press.

Haeberli, W., 1995, Glacier fluctuations and climate change detection. *Geografia Fisica e Dinamica Quaternaria*, 18, pp. 191-199.

Haeberli, W., Hoelzle, M., Paul F., and Zemp, M., 2007, Integrated monitoring of mountain glaciers as key indicators of global climate change: the European Alps. *Annals of Glaciology* 46(1): pp. 150-160. DOI: 10.3189/172756407782871512.

Hall, D. K., Williams, R. S., and Bayr, K. J., 1992, Glacier recession in Iceland and Austria. *Eos, Transactions American Geophysical Union*, 73(12), pp. 129-141.

Hambrey, M. J., Bennett, M. R., Dowdeswell, J. A., Glasser, N. F. and Huddart, D. 1999, Debris entrainment and transfer in polythermal valley glaciers, *Journal of Glaciology*, 45(149), pp. 69–86.

Han, H., Wang, J., Wei, J. and liu, S., 2010, Backwasting rate on debris covered Koxkar glacier, Tuomuer Mountain, China. *Journal of Glaciology*, 56(196), pp. 287-296.

## REFERENCES

---

Hewitt, K., 2009, Rock avalanches that travel onto glaciers and related developments, Karakoram Himalaya, Inner Asia, *Geomorphology*, 103(1), pp. 66-79.

Hewitt, K., 2014, Glaciers of the Karakoram Himalaya: Glacial Environments, Processes, Hazard sand Resources. New York, NY, USA: Springer.

Hoelzle, M., Haeberli, W., Dischl, M. and Peschke, W., 2003, Secular glacier mass balances derived from cumulative glacier length changes. *Global and Planetary Change*, 36(4), pp. 295-306.

Hooke, R.L., 2005, Principles of glacier mechanics, Cambridge university press.

IPCC (2013) Climate change 2013: the physical science basis. Contribution of working group I to the Fifth Assessment Report of the Intergovernmental Panel on Climate Change.

Juen, M., Mayer, C., Lambrecht, A., Han, H. and Liu, S., 2014, Impact of varying debris cover thickness on ablation: a case study for Koxkar Glacier in the Tien Shan. *The Cryosphere*, 8(2), pp. 377-386.

Kääb, A., Reynolds, J. M., and Haeberli, W., 2005, Glacier and permafrost hazards in high mountains. In *Global Change and Mountain Regions* (pp. 225-234). Springer Netherlands.

Kääb, A., Huggel, C., and Fischer, L., 2006, Remote sensing technologies for monitoring climate change impacts on glacier-and permafrost-related hazards.

Kääb, A., Bolch, T., Casey, K., Heid, T., Kargel, J. S., Leonard, G. J., Paul, F., and Raup, B. H., 2014, Glacier mapping and monitoring using multispectral data. In *Global Land Ice Measurements from Space* (pp. 75-112). Springer Berlin Heidelberg.

Karimi, N., Farokhnia, A., Karimi, L., Eftekhari, M., and Ghalkhani, H., 2012, Combining optical and thermal remote sensing data for mapping debris-covered glaciers (Alamkouh Glaciers, Iran), *Cold Regions Science and Technology*, 71, pp. 73-83.

Kääb, 2012, Spectral response of Snow and ice, “Remote Sensing of Glaciers and Ice Caps” ESA Earth Observation Summer School Earth System Monitoring and Modelling, Department of Geosciences, University of Oslo.

## REFERENCES

---

- Kargel, J. S., ed., 2014, Global Land Ice Measurements from Space. Springer.
- Kaser, G., Fountain, A. G. and Jansson, P. A, 2002, manual for monitoring the mass balance of mountain glaciers, IHP-VI- Technical documents in hydrology, pp. 59.
- Kearsley, G. W., 1993, Tourism and resource development conflicts on the Kawarau and Shotover rivers, Otago, New Zealand. *GeoJournal*, 29(3), pp. 263-270.
- Kerle, N., Janssen, L.L., and Huurneman, G.C, 2004, Principles of remote sensing. ITC, Educational textbook series, 2.
- Khan, A., Naz, B. S., and Bowling, L. C., 2015, Separating snow, clean and debris covered ice in the Upper Indus Basin, Hindukush-Karakoram-Himalayas, using Landsat images between 1998 and 2002. *Journal of Hydrology*, 521, pp. 46-64.
- Kirkbride, M. P., 1993, The temporal significance of transitions from melting to calving termini at glaciers in the central Southern Alps, New Zealand. *Holocene*, 3, pp.232–240.
- Kohshima, S., Seko, K. and Yoshimura, Y., 1993, Biotic acceleration of glacier melting in Yala Glacier, Langtang region, Nepal Himalaya. In: *Snow and Glacier Hydrology* (ed. by G. J. Young) (Proc. Kathmandu Symp., November 1992), pp. 309-316. IAHS Publ. no. 218.
- Liang, S., 2005, Quantitative remote sensing of land surfaces. John Wiley and Sons.
- Liu, Q., Mayer, C. and Liu, S., 2013, Distribution and recent variations of supraglacial lakes on dendritic-type glaciers in the Khan Tengri-Tomur Mountains, Central Asia. *The Cryosphere Discussions*, 7, pp. 4545-4584.
- Liu, S. Y., Yao, X. J., Guo, W. Q., Xu, J. L., Shangguan, D. H., Wei, J. F., Bao, W. J., and Wu, L. Z., 2015, The contemporary glaciers in China based on the Second Chinese Glacier Inventory. *Acta Geographica Sinica*, 70(1), 3-16.
- Lorius, C., Jouzel, J., Raynaud, D., Hansen, J., and Le Treut, H., 1990, The ice-core record: climate sensitivity and future greenhouse warming. *Nature*, 347(6289), pp. 139-145.
- Lougeay, R., 1974, Detection of buried glacial and ground ice with thermal infrared remote sensing. *Advanced Concepts and Techniques in the Study of Snow and Ice Resources*, National Academy of Sciences, Washington, DC.

## REFERENCES

---

- Luckman, A., Quincey, D., and Bevan, S., 2007, The potential of satellite radar interferometry and feature tracking for monitoring flow rates of Himalayan glaciers. *Remote sensing of Environment*, 111(2), pp. 172-181.
- Margreth, S., and Funk, M., 1999, Hazard mapping for ice and combined snow/ice avalanches—two case studies from the Swiss and Italian Alps. *Cold Regions Science and Technology*, 30(1), pp. 159-173.
- McNabb, R. W., and Hock, R., 2014, Alaska Tidewater Glacier Terminus Positions, 1948–2012, *Journal of Geophysical Research: Earth Surface*, 119 (2), pp. 153–167.
- McNabb, R. W., R. Hock, and M. Huss, 2015, Variations in Alaska Tidewater Glacier Frontal Ablation, 1985–2013, *Journal of Geophysical Research: Earth Surface*, 120 (1), pp. 120–136.
- Mertie, J. B., Jr. 1933, Notes on the Geography and Geology of Lituya Bay, in U.S. Geological Survey, Mineral resources of Alaska, Report on Progress of Investigations in 1930: U.S. Geological Survey Bulletin 836, pp. 117–135. Reston, VA: U.S. Geological Survey.
- Meier, M. F., 1980, Remote sensing of snow and ice/La télédétection de neige et de glace. *Hydrological Sciences Journal*, 25(3), pp. 307-330.
- Mihalcea, C., Mayer, C., Diolaiuti, G., Lambrecht, A., Smiraglia, C., and Tartari, G., 2006, Ice ablation and meteorological conditions on the debris-covered area of Baltoro glacier, Karakoram, Pakistan. *Annals of Glaciology*, 43(1), pp. 292-300.
- Minora, U., Senese, A., Bocchiola, D., Soncini, A., D'agata, C., Ambrosini, R., Mayer, C., Lambrecht, E., Vuillermoz, C., Smiraglia, C., and Diolaiuti, G , 2015, A simple model to evaluate ice melt over the ablation area of glaciers in the Central Karakoram National Park, Pakistan, *Annals of Glaciology Vol 56 No 70*, pp. 202-216.
- Molnia, B. F., 2008, Glaciers of North America—Glaciers of Alaska, in *Satellite Image Atlas of Glaciers of the World*, edited by J.R.S., Williams and J.G., Ferrigno, pp. 52–83, United States Geological Survey. USGS Prof. Pap. 1386-K.
- Moribayashi, S. and Higuchi, K., 1977, Characteristics of glaciers in the Khumbu region and their recent variations. *J. Japan. Soc. Snow Ice (Seppyo)* 39, special issue, pp. 3-6.

## REFERENCES

---

Müller, F., Caflisch, T., and Müller, G., 1977, Instructions for compilation and assemblage of data for a World Glacier Inventory. Zürich: Department of Geography, Swiss Federal Institute of Technology (ETH).

Henrik M. (ed.), 2008, Greenland Ice and Water for Export, NIRAS Greenland.

Nagai, H., Fujita, K., Nuimura, T., and Sakai, A., 2013, Southwest-facing slopes control the formation of debris-covered glaciers in the Bhutan Himalaya, *Cryosphere*, vol. 7, pp. 1303–1314.

Nakawo, M., 1979, Supraglacial debris of G2 glacier in Hidden Valley, Mukut Himal, Nepal. *Journal of Glaciology*, 22(87), 273-283.

Nakawo, M., and Young, G.J., 1981, Field experiments to determine the effect of a debris layer on ablation of glacier ice. *Annals of Glaciology*, 2(1), pp. 85-91.

Nakawo, M., and Young, G. J., 1982, Estimate of glacier ablation under a debris layer from surface temperature and meteorological variables, *Journal of Glaciology*, 28(98), pp. 29-34.

Nakawo, M., and Rana, B., 1999, Estimate of ablation rate of glacier ice under a supraglacial debris layer, *Geografiska Annaler: Series A, Physical Geography*, 81(4), pp. 695-701.

Nesje, A., and Dahl, S. O., 2016, *Glaciers and environmental change*. Routledge.

Nicholas, M., Short, Sr., 1999, THE REMOTE SENSING TUTORIAL: section1. Contrast Stretching and Density Slicing. online tutorial book, [http://www.fas.org/irp/imint/docs/rst/Sect1/Sect1\\_12a.html](http://www.fas.org/irp/imint/docs/rst/Sect1/Sect1_12a.html).

Nicholson, L. and Benn, D.I., 2006, Calculating ice melt beneath a debris layer using meteorological data” *J GLACIOL*, vol. 52, no. 178, pp. 463-470.

Nuimura, T., Sakai, A., Taniguchi, K., Nagai, H., Lamsal, D., Tsutaki, S., Kozawa, A., Hoshina, Y., Takenaka, S., Omiya, S., Tsunematsu, K., Tshering, P., and Fujita, K., 2014, The GAMDAM Glacier Inventory: A quality controlled inventory of Asian glaciers, *The Cryosphere*, 9, pp. 849-864.

Oerlemans, J., 2005, Extracting a climate signal from 169 glacier records. *Science*, 308(5722), pp. 675-677.

## REFERENCES

---

Ohmura, A., 2010, Completing the world glacier inventory. *Annals of Glaciology*, 50(53), pp. 144-148.

Østrem, G., 1959, Ice Melting under a Thin Layer of Moraine, and the Existence of Ice Cores in Moraine Ridges. *Geografiska Annaler*, 41(4), pp. 228-230. Retrieved from <http://www.jstor.org/stable/4626805>.

Østrem, G. and Brugman, M., 1991, Glacier-mass balance measurements : a manual for field and office work, National Hydrology Research Institute. NHRI Science Report, Saskatoon, Sask.

Owen, L.A., and Derbyshire, E., 1993, Quaternary and Holocene intermontane basin sedimentation in the Karakoram Mountains. In Shroder, J. F. (ed.), *Himalaya to the Sea*. London: Routledge, pp. 108–131.

Owen, L.A., and England, J. (1998). Observations on rock glaciers in the Himalayas and Karakoram Mountains of northern Pakistan and India. *Geomorphology*, 26(1), 199-213.

Paterson W.S.B., 1994, *The physics of glaciers*, 3rd Edition, Butterworth-Heinemann.

Paul, F., 2000, Evaluation of different methods for glacier mapping using Landsat TM. In Workshop on Land Ice and Snow, Dresden/FRG, June (Vol. 1617).

Paul, F., Kääb, A., Maisch, M., Kellenberger, T., and Haeberli, W., 2002, The new remote-sensing-derived Swiss glacier inventory: I. Methods. *Annals of Glaciology*, 34(1), pp. 355-361.

Paul, F., Huggel, C., and Kääb, A., 2004, Combining satellite multispectral image data and a digital elevation model for mapping debris-covered glaciers, *Remote sensing of Environment*, 89(4), pp. 510-518.

Paul, F., Barrand, N. E., Baumann, S., Berthier, E., Bolch, T., Casey, K., Frey, H., Joshi, S. P., Knovalov, V., Bris, R. Le, Mölg, N., Nosenko, G., Nuth, C., Pope, A., Racoviteanu, A., Rastner, P., Raup, B., Scharrer, K., Steffen, S., and Winsvold, S., 2013, On the accuracy of glacier outlines derived from remote-sensing data, *Annals of Glaciology*, 54(63), pp. 171-182.

## REFERENCES

---

- Paul, F., Winsvold, S. H., Kääb, A., Nagler, T., and Schwaizer, G., 2016, Glacier Remote Sensing Using Sentinel-2. Part II: Mapping Glacier Extents and Surface Facies, and Comparison to Landsat 8. *Remote Sensing*, 8(7), 575.
- Pellikka, P., and Rees, W.G. (Eds.), 2009, *Remote sensing of glaciers: techniques for topographic, spatial and thematic mapping of glaciers*. CRC Press.
- Pelto, M. S., and Hedlund, C., 2001, Terminus behavior and response time of North Cascade glaciers, Washington, USA, *Journal of Glaciology*, 47(158), pp. 497-506.
- Petersen, J. F., Sack, D., and Gabler, R. E., 2016, *Physical geography*, Nelson Education, Chapter 19: Glacial systems and landforms, pp. 525-535.
- Petit, J. R., Jouzel, J., Raynaud, D., Barkov, N. I., Barnola, J. M., Basile, I., Bender, M., Chappellaz, J., Davis, M., Delaygue, G., Delmotte, M., Kotlyakov, V. M., Legrand, M., Lipenkov, V. Y., Lorius, C., PÉpin, L., Ritz, C., Saltzman, E. and Stievenard, M., 1999, Climate and atmospheric history of the past 420,000 years from the Vostok ice core, Antarctica. *Nature*, 399(6735), pp. 429-436.
- Pfeffer, W. T., Harper, J. T., and O'Neal, S., 2008, Kinematic constraints on glacier contributions to 21st-century sea-level rise. *Science*, 321(5894), pp. 1340-1343.
- Pfeffer, W.T., Arendt, A.A., Bliss, A., Bolch, T., Cogley, J.G., Gardner, A.S., Hagen, J., O., Hock, R., Kaser, G., Kienholz, C., Miles, E.S., Moholdt, G., Mölg, N., Paul, F., Radic, V., Rastner, P., Raup, B.H., Rich, J., Sharp, M.J., and the Randolph Consortium, 2014, The Randolph Glacier Inventory: a globally complete inventory of glaciers. *Journal of Glaciology*, 60, pp. 537–552.
- Pidwirny, M., 2006, *Glacial Processes, Fundamentals of Physical Geography, 2nd Edition*. Date Viewed. <http://www.physicalgeography.net/fundamentals/10ae.html>.
- Poore, R. Z., Williams Jr, R. S., and Tracey, C., 2000, Sea level and climate, USGS Fact Sheet 002.
- Post, A. 1967. "Effects of the March 1964 Alaska Earthquake on Glaciers." U.S. Geological Survey, 435, Professional Paper 544 –D.
- Pratap, B., Dobhal, D. P., Mehta, M., and Bhambri, R., 2015, Influence of debris cover and altitude on glacier surface melting: a case study on Dokriani Glacier, central Himalaya, India, *Annals of Glaciology*, 56(70), pp. 9-16.

## REFERENCES

---

- Quincey, D. J., Lucas, R.M., Richardson, S.D., Glasser, N.F., Hambrey, M.J., and Reynolds, J. M., 2005, Optical remote sensing techniques in high-mountain environments: applications to glacial hazards. *Progress in Physical Geography*, 29, pp.475–505.
- Racoviteanu, A. E., Paul, F., Raup, B., Khalsa, S. J. S., and Armstrong, R., 2010, Challenges and recommendations in mapping of glacier parameters from space: results of the 2008 Global Land Ice Measurements from Space (GLIMS) workshop, Boulder, Colorado, USA, *Annals of Glaciology*, 50(53), pp. 53-69.
- Racoviteanu, A., and Williams, M. W., 2012, Decision tree and texture analysis for mapping debris-covered glaciers in the Kangchenjunga area, eastern Himalaya. *Remote Sensing*, 4(10), pp. 3078-3109.
- Ranzi, R., Grossi, G., Iacovelli, L., and Taschner, S., 2004, Use of multispectral ASTER images for mapping debris-covered glaciers within the GLIMS Project. In *Geoscience and Remote Sensing Symposium, 2004. IGARSS'04. Proceedings. 2004 September, IEEE International* (Vol. 2, pp. 1144-1147).
- Rankl, M., Kienholz, C., and Braun, M., 2014, Glacier changes in the Karakoram region mapped by multimission satellite imagery, *The Cryosphere*, 8(3), pp. 977-989.
- Raup, B., and Khalsa, S. J. S., 2007, GLIMS analysis tutorial. Available from World Wide Web: [http://www.glims.org/MapsAndDocs/assets/GLIMS\\_Analysis\\_Tutorial\\_a4.pdf](http://www.glims.org/MapsAndDocs/assets/GLIMS_Analysis_Tutorial_a4.pdf).
- Raup, B. H., Kääb, A., Kargel, J. S., Bishop, M. P., Hamilton, G., Lee, E., Paul, F., Rau, F., Soltesz, D., Khalsa, S. J. S., Beedle, M., and Helm, C., 2007, Remote Sensing and GIS technology in the Global Land Ice Measurements from Space (GLIMS) Project, *Computers and Geosciences*, 33(1), pp. 104-125.
- Rau, F., Mauz, F., Vogt, S., Khalsa, S.J.S., and Raup, B., 2005, Illustrated GLIMS glacier classification manual. Institut fr Physische Geographie Freiburg, NSIDC.
- Rastner, P., Bolch, T., Mölg, N., Machguth, H., Le Bris, R., and Paul, F, 2012, The first complete inventory of the local glaciers and ice caps on Greenland. *The Cryosphere*, 6(6), pp.1483-1495.
- Richards, J. A., Jia, X., 1999, *Remote sensing digital image analysis* (Vol. 3). Berlin: Springer-Verlag, pp. 249-263.
- Reznichenko, N., Davies, T., Shulmeister, J., and McSaveney, M., 2010, Effects of debris on ice-surface melting rates: an experimental study. *Journal of Glaciology*, 56(197), pp. 384-394.

## REFERENCES

---

- Ritchie, J. B., Lingle, C. S., Motyka, R. J., and Truffer, M., 2008, Seasonal Fluctuations in the Advance of a Tidewater Glacier and Potential Causes: Hubbard Glacier, Alaska, USA, *Journal of Glaciology*, 54 (186), pp. 401–411.
- Rott, H., 1994, Thematic studies in alpine areas by means of polarimetric SAR and optical imagery, *Advances in Space Research*, 14(3), pp. 217-226.
- Scherler, D., Bookhagen, B., and Strecker, M. R., 2011, Spatially variable response of Himalayan glaciers to climate change affected by debris cover, *Nature geoscience*, 4(3), pp. 156-159.
- Schomacker, A., 2011, Moraine. In *Encyclopedia of Snow, Ice and Glaciers* (pp. 747-756). Springer Netherlands.
- Shi, Y., Liu, S., Ye, B., et al., 2008, Concise glacier inventory of China. Shanghai, Shanghai Popular Science, Shanghai, China.
- Shroder, J. F., Bishop, M. P., Copland, L., and Sloan, V. F., 2000, Debris-covered glaciers and rock glaciers in the Nanga Parbat Himalaya, Pakistan, *Geografiska Annaler: Series A, Physical Geography*, 82(1), pp. 17-31.
- Shukla, A., Gupta, R. P., and Arora, M. K., 2009, Estimation of debris cover and its temporal variation using optical satellite sensor data: a case study in Chenab basin, Himalaya, *Journal of Glaciology*, 55(191), pp. 444-452.
- Shukla, A., Gupta, R., and Arora, M. K., 2010a, Delineation of debris-covered glacier boundaries using optical and thermal remote sensing data, *Remote Sensing Letters*, 1(1), pp. 11-17.
- Shukla, A., Arora, M. K., and Gupta, R. P., 2010b, Synergistic approach for mapping debris-covered glaciers using optical–thermal remote sensing data with inputs from geomorphometric parameters, *Remote Sensing of Environment*, 114(7), pp. 1378-1387.
- Shukla, A., and Ali, I., 2016, A hierarchical knowledge-based classification for glacier terrain mapping: a case study from Kolahoi Glacier, Kashmir Himalaya, *Annals of Glaciology*, 57(71), pp. 1-10.
- Silverio, W., and Jaquet, J. M., 2005, Glacial cover mapping (1987–1996) of the Cordillera Blanca (Peru) using satellite imagery. *Remote Sensing of Environment*, 95(3), pp. 342-350.
- Sinha, R. and Ravindra, R., 2013, Earth system processes and disaster management, Springer, pp. 38-39.

---

## REFERENCES

Solomon, S., D. Qin, M. Manning, M. Marquis, K. Averyt, M. M. B. Tignor, H. L. Miller Jr., and Z. Chen. 2007. Climate Change 2007 – The Physical Science Basis: Working Group I Contribution to the Fourth Assessment Report of the IPCC. Vol. 4. Cambridge: Cambridge University Press.

Stokes, C. R., Popovnin, V., Aleynikov, A., Gurney, S. D., and Shahgedanova, M., 2007, Recent glacier retreat in the Caucasus Mountains, Russia, and associated increase in supraglacial debris cover and supra-/proglacial lake development. *Annals of Glaciology*, 46(1), pp. 195-203.

Strozzi, T., Luckman, A., Murray, T., Wegmüller, U., and Werner, C. L., 2002, Glacier motion estimation using SAR offset-tracking procedures, *IEEE Transactions on Geoscience and Remote Sensing*, 40(11), pp. 2384-2391.

Suzuki, R., 2011, Debris thermal properties and impact on ice ablation. In *Encyclopedia of Snow, Ice and Glaciers* (pp. 178-180). Springer Netherlands.

Taschner, S., and Ranzi. R., 2002, Comparing the opportunities of Landsat-TM and Aster data for monitoring a debris covered glacier in the Italian Alps within the GLIMS project, *Geoscience and Remote Sensing Symposium, 2002. IGARSS'02. 2002 IEEE International*. Vol. 2. IEEE, 2002.

Tachikawa, T., Kaku, M., Iwasaki, A., Gesch, D. B., Oimoen, M. J., Zhang, Z., Danielson, J. J., Krieger, T., Curtis, B., Haase, J., Abrams, M., and Carabajal, C., 2011, ASTER global digital elevation model version 2-summary of validation results. NASA.

Thomas, J., and S. C. Rai, 2005, An overview of glaciers, glacier retreat, and subsequent impacts in Nepal, India, and China, report, pp. 70, WWF Nepal Programme, Kathmandu.

Veettil, B. K., Bremer, U. F., Grondona, A. E. B., and De Souza, S. F., 2014, Recent changes occurred in the terminus of the Debris-covered Bilafond Glacier in the Karakoram Himalayas using remotely sensed images and digital elevation models (1978–2011). *Journal of Mountain Science*, 11(2), pp. 398-406.

Vihma, T., 2011, Atmosphere-snow/ice interactions. *Encyclopedia of Snow, Ice and Glaciers*, pp.66-75.

## REFERENCES

---

- Waldinger, R., 1999, The spatial distribution of alpine glaciers and snowlines: Influencing factors and controls, [Online]. Available: <http://www.utexas.edu/depts/grg/hudson/grg394k/studentprojects/waldinger/waldinger.html>.
- Warren, S.G. and Brandt, R.E., 2008, Optical constants of ice from the ultraviolet to the microwave: A revised compilation. *Journal of Geophysical Research-Atmospheres*. 113(D14).
- Westermann, S., Duguay, C. R., Grosse, G., and Kääb, A., 2015, Remote sensing of permafrost and frozen ground. *Remote Sensing of the Cryosphere*, pp.307-344.
- Whalley, W. B., Martin, H. E., and Gellatly, A. F., 1986, The problem of hidden ice in glacier mapping. *Annals of Glaciology*, 8, pp. 181-183.
- Williams, R. S., 1983, UNITED STATES GEOLOGICAL SURVEY. Glaciers: clues to future climate? US Department of the Interior, Geological Survey, pp.17.
- Williams Jr, R. S., 1986, Glacier inventories of Iceland: evaluation and use of sources of data. *Annals of Glaciology*, 8, pp. 184-191.
- Wirz, V., Gruber, S., Purves, R.S., Beutel, J., Gärtner-Roer, I., Gubler, S., and Vieli, A., 2015, Short-term velocity variations of three rock glaciers and their relationship with meteorological conditions. *Earth Surface Dynamics Discussions*, 3, pp. 459-514.
- Zemp, M., Frey, H., Gärtner-Roer, I., Nussbaumer, S. U., Hoelzle, M., Paul, F., Haeberli, W., Denzinger, F., AhlstrØm, A.P., Anderson, B., Bajracharya, S., Baroni, C., Braun, L.N., Cáceres, B.E., Casassa, G., Cobos, G., Dávila, L.R., Granados, H.D., Demuth, M.N., Espizua, L., Fischer, A., Fujita, K., Gadek, G., Ghazanfar, A., Hagen, J.O., Holmlund, P., Karimi, N., Li Z., Pelto, M., Pitte, P., Popovnin, V.V., Portocarrero, C.A., Prinz, R., Sangewar, C.V., Severskiy, I., Sigurðsson, O., Soruco, A., Usualiev, R., and Vincent, C., 2015, Historically unprecedented global glacier decline in the early 21st century. *Journal of Glaciology*, 61(228), pp. 745-762.